Geology and Geochemistry of a Proterozoic Supracrustal and Intrusive Sequence in the Central Wet Mountains, Colorado

by
Antonio Lanzirotti

Submitted in Partial Fullfillment
of the Requirements for the Degree of
Masters of Science in Geochemistry

New Mexico Institute of Mining and Technology
Socorro, New Mexico
May 24, 1988

Gott würfelt nicht.

-Albert Einstein

Abstract

The early Proterozoic supracrustal and intrusive rocks of the central Wet Mountains in south-central Colorado were analyzed geochemically and petrographically. The terrane consists of supracrustal metasedimentary units, amphibolites, and leucogranitic gneisses variably deformed and metamorphosed to amphibolite and granulite grades. Amphibolites (plagioclase-hornblende gneisses) seem to represent metamorphosed, basaltic dikes and sills with calc-alkaline affinities and define two groups, one with high-Fe (>7% FeO-T) and low Mg (<9% MgO) which is seen over the entire study area and has geochemical affinities to calc-alkaline basalts erupted from immature island arc settings, and another with low-Fe (<7% FeO-T) and high Mg (>9% MgO) which is seen in the Bull Domingo Hills amphibolite complex (BDH). The second group is extremely REE depleted (<10x chondrite) with convex upward REE patterns; a Rayleigh closed system FXL model seems to work best in explaining their origin as cumulates of a 50% FXL event (plagioclase, clinopyroxene, olivine, magnetite) of the first amphibolite group. The liquid from this FXL is geochemically similar to quartz diorites exposed in the Wet Mountains.

Paragneisses (biotite-quartz-plagioclase gneiss) from the terrane show sedimentary type trends and geochemical similarities to modern and Proterozoic quartz-wackes. They also show geochemical affinities to sediments from basins associated with continental margin arcs.

Leucogranites are concordant to the regional foliation and occur as sills infolded with the supracrustal units. They are peraluminous and show similarities to S-type granites. They bear a lithologic similarity to leucogranites from collisional terranes and geochemically appear to have been emplaced at low water pressures. They have strongly enriched LREE patterns (La/Sm = 20) and affinities to granites from within-plate and post-collisional tectonic settings.

Granulites have moderately enriched LREE patterns (80x chondrites) and positive Eu anomalies. Fluid inclusions from granulites are CO_2 dominated with densities close to 1.1 g/cm^3. Scapolite is seen as a prograde mineral and appears to have formed at temperatures above 850°C and pressures of about 9 kbars.

Metasediments and amphibolites seem to have been deposited in a back arc basin developed in or near continental crust prior to 1720 Ma. They were subsequently deformed and metamorphosed by a deformational event at 1710 Ma. This event may represent accretion of the Pecos arc to a continental margin arc in southern Colorado at about 1710 Ma. This collision might result in crustal thickening and granulite facies metamorphism. Water purging from the system may result in anatectic melting of the metasedimentary gneisses to form the leucogranites. Subsequent uplift of the granulites results in retrogression to amphibolite grade.

Acknowledgements

Contents

List of Figures

List of Tables

Introduction

The earliest detailed geologic studies in the central Wet Mountains were conducted by the U. S. Geological Survey in the Silvercliff and Rosita Hills areas (Cross, 1896). Early studies were primarily concerned with the occurrences of gold and silver associated with Tertiary veins, dikes, and breccias. It wasn't until the detailed geologic work of Brock and Singewald (1968) and Christman (1959) in evaluating thorium deposits in the Wet Mountains that it became apparent that the dominant lithologies in the area are gneisses of Precambrian age. Their detailed mapping in the Mount Tyndall quadrangle resulted in the identification of 30 separate Precambrian units.

However, such extreme detail in mapping occasionally results in confusion. Units labeled ab (alaskitic granite gneiss and biotite gneiss), af (alaskitic granite gneiss and charnockite gneiss), and ah (alaskitic granite gneiss and hornblende gneiss) all represent gneisses in various degrees of digestion within alaskitic granite and units such as afh (alaskitic granite gneiss, charnockite gneiss, and hornblende gneiss) represent mixtures of three gneissic varieties or where the three occur in too close a proximity to be mapped individually. By eliminating units such as these, the Wet Mountains terrane can be defined by four major rock types. The biotite gneisses of Brock and Singewald seem to be metasediments and will be referred to as such. The hornblende gneisses appear to represent basaltic dikes and sills and perhaps flows and will be referred to as amphibolites. There are extensive amounts of granitic rock of various ages, from syn-tectonic to post-tectonic plutons and from alaskitic to dioritic compositions. Brock and Singewald's original identification of charnockites in the Wet Mountains was correct. The word charnockite, however, often implies a rock with granitic composition, whereas the

granulites of the Wet Mountains are compositionally diverse, having mafic, felsic, and occasionally calc-silicate compositions. Other rock types, such as metapelites, calc-silicates, quartzites, and ultramafics are rare.

Location

The Wet Mountains (Fig. 1) are a major uplift south of the Front Range and adjacent to the Great Plains in central Colorado. The Arkansas River and the Cañon City Embayment bound the Wet Mountains to the north, separating them from the Front Range, and the Wet Mountain Valley, a Laramide feature, separates the Wet Mountains from the Sangre de Cristo range to the west. Sampling was concentrated primarily in an east-west traverse through the central Wet Mountains, with most samples coming from the Beckwith Mountain, Westcliffe, Mount Tyndall, and Hardscrabble Peak quadrangles. The sampling area was a 25 km wide section extending from 105°37'30" longitude east to 105°07'30" (see Fig. 2).

Purpose

This study will give detailed descriptions of the rock types exposed in the Wet Mountains and, through these descriptions, make inferences about rock protoliths. The conclusions will be based upon field, petrologic, lithologic, and geochemical evidence and will build upon these relationships to characterize the rock types in terms of a petrotectonic origin and a depositional, structural, and metamorphic history. In a larger sense, the relationships will be evaluated in terms of how the Wet Mountains fit into a possible tectonic model for the origin of the early crust in Colorado.
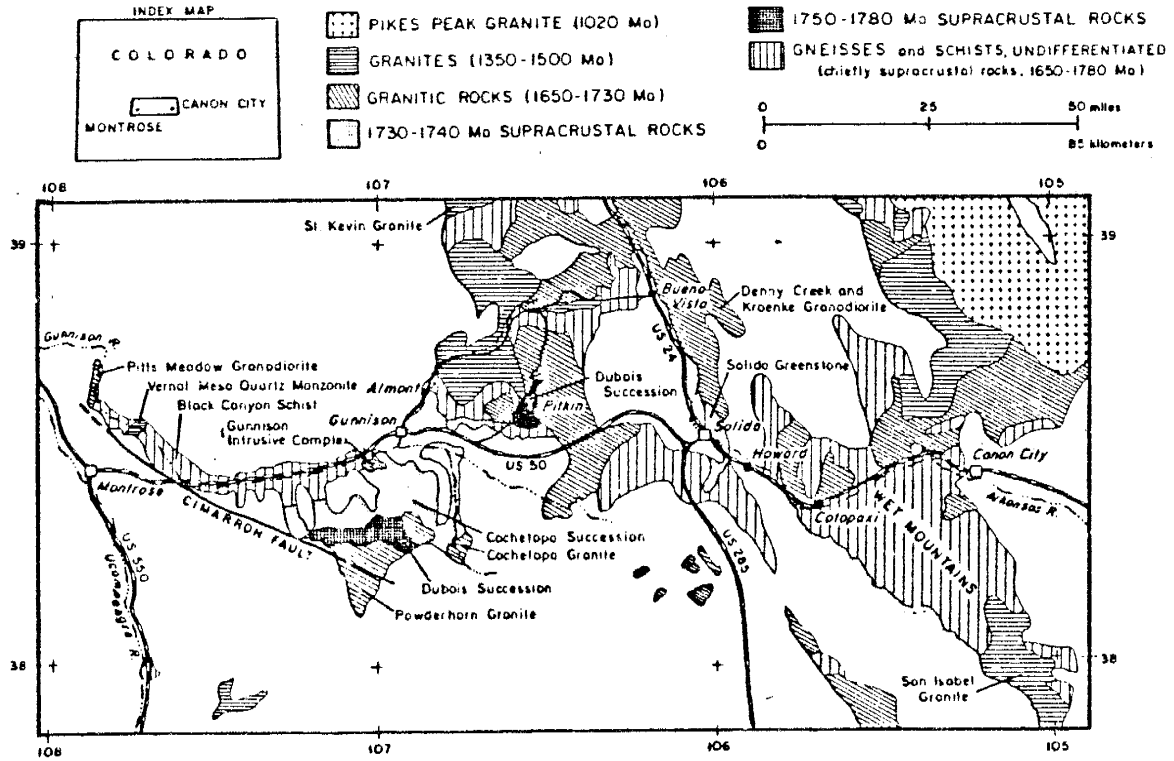
Figure 1: Generalized geologic map of Proterozoic rocks in central Colorado (from Knoper and Condie, 1986).
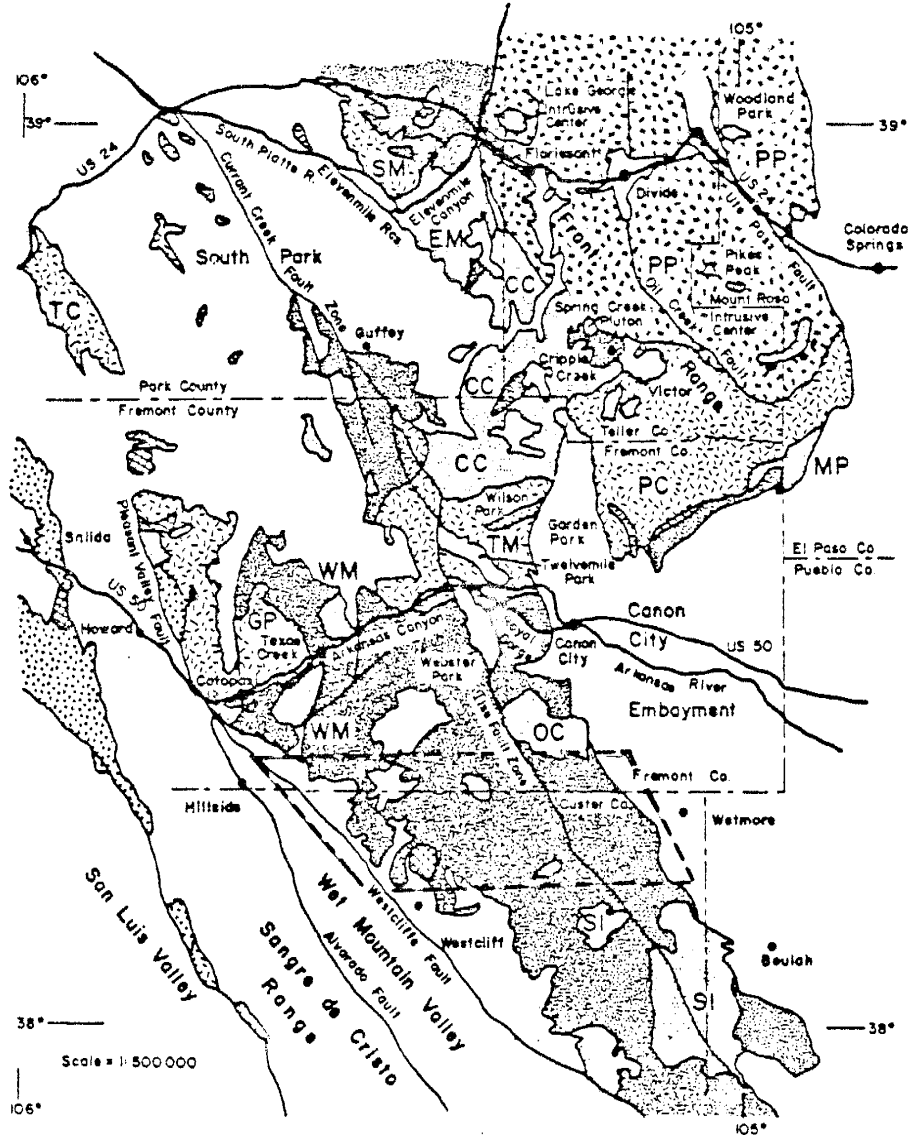
Figure 2: Geologic map of the southern Front Range and the northern Wet Mountains (from Cullers and Wobus, 1986). Outlined area is area encompassed by this study. Explanation in Fig. 3.

EXPLANATION

Phanerozoic Rocks, Undivided

Proterozoic Y

Alkalic intrusives assoc. with Pikes Peak Batholith

Pikes Peak Granite

Granitic Rocks of Berthoud (silver plume) Intrusive Suite
  Specific plutons (alphabetical listing):
    CC= Cripple Creek Batholith (1410 m.y.)
    EM= Elevenmile Canyon Stock (1440 m.y.)
    MP= Mount Pittsburg Stock
    OC= Oak Creek Stock (1440 m.y.)
    SI = San Isabel Batholith (1360 m.y.)
    WM= West McCoy Gulch Stock (1460 m.y.)

Proterozoic X

Granitic Rocks of Routt (Boulder Creek) Intrusive Suite
  Specific plutons (alphabetical listing):
    GP= Garrel Peak - Cotopaxi Batholith (1670 m.y.)
    PC= Phantom Canyon Batholith (1670 m.y.)
    SM= Stoll Mtn. Batholith
    TC= Trout Creek Batholith (1670 m.y.)
    TM= Twin Mtn. - Crampton Mtn. Batholith (1700 m.y.)

Metagabbro (BDH complex)

Metavolanic Rocks and Associated Metasediments (1710-1740 m.y.)

Quartzite - Mica Schist of Blue Ridge and Phantom Canyon

Metasedimentary Rocks, Undivided (Derived Primarily from
  Pelitic Sediments; Volcanic Components Minor)

Figure 3: Explanation to Figure 2

It should be emphasized, however, that due to the size of the field area and the nature of this study that much of the data should be considered as being reconnaissance in nature. Much more detailed work must follow in order to clarify many of the details and questions which this study will raise.

Methods

Field work was initiated during May of 1985 and continued intensively for the following three months, during which samples were collected from some 200 locations. Some follow-up field work was done the following summer. Of the samples collected, about 45 were analyzed for major and trace element contents. Analyses were done by neutron activation analysis (NAA), using the ND-6600 system, and by X-ray fluorescence (XRF), using a Rigaku XRF spectrometer. Two granulites underwent thermometric fluid inclusion analysis.

Thin sections were made from about twenty samples and, in addition to geo-chemical and petrologic analysis, some structural analysis is presented, primarily based upon data collected by Brock and Singewald (1968).

General Geology

The Wet Mountains are an early Laramide uplift about 75 km long and 8 to 16 km wide, trending north-northwest on the site of the late Paleozoic Front Range highland. Their thin sedimentary cover was easily removed during uplift, exposing the Precambrian terrane (Tweto, 1975). The range is fault bounded on both the east and west by the Wet Mountains and Westcliffe faults respectively. Both faults are Laramide structures which underwent continued movement into the late Cenozoic (Taylor, 1975).

Precambrian units constitute upwards of 75% of the study area with metasediments, amphibolites, and granitic gneisses representing the bulk of the Proterozoic lithologies exposed. All units show evidence of high grade ductile deformation, with a minimum of two periods of deformation, although the degree of deformation and metamorphism is not consistent. Metamorphic foliation tends to parallel the original compositional layering and primary textures are rare. Much of the area has also been extensively migmatized. No rock types are seen less than middle amphibolite metamorphic grade and there is strong evidence in certain areas of grades as high as granulite facies. Tweto (1977) suggests that the entire area, along with the southern Front Range, was metamorphosed during a single event at least 1700 Ma ago, based upon structural constraints on metamorphic assemblages.

A U-Pb zircon date on one of the charnockites by Bickford (1986) gives an age of 1694±25 Ma, on the basis of analysis of a suite of exceptionally clear, euhedral zircons. Since zircons commonly recrystallize under granulite facies conditions, there is a strong suggestion that this is a metamorphic age. Also, two U-Pb dates on granites from the Parkdale area, which intruded into probable equivalents of the central Wet Mountains supracrustals, yield ages of 1705 Ma (Bickford, 1986),

suggesting a terrane older than 1700 Ma with mantle separation ages between 1800 and 2000 Ma (Nelson and DePaolo, 1985).

The gneissic rocks are intruded by granitic plutons at four major periods during the Proterozoic: 1700 Ma, 1670±30 Ma, 1410±50 Ma, and about 1000 Ma (Cullers and Wobus, 1986), each at a successively shallower crustal level as uplift proceeded (Wobus, 1969, Hutchinson and Hedge, 1967).

Amphibolites and Ultramafics

Occurrence and Form

Amphibolites represent 15 to 20 % of the exposed Proterozoic sequences, representing almost exclusively dikes and sills or perhaps basaltic flows. Evidence for their being hypabyssal intrusives comes primarily from their relationships to other rock types and from the textural variation within individual units. Although some are fine grained, most are medium to coarse grained and show significant variations in crystal size within individually mappable units. Most have crystal diameters on the order of 1 mm although some have cross-sectional areas of about 5 mm, and are generally equigranular and well foliated. Their "gabbroic" texture, however, may be a product of recrystallization and these units may in fact represent flows.

The amphibolites are generally folded and concordant to regional foliation, although they are occasionally discordant, alternating with alaskitic and biotite gneisses, suggesting they primarily represent sills (Brock and Singewald, 1968). Ultramafics are an extremely minor rock type and commonly occur as bronzite bearing units (Fig. 5) which are always fault bounded and tectonized. The brown, mottled specks on the rock surface are altered bronzite crystals, individual crystals of which may be found as large as 4 cm in length. Although similar ultramafic bodies occur in other Precambrian terranes, such as the bronzite-picrite dikes in the Scourie dike complex (Tarney, 1986), cumulus textures in outcrop and thin section suggest that these are ultramafic cumulates. Compositionally, the ultramafic gneisses are websterites, composed primarily of hypersthene-bronzite

Figure 4: Typical amphibolite in hand specimen

and clinopyroxene, but also contain olivine and very minor plagioclase (Fig. 6). One particular unit can be traced for about 7 km to the northwest as a relatively thin body.

Modeling of the ultramafics as cumulates of fractional crystallization of the amphibolites prove unsuccessful. Although their textures are suggestive of cumulates, their linear outcrop exposure implies that they represent dikes or sills and, though they may represent primitive magmas, lack of more detailed data prevents evaluation of this possibility. Additionally, the common presence of fault zones in association with websterite occurrence may imply a genetic, tectonic origin which cannot be precluded.

Petrography

The amphibolites commonly have a granoblastic texture with individual crystals being xenoblastic to hypidioblastic, and some amphibolites appear to be subophitic to blastophitic. All the amphibolites appear to be gneissic with foliation highly dependent upon amphibole habit. Most of the thin sections display a polygonal texture rich in triple junctions although there appears to be some breakage of the amphiboles along {010} to produce polycrystalline aggregates. Brittle deformation in the amphiboles along the edges coupled with preferential alignment of amphiboles along S_1 suggests that they may be pre-kinematic. Plagioclase is occasionally poikiloblastic, including within it amphiboles and minor mineral phases. Amphiboles range in size from 0.25 mm in diameter to 2 mm by 1 mm, are hornblendes compositionally, and occasionally will cluster into aggregates.

Determination of anorthite (An) content in the plagioclases is difficult at high metamorphic grades. The Michel-Lévy method is not very useful due to the rarity

Figure 5: Field photo of bronzite bearing, ultramafic cumulate. Large brown crystals are weathered bronzites.
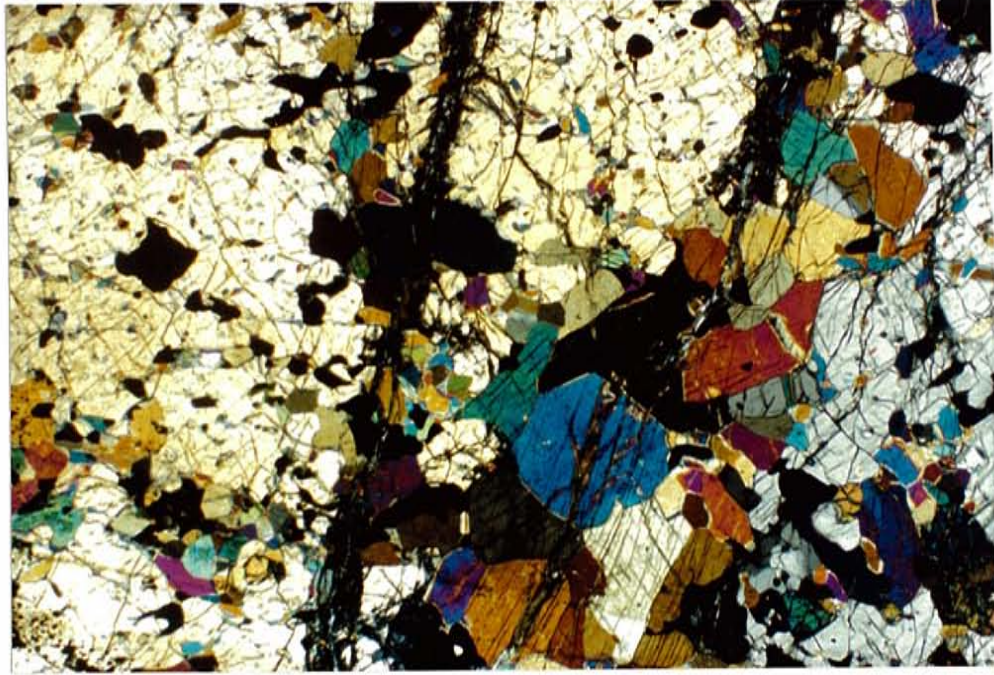
Figure 6: Photomicrograph of websterite sample LSC-2. Large yellow crystal is bronzite, bright blue crystals are clinopyroxene, brown to green crystals are hornblende. Purple crystals are olivine. Opaques are spinel. Sample has been tectonized. Scale 1cm=0.5mm, X-polz. light.

with which one can find a {010} crystallographic plane normal to the plane of the section and therefore the Fouqué method is much more applicable. In the Fouqué method it is only necessary to secure a centered bisectrix figure with either a positive or negative optic sign. With positive figures the extinction angle of the faster ray against {010} is measured and with negative figures the faster ray is measured against {001}. Using this method the plagioclases have An contents of 48 to 67%.

Amphibole constitutes about 50% of the sections examined (visual estimate), whereas plagioclase constitutes about 45%. Zircon makes up as much as 3% of some sections with other minor phases making up the balance, including apatite, quartz, and occasionally sphene and alteration products due to saussuritisation and epidotization, although these were not analyzed chemically.

Geochemistry

Table I contains geochemical analyses of selected amphibolites and ultramafics (LSC-2 and LSG-11). When plotted on a Jensen cation plot (Fig. 7), the amphibolites scatter in the basalt and tholeiite fields and appear to have affinities to both calc-alkaline and tholeiitic basalts. Those samples which plot in the basaltic komatiite field are websterites or samples from the Bull Domingo Hills (BDH) amphibolite complex. On a Nb/Y vs Zr/TiO_2 diagram (Winchester and Floyd, 1977; Fig. 8) the amphibolites bear chemical similarities to tholeiites and basaltic andesites. Those plotting in the andesite field may have been altered for, when the amphibolites are plotted on a $MgO/10$-$SiO_2/100$-CaO/Al_2O_3 ternary alteration screen (Davis, 1979; Fig. 9), the samples with andesitic affinities fall outside the unaltered field. Samples plotting near the $MgO/10$ apex are samples of ultramafics. It should be noted here analyzed samples were selected on the basis of a
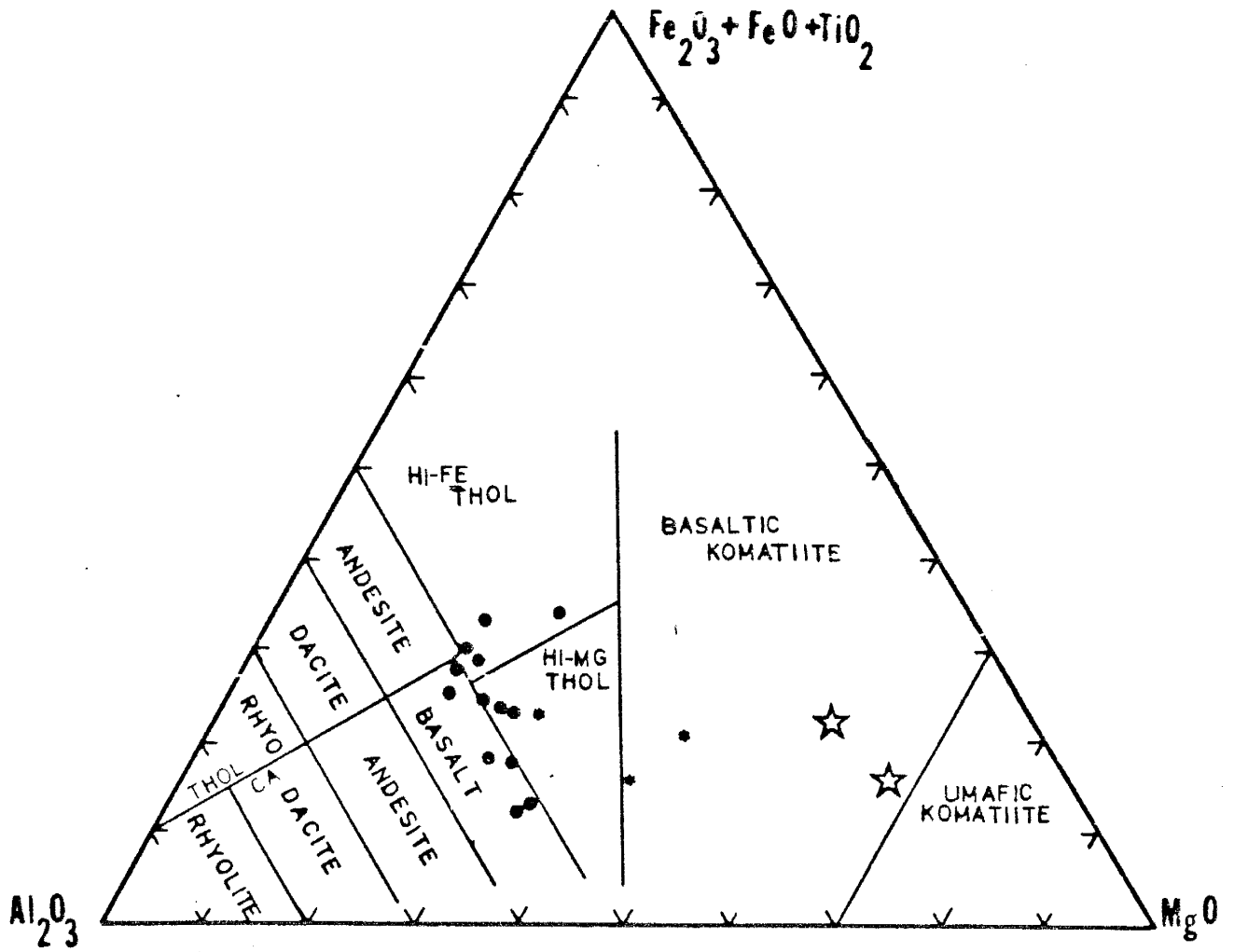
Figure 7: Jensen cation plot of Wet Mountains amphibolites. Solid circles are amphibolites, asterisks are Bull Domingo Hills (BDH) samples, stars are websterites. THOL and CA separate tholeiitic from calc-alkali fields (Jensen, 1976).
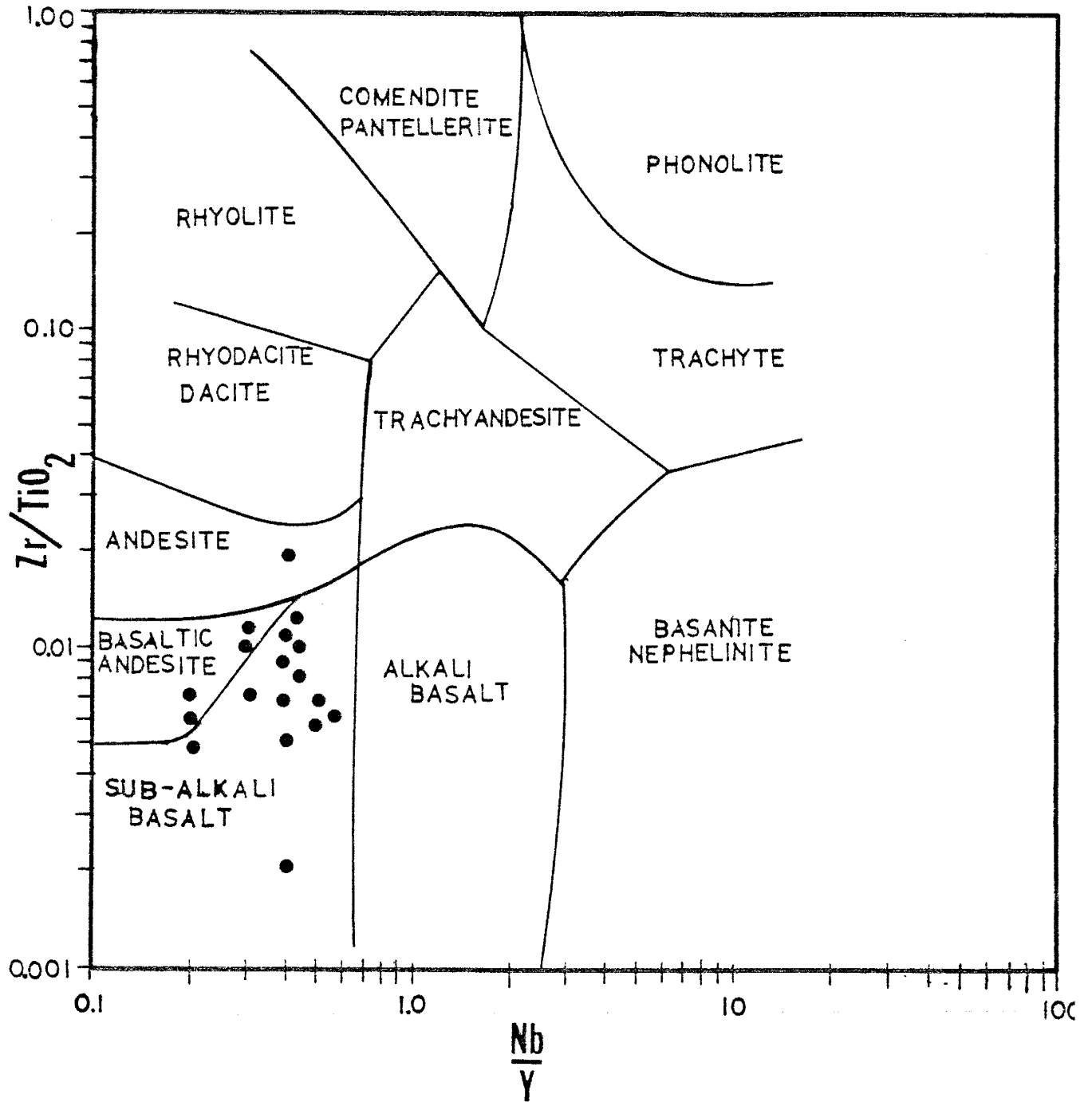
Figure 8: Nb/Y vs Zr/TiO_2 plot showing the distribution of amphibolites from the Wet Mountains (after Winchester and Floyd, 1977).
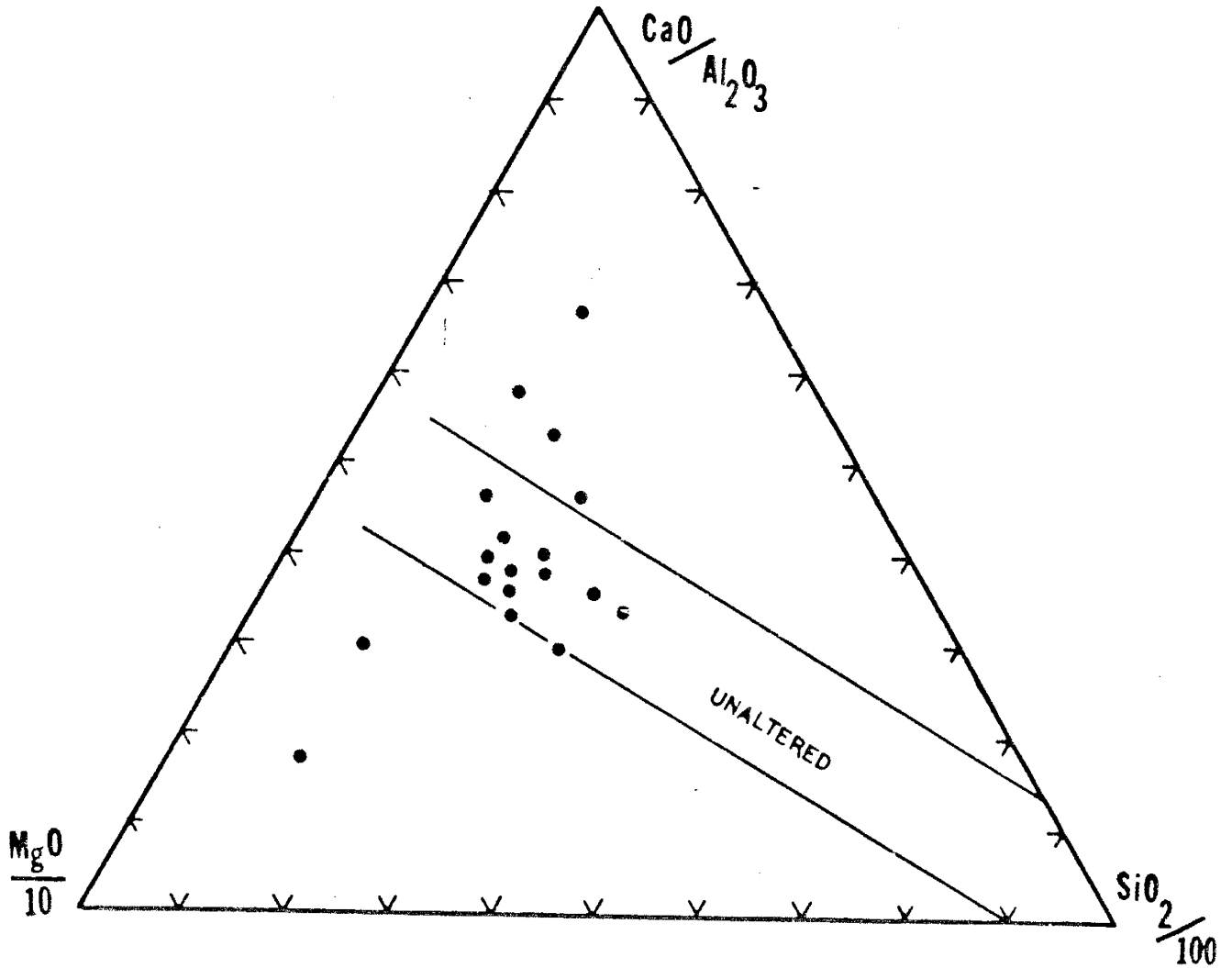
Figure 9: Amphibolites and ultramafic units from the Wet Mountains are plotted on a Mg-Si-Ca/Al alteration screen (Davis, 1979). Two samples plotting towards the MgO apex are ultramafics.

lack of amygdules, staining, quartz veins, and possible alteration products, such as epidote or calcite, in hand specimen. Also, samples which appear to have been affected by retrogressive metamorphism were were not analyzed. None-the-less, the area has been affected by high-grade metamorphism and care should be taken in interpreting the chemical data. Most chemical migration during metamorphism, however, with the exception of fluid migration, is generally on a mm to cm scale and thus should not significantly affect bulk samples (Mason and Moore, 1982). The migration of atoms or ions through solids is generally agreed to be insignificant under regional metamorphic conditions, since measurement of diffusion rates indicates that such a migration of ions in silicates is extremely slow, even on the scale of metamorphic events (Mason and Moore, 1982). Large scale redistribution of elements (even REE) is only significant when metamorphic or metasomatic fluids are generated or introduced (Henderson, 1984). Luckily, the amphibolite grade gneisses of the Wet Mtns appear not to have been affected by such processes. The granulites, on the other hand, given the effects of CO_2 flushing and anatexis, have seen chemical redistribution. It has been shown, however, that even under these conditions elements such as Zr, Hf, Ta, Ba, Sr, and the REE (particularly the heavy REE) are generally immobile (Condie et. al., 1982, Muecke, 1979).

On a chondrite normalized rare earth element (REE) diagram (Fig. 10), the amphibolites show depletions in the heavy REE relative to chondrites, with light REEs having values of about 30 times chondrites and heavy REEs about 10 times chondrites. Although the patterns are LREE enriched, overall the patterns are relatively flat and show no indication of decoupling of the LREE from the HREE, with the exception of the altered samples (not included in diagram). The amphibolites also display a minor negative Eu anomaly.

On a FeO-T vs MgO diagram (Fig. 11, Jolly, 1980) the amphibolites plot
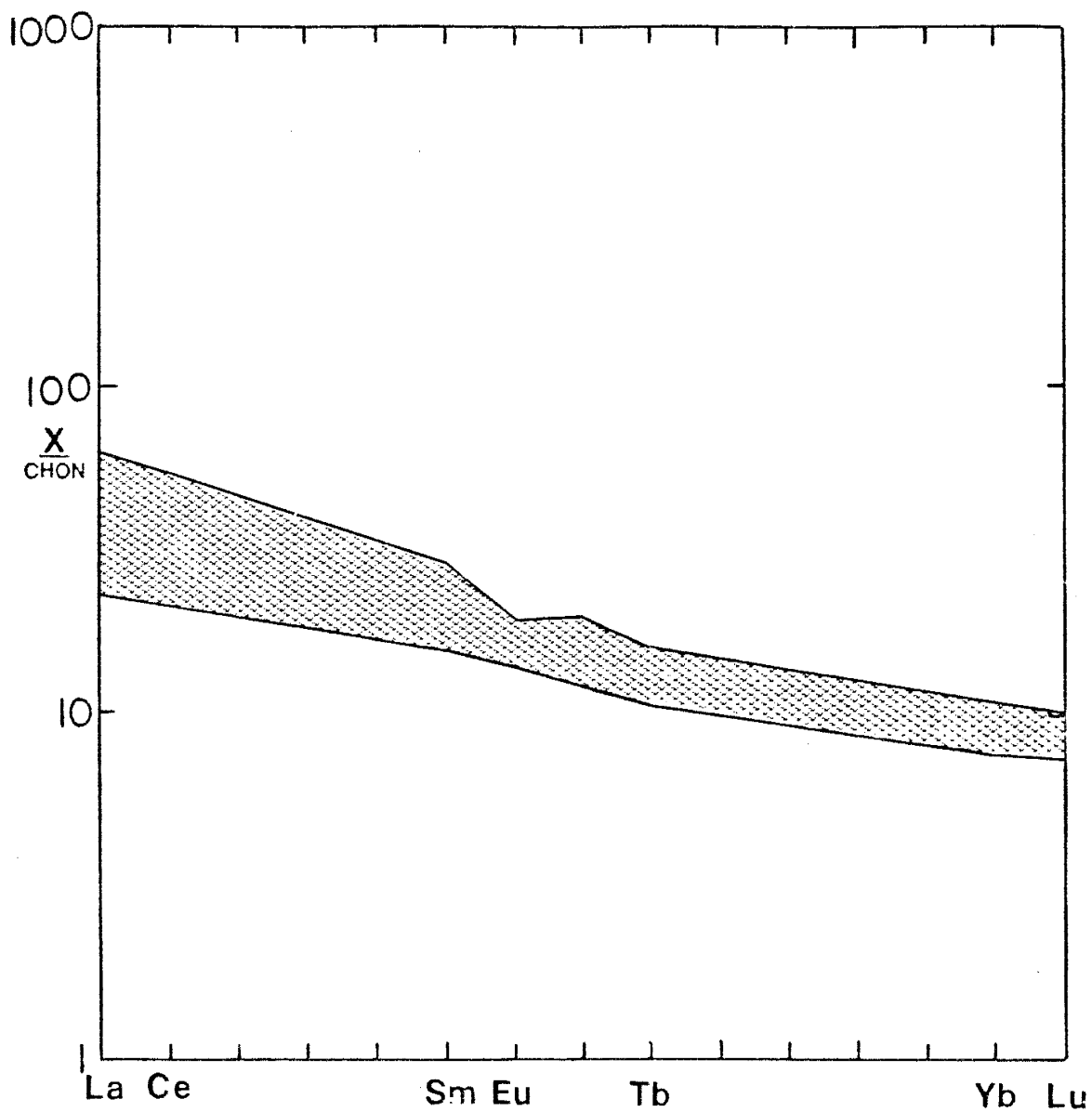
Figure 10: Chondrite normalized REE plot showing range (10 samples) for Wet Mountains amphibolites. Samples which appear to be altered and ultramafics are not plotted.

primarily in the calc-alkaline field, although there may be a slight Fe fractionation trend. The FeO-T increases from 6% to about 13% with the three samples plotting at about 6% being from the BDH amphibolite complex. Overall, however, the amphibolites do not display an Fe-enrichment trend and are dominantly calc-alkaline.

The amphibolites can be derived by batch melting of a garnet lherzolite source. Starting with a Wright-Doherty least squares mixing approach (Wright and Doherty, 1970) it is possible to produce the amphibolites by 5% batch melting of a garnet lherzolite. With trace element modeling, 10% batch melting will produce a liquid with a similar trace element composition to the amphibolites. This trace element modeling is shown diagrammatically in Fig. 12, a Lu vs Sm plot where plotted are the amphibolites (solid circles), ultramafics (stars) and a line representing the chemical changes produced in the liquid with continued melting. Again, the three points with Sm values less than 1 ppm are from the BDH complex.

When the amphibolites are plotted on an isomolar, pseudo-liquidus phase diagram (after Elthon, 1983), they lie close to the 1 atm phase equilibrium join, suggesting they may have crystallized very close to the surface (Fig. 13), which would support their origin as shallow, hypabyssal intrusives.
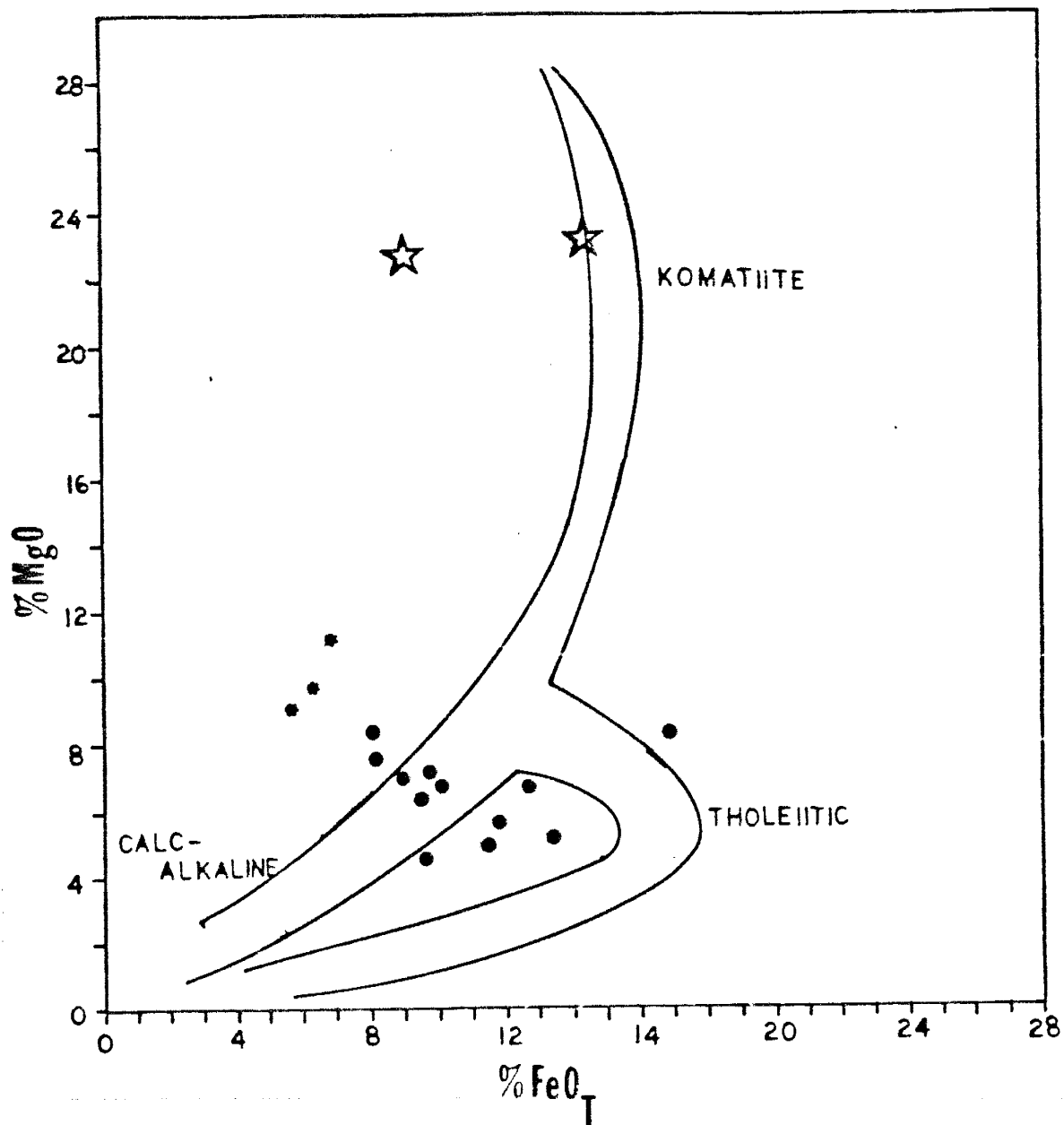
Figure 11: FeO-T vs MgO plot showing the calc-alkaline nature of the Wet Mountains amphibolites. Asterisks are BDH samples, stars are ultramafics, dots are amphibolites (after Jolly, 1980).
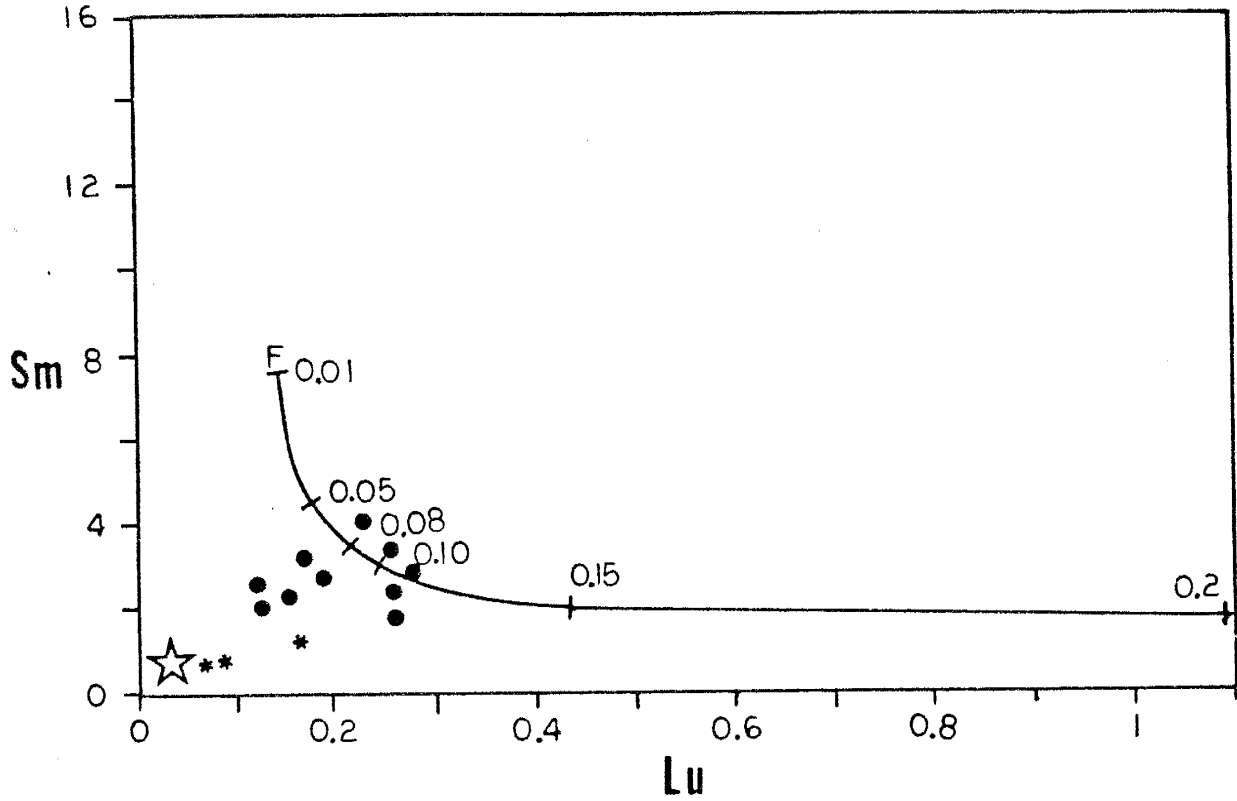
Figure 12: Lu vs Sm plot showing trace element modeling of the Wet Mountains amphibolites as liquids derived from batch melting a garnet lherzolite source. Solid line represents chemical composition of melt at various degrees of melting (F). Stars are ultramafics, dots are amphibolites, asterisks are BDH samples.
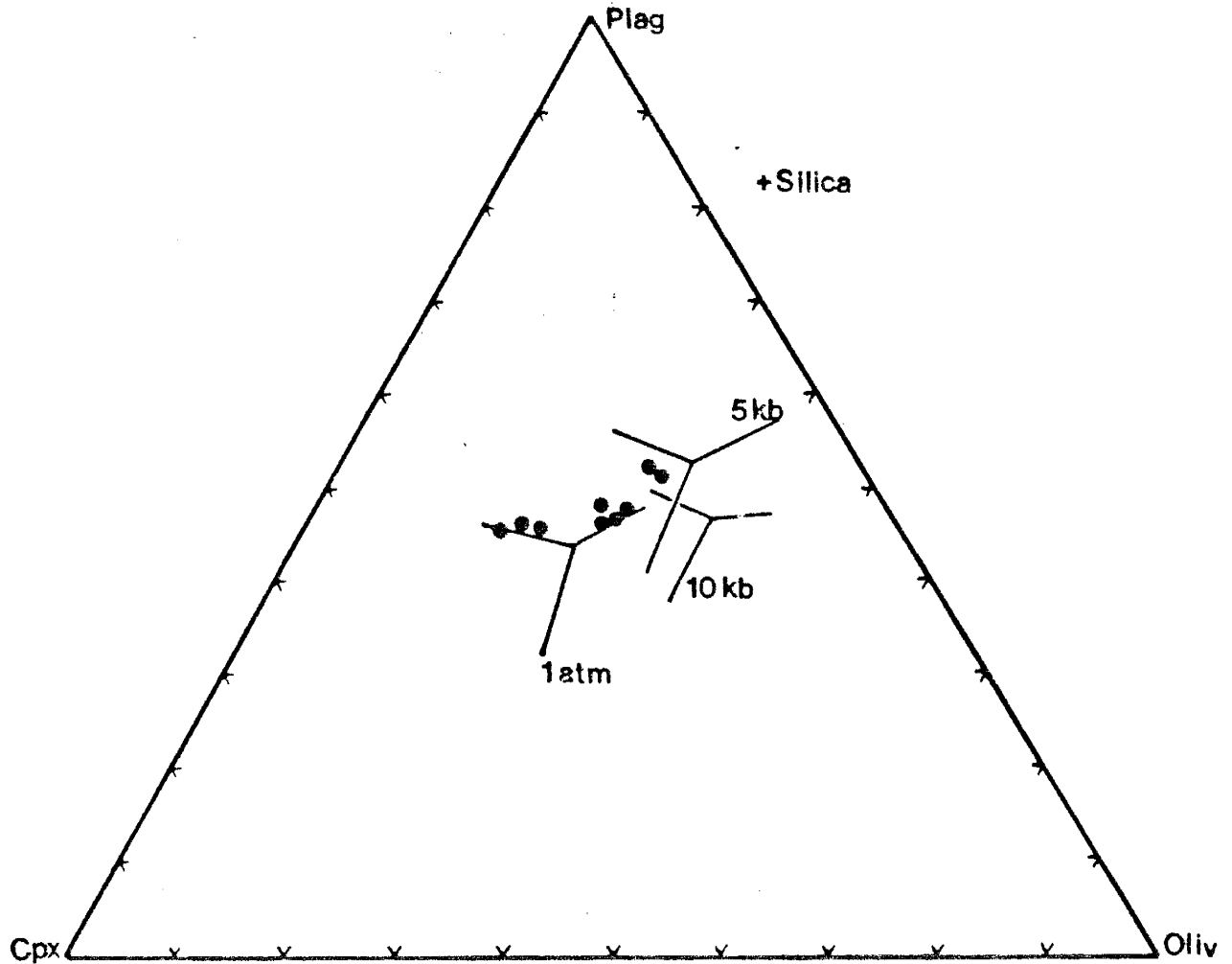
Figure 13: Wet Mountains amphibolites plotted on a pseudo-liquidus, ternary phase diagram projected from silica (after Elthon, 1983). Shown are phase equilibria for 1atm, and 5 and 10kbar pressures.

Tectonic Affinities

A tectonomagmatic discrimination of ancient volcanic rocks is best done by incorporating geologic, petrologic, mineralogic, and geochemical data since, as Pearce (1987) correctly points out, relying solely on one parameter can be dangerous. Various geochemical schemes have been proposed for classifying petrotectonic assemblages but the MORB normalized spidergram approach is probably the best known and the most useful. Analyses in a MORB normalized spidergram are presented in the form of a geochemical pattern normalized to the average tholeiitic Mid-Ocean Ridge Basalt (MORB) of Pearce (1983). Ordering in the diagram is such that the incompatibility of both mobile and immobile elements increases from the outside to the center of the pattern; large ion lithophile elements (LILE) on the left and high field strength elements (HFSE) on the right. MORB-normalized diagrams are helpful in that basaltic units erupted in various tectonic settings can be distinguished by the degree to which selective enrichment of trace elements occurs in those settings. Figures 14, 15, and 16 show typical ranges of values for basalts from within plate settings, continental and island arc settings with their associated immature back-arc basins, and immature island arc settings, superposed over the MORB-normalized pattern of the Wet Mountains amphibolites. Within plate settings show a relative enrichment in all the elements relative to MORB, producing a hump pattern due to enrichment through crustal contamination and selective enrichment related to incompatibility with respect to garnet lherzolite in the mantle. Island arc settings show relative depletions in Ta, Nb, Zr, Hf, and Ti due to a selective enrichment in LIL elements and REEs in subduction zones. Immature island arcs show larger relative depletions in these elements since they are less evolved. The Wet Mountains amphibolites display a subduction zone

signature closest to the pattern for immature island arcs.

The Zr vs TiO_2 diagram (Pharoah and Pearce, 1984; Fig. 17) distinguishes between arc, MORB, and within-plate sources for mafic volcanics. The Wet Mountains amphibolites fall dominantly in the arc field, with some overlap into the MORB field, and with three samples plotting at less than 1.1 ppm Zr (BDH samples). The Ta/Yb vs Th/Yb plot (Pearce, 1982; Fig. 18) distinguishes between oceanic and continental arc sources and also non-subduction and MORB sources. Although the Wet Mountains amphibolites scatter along the oceanic/island arc boundary, they plot outside the non-subduction related basalt field, suggesting they are subduction related basalts with affinities to both oceanic and continental arcs. The Th-Ta-Hf/3 ternary diagram of Wood (1979; Fig. 19) distinguishes subduction related, MORB, and within-plate sources for basaltic rocks. On the Th-Ta-Hf/3 diagram, the Wet Mountains samples show affinities to subduction zone related basalts with calc-alkaline chemistry. The arc signature is seen consistently on most of the discrimination diagrams which are applicable and implies a chemical similarity between the amphibolites sampled in the Wet Mountains and subduction related basalts emplaced in evolved arc settings.

A subduction related setting is consistent with the calc-alkaline nature of the amphibolites, the nature of the metasediments with which they are intercalated, and the nature of the volcanic rocks in the surrounding Proterozoic terranes.
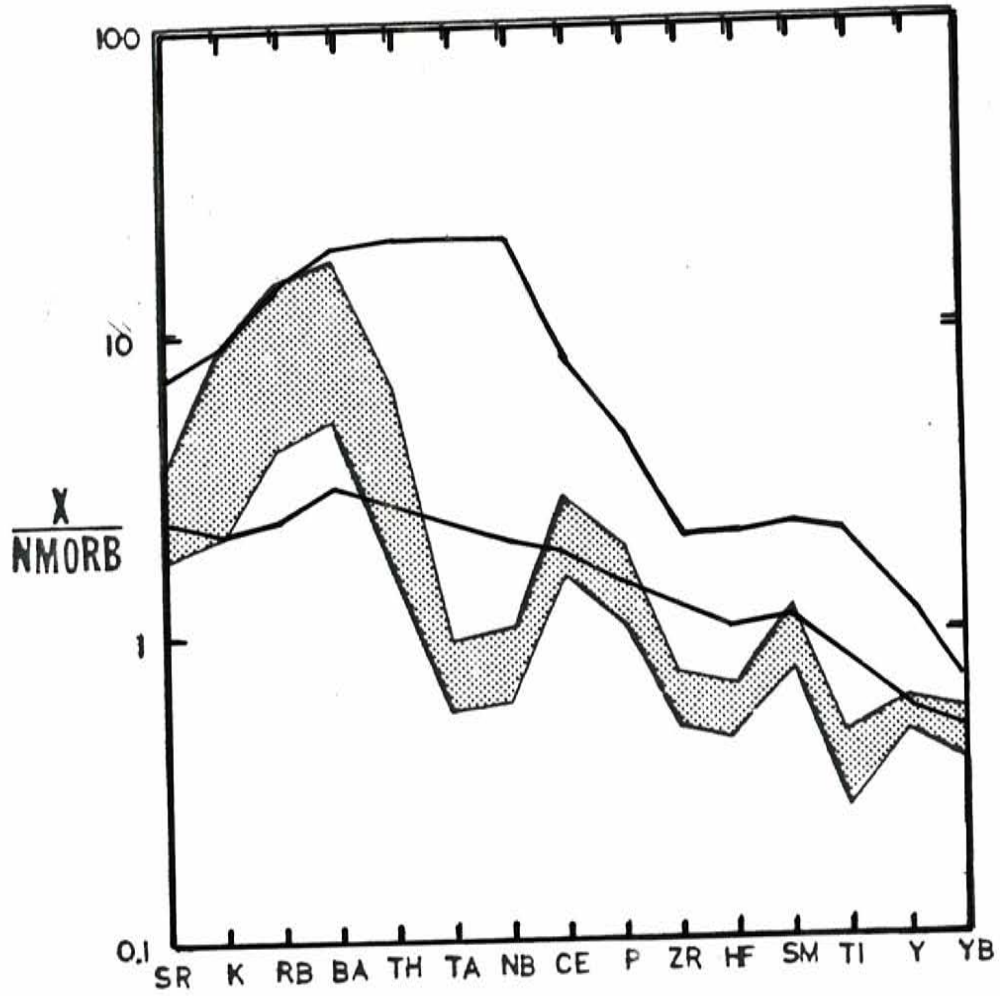
Figure 14: MORB normalized, incompatible element distribution in amphibolites from the Wet Mountains (stippled field, range of 8 samples) and that common in within-plate basalts (overlay), after Pearce (1983).
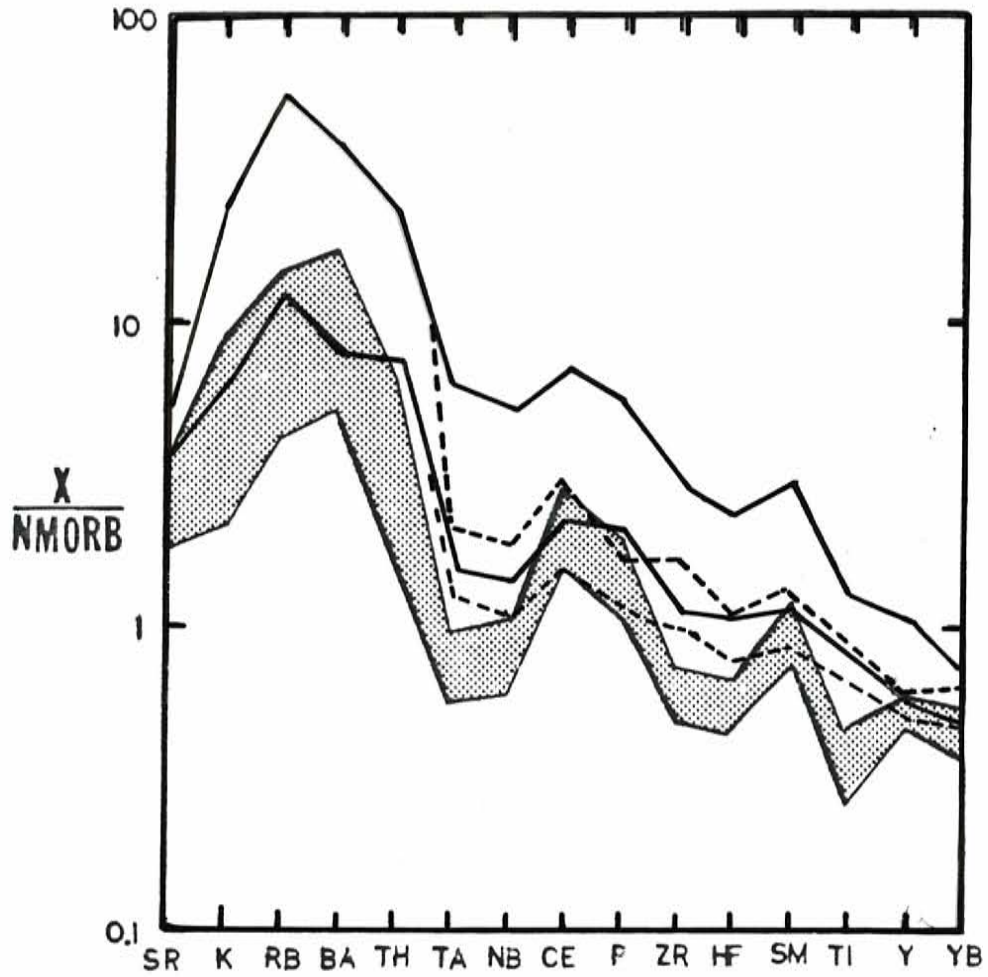
Figure 15: MORB normalized spidergram of Wet Mountains amphibolites compared to basalts from continental margin arcs, and their associated back-arc basins (solid line envelope), and basalts from evolved island arcs, and their associated back-arc basins (dashed line envelope).
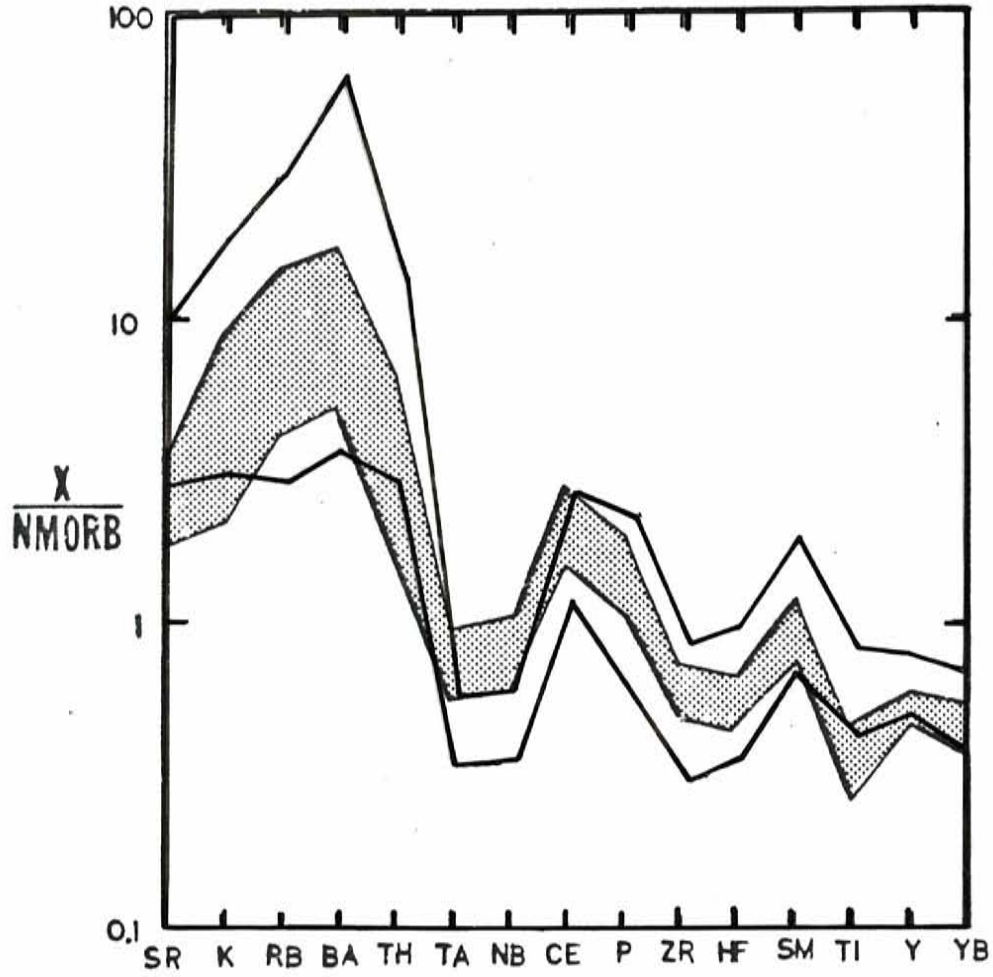
Figure 16: MORB normalized spidergram of Wet Mountains amphibolites compared to basalts from immature island arc settings.
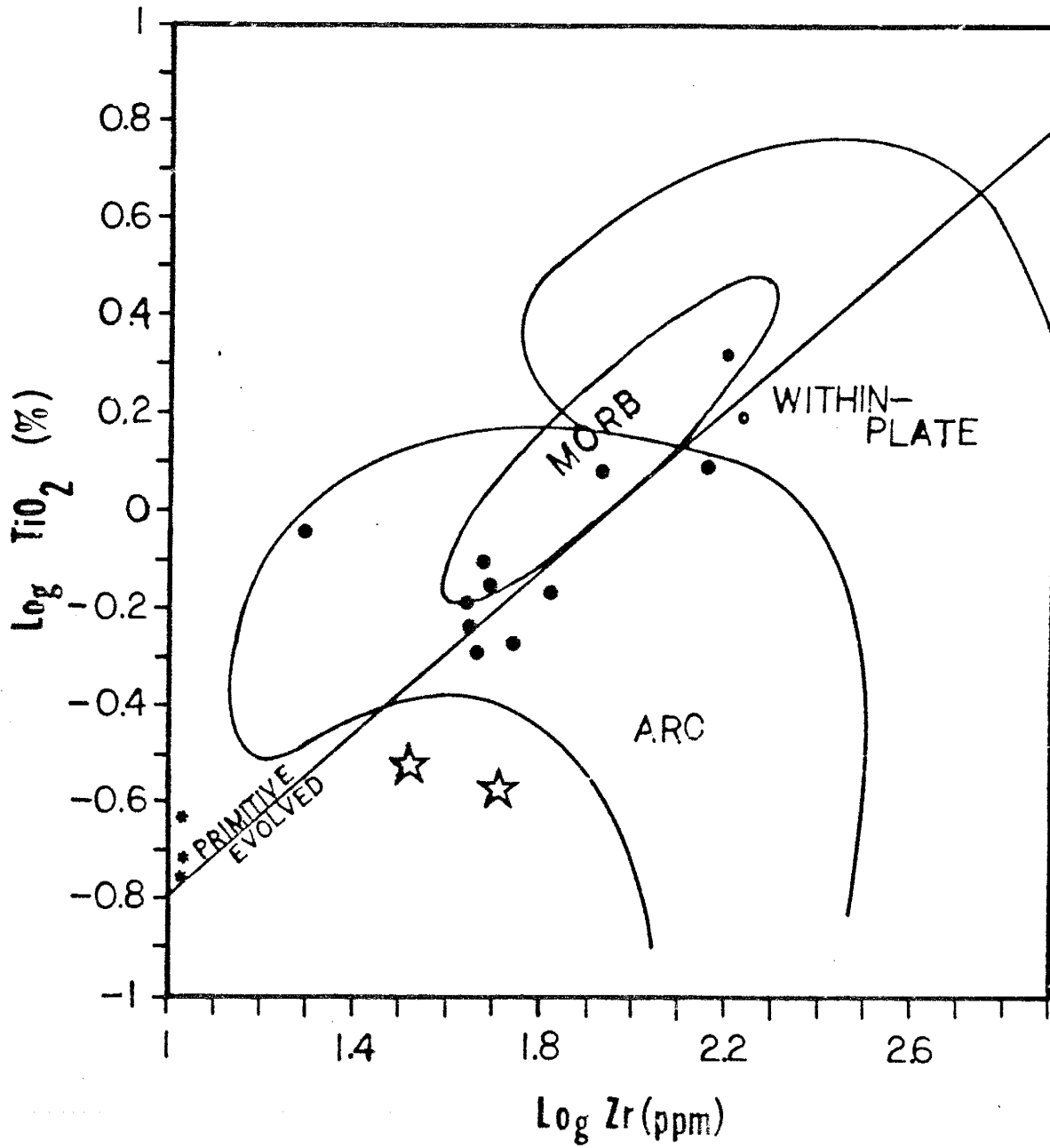
Figure 17: Zr vs TiO$_2$ chemical discrimination diagram (after Pharaoh and Pearce, 1984) for basalts. Solid circles are amphibolites, open circles are altered samples, asterisks are BDH samples and stars are websterites. Samples plotting below the primitive-evolved boundary have undergone magnetite and ilmenite fractionation.
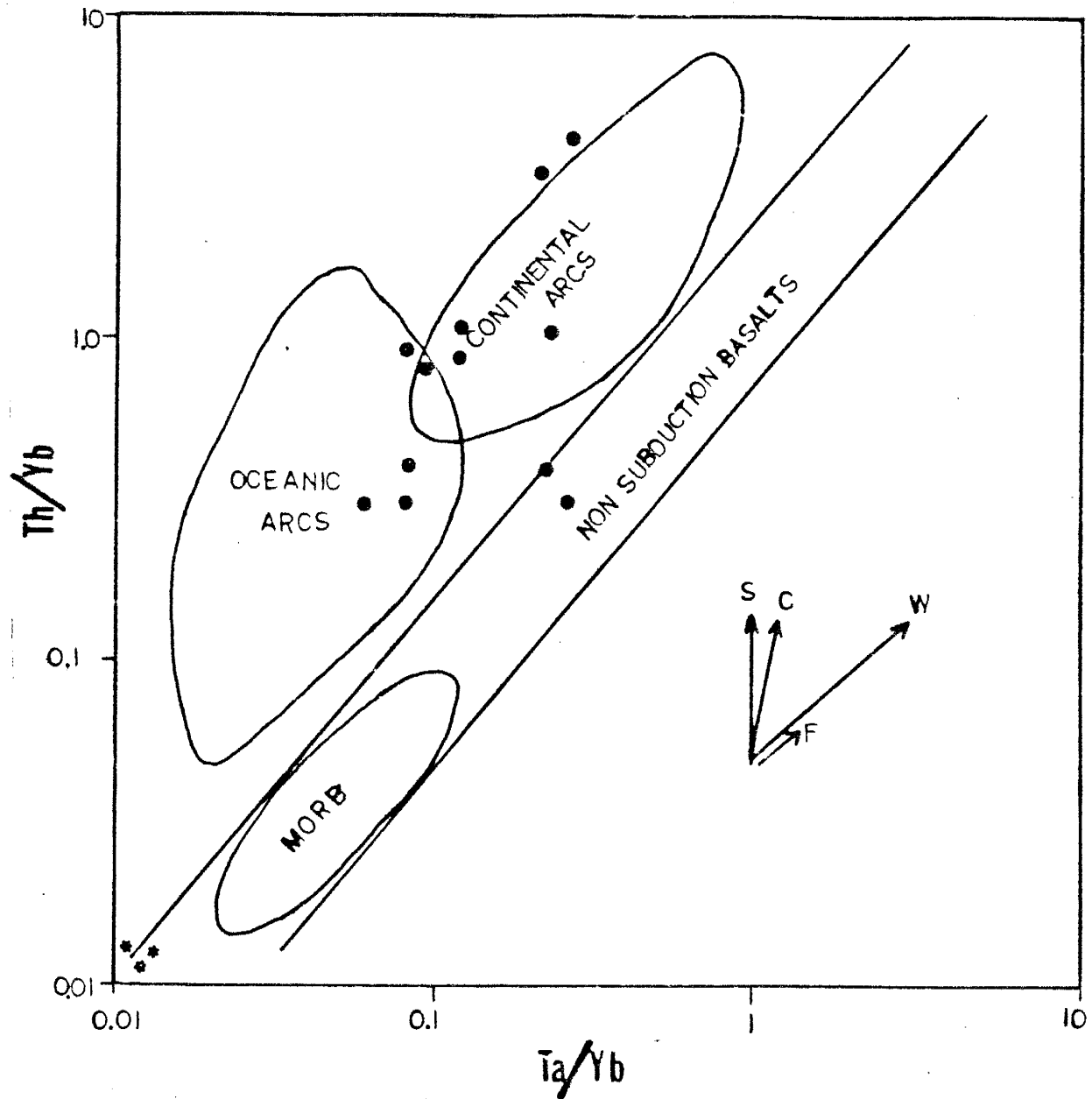
Figure 18: Ta/Yb vs Th/Yb chemical discrimination diagram (after Pearce, 1983) for basalts. Arrows show how certain magmatic processes affect magma chemistry. S is subduction zone enrichment, C is crustal contamination, W is within-plate enrichment, F is fractional crystallization. Dots are amphibolites, asterisks are BDH samples.
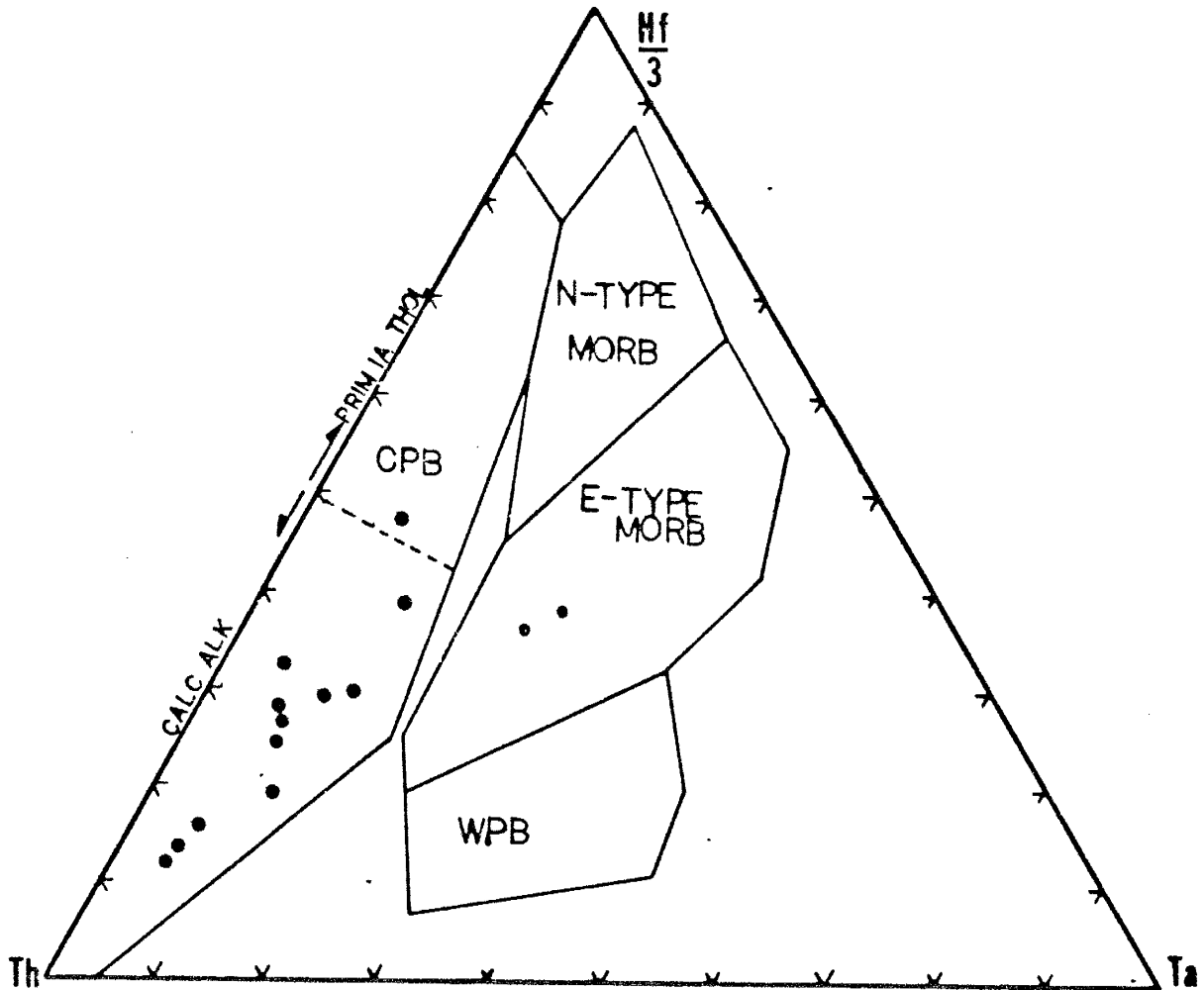
Figure 19: Th-Ta-Hf/3 chemical discrimination diagram (after Wood and Joron, 1979) for basalts. WPB is field of within-plate basalts (including continental rifts), CPB are basalts from collisional plate boundaries (subduction zone related), and CPB is divided in calc-alkaline and primitive island arc tholeiite field. Dots are amphibolites, open circles are altered samples.

Sample	LHS-36	LWC-31	LSG-11	LMT-50	LHS-2	LSC-2
SiO_2	47.42	49.79	48.47	39.14	39.63	43.02
TiO_2	0.64	0.67	0.30	2.05	1.48	0.51
Al_2O_3	18.50	15.60	7.26	21.77	14.64	9.25
Fe_2O_3-T	9.02	10.78	10.15	14.05	18.81	16.24
MgO	7.64	6.95	22.52	6.71	8.23	23.8
CaO	11.03	11.43	8.27	14.00	11.47	5.07
Na_2O	2.88	2.76	0.64	1.39	2.15	0.52
K_2O	1.33	0.94	0.19	0.30	1.43	0.11
MnO	0.15	0.17	0.18	0.11	0.20	0.20
P_2O_5	0.13	0.23	0.17	0.47	0.50	0.28
LOI	1.10	0.46	0.65	0.34	1.08	1.21
Σ	99.83	99.79	98.81	100.33	99.62	99.48
Rb	28.9	10.8	BD	8.3	55.5	3.9
Ba	203	401	65	44	121	41
Cs	0.2	BD	BD	BD	BD	0.5
Sr	408.9	565.5	52.2	809.2	361.2	122.7
Pb	17.2	12.6	7.4	8.9	8.9	13.3
Th	0.5	1.3	0.7	15.7	0.3	BD
U	0.2	0.7	0.6	4.2	0.4	0.2
Sc	33.1	25.5	25.1	32.9	29.2	11.9
V	208.3	225.8	131.0	289.6	837.4	99.2
Cr	330.5	288.0	1943.5	187.0	33.8	1079.5
Co	42.8	30.2	82.7	43.6	56.9	102.1
Ni	123.0	79.5	830.0	92.5	17.0	865.0
Y	15.5	17.7	10.1	34.6	14.4	13.1
Zr	44.5	65.8	33.0	157.4	20.0	46.3
Nb	3.8	7.3	3.8	12.7	5.5	5.3
Hf	1.6	1.6	1.1	6.8	0.6	0.9
Ta	0.10	0.17	0.07	1.00	BD	0.13
La	6.2	12.0	5.6	35.7	4.5	7.5
Ce	15.2	27.2	15.5	85.9	12.1	20.1
Sm	2.45	4.01	1.95	8.45	2.48	2.26
Eu	0.87	0.99	0.54	2.58	0.76	0.65
Tb	0.53	0.66	0.31	1.15	0.41	0.29
Yb	1.54	1.31	0.84	3.79	0.96	0.95
Lu	0.26	0.26	0.12	0.64	0.12	0.15

Table I: Geochemistry of amphibolites

[BD = below detection, Fe_2O_3 as total Fe, major elements in wt. % oxides, trace elements in ppm, LOI=loss on ignition, Σ=sum of oxides.]

Sample	LWC-26	LSG-10	LMT-19	LOC-10	LHS-31	LBM-2
SiO_2	49.35	47.32	47.96	51.36	55.70	48.56
TiO_2	0.70	0.77	0.61	1.21	1.57	0.53
Al_2O_3	16.04	16.22	17.60	14.62	14.06	13.44
Fe_2O_3-T	10.94	12.88	8.89	14.89	10.45	9.75
MgO	6.86	5.27	8.30	5.16	4.79	7.06
CaO	12.10	13.67	12.53	8.15	7.18	17.58
Na_2O	2.10	3.04	2.61	3.15	3.55	1.65
K_2O	0.65	0.18	0.68	0.64	1.35	0.72
MnO	0.19	0.17	0.13	0.39	0.15	0.26
P_2O_5	0.16	0.12	0.16	0.20	0.47	0.20
LOI	0.25	0.61	0.67	0.26	0.62	0.28
Σ	99.32	100.26	100.14	100.03	99.89	100.03
Rb	10.6	5.2	6.5	6.7	64.6	30.0
Ba	148	163	205	83	316	237
Cs	0.1	BD	BD	BD	1.0	0.5
Sr	315.2	329.8	518.8	134.9	233.0	363.0
Pb	13.2	20.1	13.2	21.3	16.5	11.9
Th	0.5	BD	0.5	0.7	12.3	1.3
U	0.2	0.2	0.6	0.5	2.9	0.9
Sc	36.4	35.3	39.5	27.7	29.3	28.8
V	266.7	295.5	202.7	297.2	232.0	186.6
Cr	126.7	113.7	141.0	589.5	99.0	793.5
Co	38.0	38.3	37.1	31.5	30.7	42.0
Ni	45.0	70.5	81.0	193.0	43.0	205.0
Y	18.1	20.6	14.8	29.7	46.1	17.8
Zr	48.8	48.0	44.2	84.8	167.9	55.2
Nb	5.7	4.6	7.0	12.0	14.3	5.5
Hf	1.2	1.3	1.5	2.3	6.2	1.7
Ta	0.14	0.11	0.33	0.57	0.84	0.15
La	7.4	3.5	9.4	9.5	34.8	9.0
Ce	18.2	7.7	23.3	23.3	85.3	21.5
Sm	2.80	1.72	3.28	3.83	8.70	2.76
Eu	0.96	0.53	1.02	1.11	1.54	0.92
Tb	0.51	0.29	0.39	0.69	1.42	0.43
Yb	1.85	1.65	1.53	2.23	4.02	1.59
Lu	0.27	0.26	0.26	0.38	0.63	0.19

Table II: Geochemistry of amphibolites, con't.

Bull Domingo Hills Amphibolite Complex

Form and Occurrence

Other than a label on the geologic map of the Pueblo 1° × 2° quadrangle (Scott et. al., 1978) identifying the Bull Domingo Hills (BDH) area as a metagabbro of Precambrian age X, no study has been undertaken of this amphibolite complex. The BDH are a series of three north-south trending ridges four km north of Silvercliff. The complex is three km long, north-south,and two km wide, east-west. The BDH complex is almost exclusively composed of amphibolite which displays a pervasive layering throughout. Certain chemical trends, such as the depleted, convex upward REE patterns, are suggestive of an origin for the complex as a cumulate of a fractional crystallization (FXL) event, thus this layering may represent original layering in a layered gabbro complex. Layers have been observed to range from as thin as 3cm in width to as thick as 10cm and seem to preserve fairly constant thicknesses over distances of several meters, although it's difficult to evaluate this character over longer distances due to the lack of continuous exposure.

The layering commonly strikes north to north-northeast and dips very steeply, about 90°. The layering is defined by changes in modal mineralogy, from hornblende to plagioclase rich modes, suggestive of rhythmic layering. BDH samples tend to be medium to coarse grained, with grain diameters on the order of 2mm to 2cm, and equigranular. Fig. 20 is an example of layering in hand specimen LWC-20. In some samples, convex trains of mafic minerals converge at the base of the layers, resembling cross-bedding. Cross-bedding is commonly observed in layered igneous complexes, such as in the Skaergaard, and are generally attributed

to flowage in a partially crystallized magma. Polished sections made of LWC-20 and examined under reflected light reveal that zones of magnetite often occur at the base of individual, mafic rich layers.

It has been suggested that the layering at the BDH complex is a tectonic fabric formed through shearing. It seems, however, that shearing would result in a reduction in grain size, particularly along interlayer boundaries, while the BDH samples, by contrast, tend to be very coarse grained. It may be argued that subsequent recrystallization may increase the grain size following shearing, but this would require very specific thermal conditions which would increase the grain size significantly while preserving fine shearing textures. Shearing would also tend to elongate grains along the shear plane, particularly prismatic crystals such as hornblende. In thin-section, however, hornblendes tend to occur as stuby, hexagonal crystals with elliptical grain boundaries (Fig. 21) and triple junctions of 120°, all features commonly seen in adcumulates (Wager, 1963). The crystal habits in the hornblendes are suggestive of crystal habits seen in pyroxenes, implying that they may be pseudomorphs after clinopyroxene. Additionally, the tendency for rocks at the western margin of the study area to be at lower metamorphic grades tends to suggest that the severe degrees of recrystallization required in a shearing model would be less likely, since such severe recrystallization is not seen in the high-grade gneisses.

Basically, although a tectonic origin for the BDH layering is possible, it would require very specific thermal and structural conditions which would produce a tectonic layering while preserving the coarse grain size or recrystallize the terrane while preserving fine shearing structures. A model in which the BDH complex is composed of very coarse grained gabbroic protoliths which tend to resist extensive deformation explains the observed textures more simply. The resistance of the

Figure 20: Hand specimen of LWC-20 and LWC-6 showing different scales of layering. Layers defined by changes in hornblende and plagioclase content.
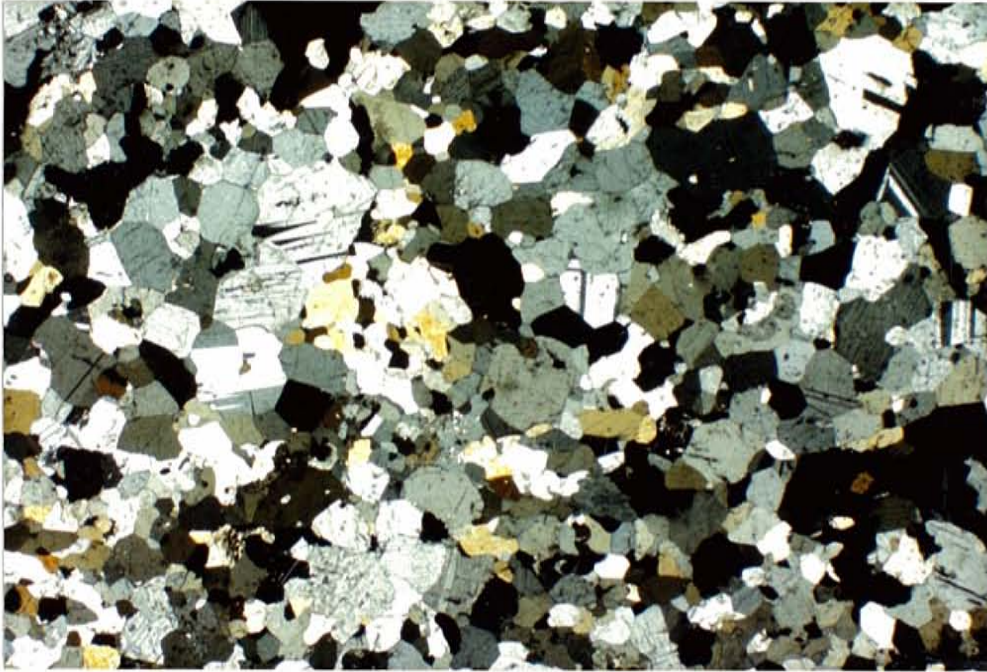
Figure 21: Photomicrograph of LWC-20 showing hexagonal habit of hornblende and plagioclase. Scale 1cm=0.5mm, X-polz. light.

coarse, gabbroic protoliths to deformation would allow a preservation of layering and cross-bedding textures in the original rock metamorphosing them in place, perhaps with a slight accentuation and warping of layers due to tectonic effects. A tectonic origin for the layering, however, cannot be uneqivocally discounted.

Petrography

Thin sections display what appears to be a polymineralic texture of plagioclase and hornblende where sub-ophitic textures are apparent. The rocks are dominantly plagioclase (65%) and hornblende (35%) rich although more hornblende may be present depending on the mineralogy of individual layers. *An* contents average 60 and magnetite and other phases are minor constituents. As discussed, reflected light studies on polished sections show that iron oxides commonly accumulate at the base of mafic-rich layers. Additionally, magnetite and sphene are occasionally observed as interstitial grains at plagioclase and/or hornblende triple junctions. Grain boundaries tend to be elliptical and 120° triple junctions are common. Hornblendes tend to be hexagonal, an uncommon habit for hornblende which may suggest that hornblende has pseudomorphed after a hexagonal crystal such as clinopyroxene. The textures observed in thin-section and polished-section are textures common to cumulates, particularly adcumulates.

Geochemistry

Twenty samples from the complex were collected but only three were analyzed chemically, one from each ridge,and these data are shown in Table III. In comparison to amphibolites from the rest of the study area the BDH samples show consistently lower values of TiO_2, Zr, Fe_2O_3, P_2O_5, Nb, and all the rare earth

elements (REE). On a REE diagram (Fig. 22) the BDH samples have highly depleted, convex upward REE patterns relative to the other amphibolites in the area, below 10x chondrites. These patterns are similar to patterns observed in mafic cumulates and ophiolites (Furnes et. al., 1985), suggesting that these rocks may represent cumulates from fractional crystallization.

Using a Wright-Doherty least squares mixing approach with olivine, plagioclase, titano-magnetite, and clinopyroxene as the crystallizing phases it is possible to produce a cumulate similar to the BDH samples by a simple closed system fractional crystallization (FXL) model, crystallizing from the Wet Mountain's amphibolites to the quartz diorites sampled from the Wet Mountains (60% FXL with 15% olivine, 49% plagioclase, 9% magnetite, and 27% clinopyroxene with squared residuals of 0.24). The low squared residuals suggests that mixing of the two end-members fits a line very closely. Trace element modeling using distribution coefficient (K_d) data (K_ds used in modeling are given in appendix) proved successful in modeling the BDH samples as cumulates of a closed system fractional crystallization trend and a Rayleigh fractionation approach. Interestingly, modeling suggests that changes in modal mineralogy and degree of fractionation are less effective in changing a cumulate chemistry than changing the composition of the parental magma. Sample LHS-36 proved an effective and reasonable choice for a primitive, parental magma with its high Mg# (65.6), low Ti content (TiO$_2$ = 0.64%), and high Cr (330ppm).

A crystallizing mode of 41% plagioclase, 44% clinopyroxene, 8% olivine, and 7% magnetite produces a reasonable trend, given the chemistry of the BDH amphibolites and possible candidates for daughter liquids, while staying inside theoretical constraints. As can be seen on V-Y (Fig. 24), Ce-Zr (Fig. 25), and Yb-La (Fig. 26) diagrams, applying a Rayleigh, closed system, fractional crystallization model to
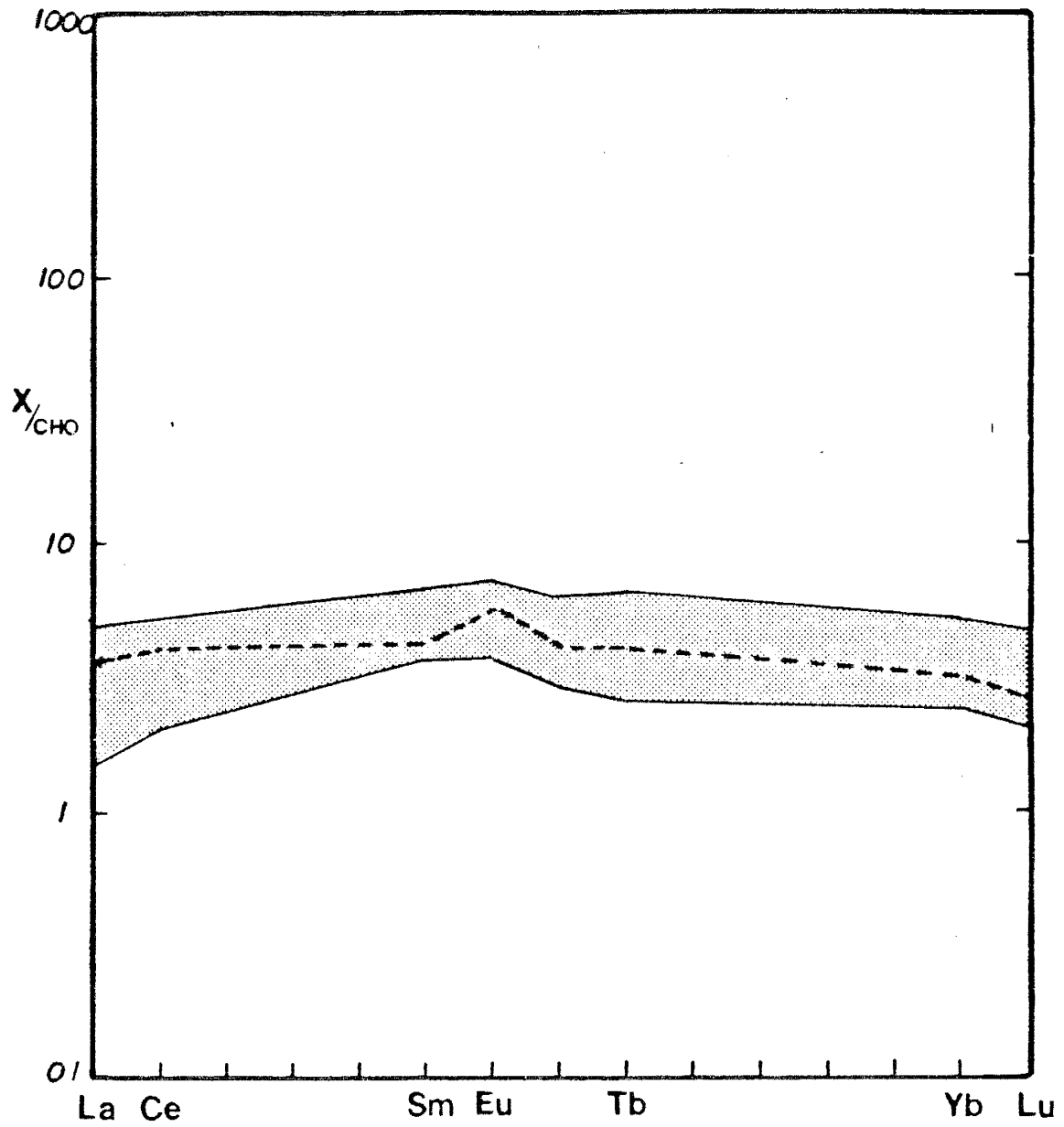
Figure 22: Chondrite normalized REE distribution of BDH samples (stippled field, range of 3 samples) and predicted value of cumulate given 50% closed system FXL (dashed line).

the samples of amphibolite from the Wet Mountains can produce a trace element chemistry in the cumulates very similar to that of the BDH samples by 50% FXL. The similarity between the model cumulate chemistry and that of the BDH samples is also seen in comparing the chondrite-normalized REE patterns (Fig. 22) or the MORB-normalized patterns (Fig. 23) of the actual samples and the model. Additionally, the liquid produced in the model bears a chemical similarity to the quartz diorites exposed in the study area, the chemical compositions of which can be seen in Table IV. Comparing the model liquid compositions to actual quartz diorite compositions, as in trace element variation diagrams such as Figs. 24, 25, or 26, or on a chondrite-normalized REE pattern (Fig. 27), the relative patterns are similar.

Samples LWC-28 and LHS-16, although bearing a major element similarity to the other quartz diorites, show dissimilarities in their trace element contents. These two samples may represent products of other magmatic mechanisms, such as open system fractional crystallization, but this has not been evaluated extensively.

Attempts to model the BDH samples as residues of partial melting are generally unsuccessful. As with a fractionation model, a partial melting model requires a viable parental source with specific trace element contents to produce a residue with a chemistry similar to that seen in the BDH samples. No such source with an acceptable mineralogy was identified in the area. The modeling does suggest, however, that a two pyroxene granulite as a parent would result in the closest possible model, but the residue of such melting would most likely still be of granulite facies mineralogy, which the BDH complex is not. Also, since migmatism tends to be less developed along the western margin of the study area, there is less probability of the large-scale partial melting required to produce such a residue. In conclusion, a fractionation model can explain the geochemical, petrographic, and
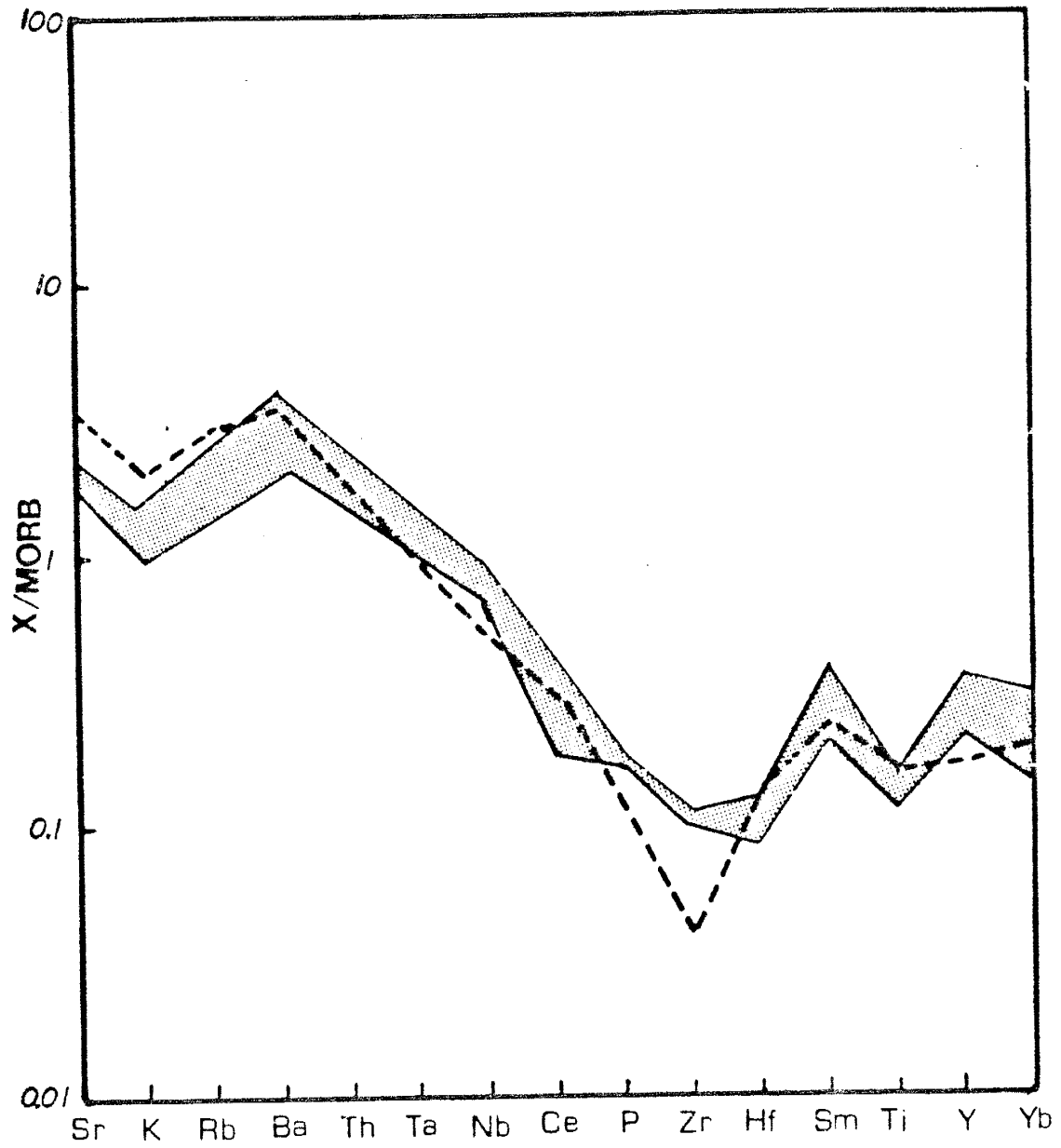
Figure 23: MORB normalized spidergram of BDH samples (stippled field, range of 3 samples) and predicted value of a modeled cumulate given 50% closed system FXL (dashed line).
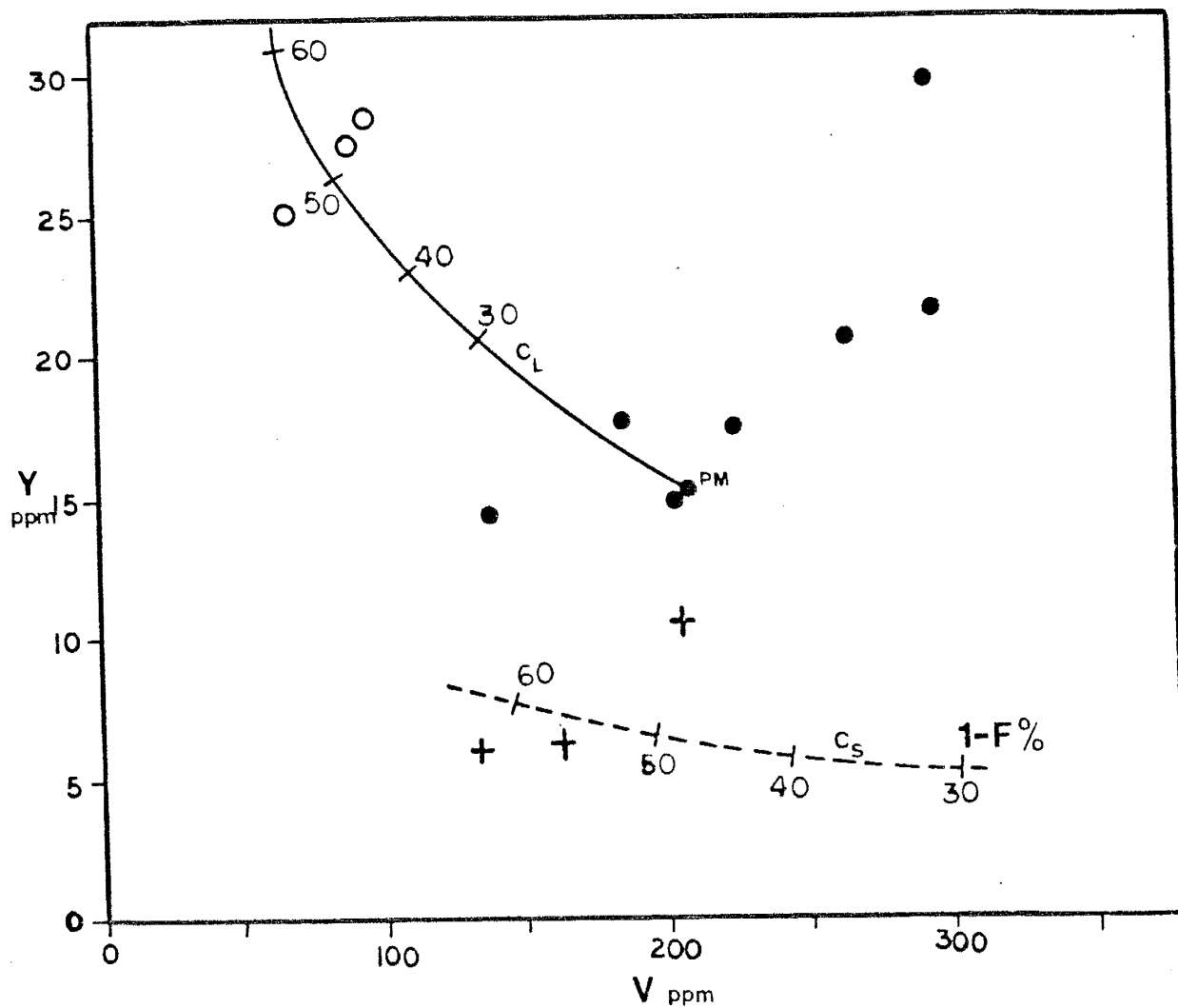
Figure 24: V vs Y diagram showing the BDH samples (crosses), amphibolites (solid circles), and quartz diorites (open circles). Solid line shows evolution of daughter liquid at various amounts of crystallization (1-F) and dashed line that of the cumulate (C_S). PM is the parental magma. Crystallizing phases are 41% plagioclase, 44% clinopyroxene, 8% olivine, and 7% magnetite.
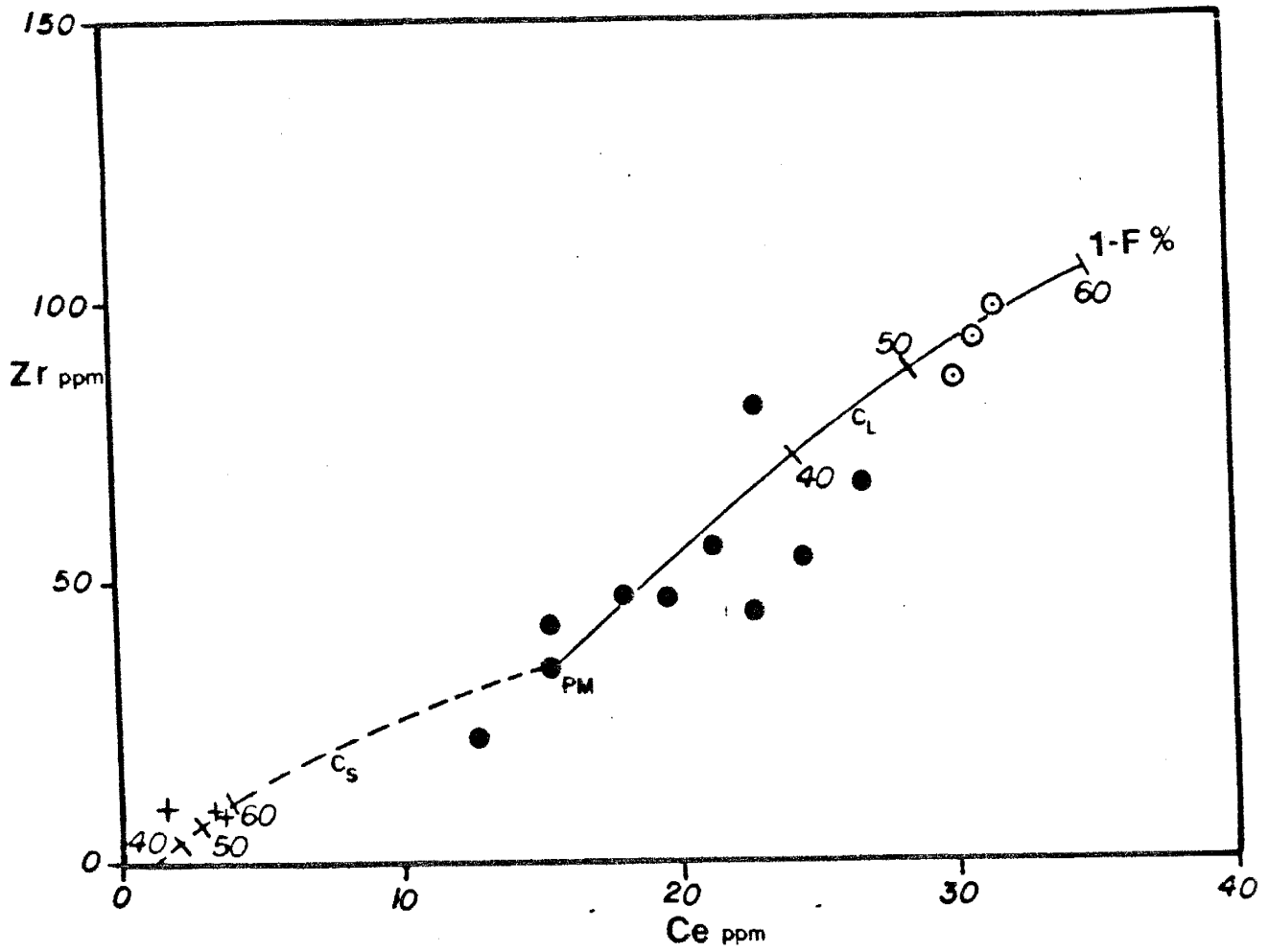
Figure 25: Closed system FXL trend on a Ce vs Zr plot. Symbols as in Fig. 24.
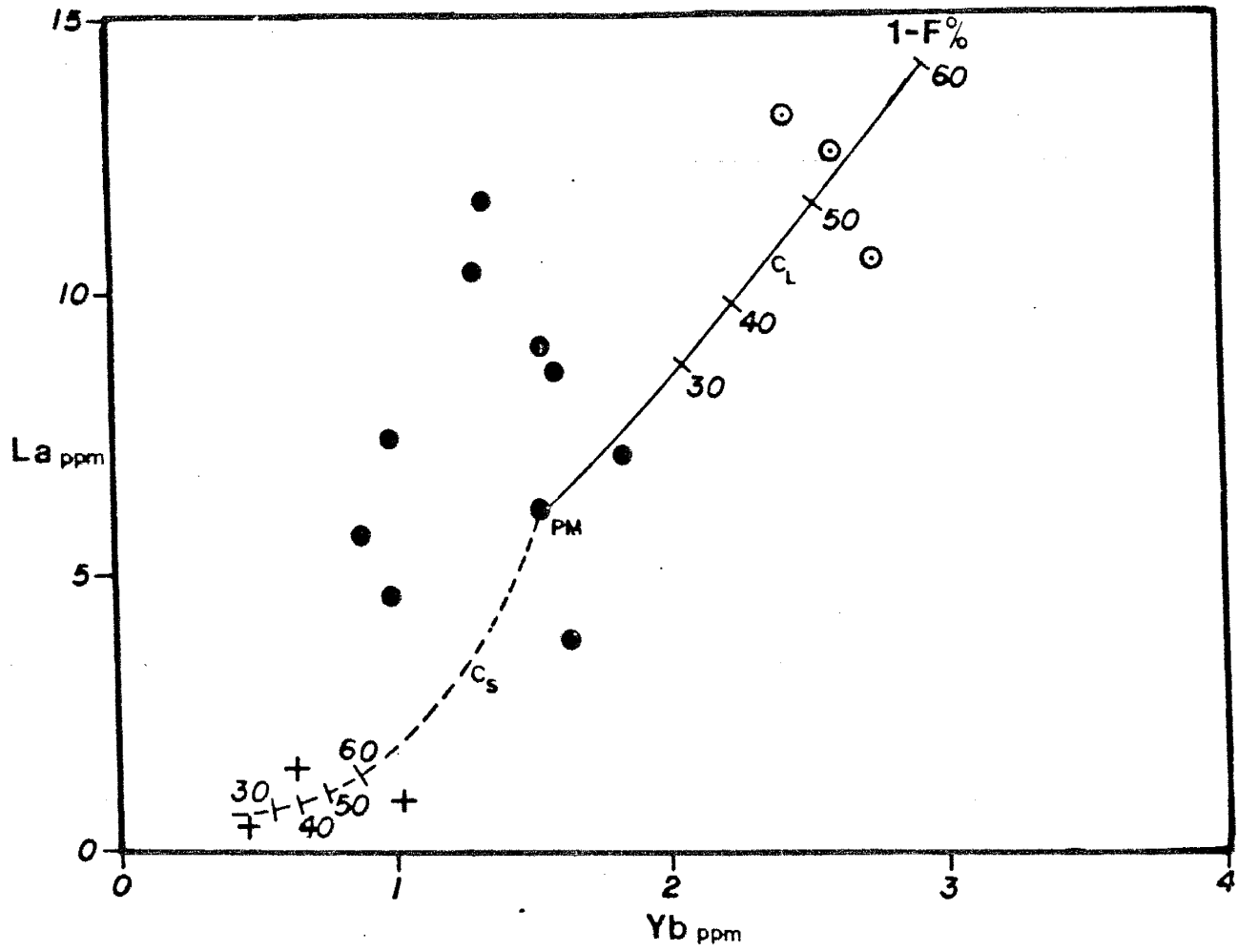
Figure 26: Closed system FXL trend on a Yb vs La plot. Symbols as in Fig. 24.
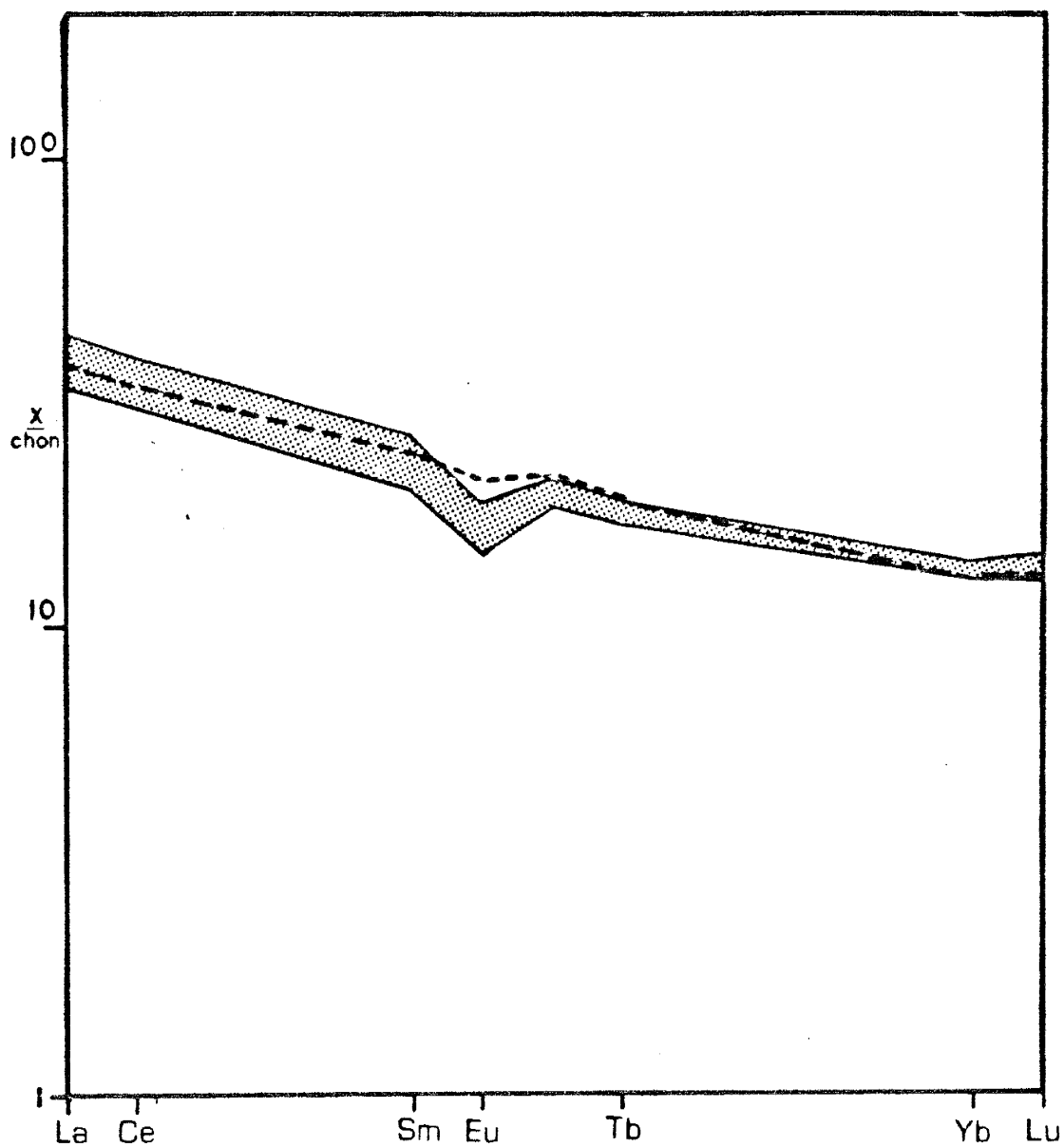
Figure 27: Chondrite normalized REE distribution of quartz diorites (stippled pattern, range of 3 samples) and predicted model value (dashed line) of 50% closed system FXL liquid.

textural patterns found in the BDH samples and the quartz diorites by fractionating rock types readily found in the area without calling upon exotic or specialized mechanisms.

Sample	LWC-13	LWC-21	LWC-33
SiO_2	48.12	47.50	46.81
TiO_2	0.23	0.17	0.18
Al_2O_3	13.40	18.11	18.93
Fe_2O_3-T	7.58	6.34	6.91
MgO	10.97	9.05	9.67
CaO	17.63	17.63	15.54
Na_2O	0.82	0.82	1.06
K_2O	0.15	0.15	0.21
MnO	0.14	0.11	0.11
P_2O_5	0.02	0.02	0.02
LOI	0.51	0.61	0.87
Σ	99.56	100.50	100.31
Rb	3.8	6.4	2.6
Ba	51	43	79
Cs	BD	0.2	BD
Sr	213.4	276.7	248.2
Pb	7.9	9.2	11.6
Th	BD	BD	BD
U	1.3	BD	0.1
Sc	87.6	46.0	53.3
V	206.9	161.9	133.1
Cr	184.0	415.0	367.0
Co	47.7	29.8	48.1
Ni	81.0	45.07	88.5
Y	10.5	6.4	6.0
Zr	9.8	10.0	9.1
Nb	2.3	3.2	2.6
Hf	0.3	0.3	0.2
Ta	BD	BD	BD
La	0.9	0.5	1.6
Ce	3.3	1.8	3.8
Sm	1.24	0.67	0.79
Eu	0.51	0.26	0.43
Tb	0.28	0.12	0.31
Yb	1.04	0.48	0.64
Lu	0.16	0.07	0.08

Table III: Geochemistry of BDH amphibolites

Sample	LHS-38	LMT-55	LOC-14	LWC-28	LHS-16
SiO_2	59.44	62.29	61.03	56.20	65.22
TiO_2	0.43	0.39	0.36	0.68	0.79
Al_2O_3	17.71	15.24	17.22	19.71	15.24
Fe_2O_3	6.53	6.68	7.00	6.65	6.44
MgO	2.01	2.24	2.19	2.23	2.20
CaO	5.34	5.83	4.97	6.59	4.28
Na_2O	4.90	4.98	5.11	5.39	2.67
K_2O	2.23	2.09	1.99	2.07	2.09
MnO	0.09	0.11	0.10	0.07	0.12
P_2O_5	0.36	0.28	0.44	0.47	0.26
LOI	0.42	0.11	0.25	0.25	0.38
Σ	99.46	100.24	100.66	100.30	99.69
Rb	60.2	57.7	59.8	51.0	87.0
Ba	421	384	381	1164	896
Cs	1.1	3.0	1.5	0.3	3.3
Sr	501.7	480.8	460.0	782.4	321.6
Pb	11.9	15.2	13.4	9.7	23.1
Th	1.1	3.0	1.5	7.3	8.6
U	1.3	1.2	1.8	2.2	2.4
Sc	31.1	34.3	30.3	13.7	11.2
V	96	90	69	118	60
Cr	22.1	28.0	25.2	14.8	9.5
Co	24.5	21.8	23.1	14.5	7.8
Ni	10.1	6.2	7.6	7.0	2.0
Y	28.7	27.6	25.1	21.5	50.0
Zr	104	93	85	153	246
Nb	10.1	10.5	8.8	9.7	15.9
Hf	3.2	2.6	4.4	4.4	7.1
Ta	0.61	0.53	0.62	0.61	1.37
La	13.5	12.6	10.5	35.8	38.0
Ce	31.8	30.9	30.0	104.7	84.9
Sm	4.62	4.35	3.61	7.93	9.19
Eu	1.31	1.24	1.03	2.06	1.76
Tb	0.88	0.78	0.83	0.83	1.30
Yb	2.43	2.61	2.73	2.19	6.40
Lu	0.43	0.45	0.49	0.36	1.08

Table IV: Geochemistry of quartz diorites

Paragneisses

The metasediments of the Wet Mountains constitute the largest portion of the supracrustal units exposed, perhaps 60%, and consist of several rock types, the most abundant being biotite-quartz-plagioclase gneisses, about 90% of the paragneisses. Other metasediments include sillimanitic and garnetiferous gneisses and quartzites, all of which are strongly foliated parallel to the strike of the beds. All the paragneisses interfinger and intergrade with each other along strike and are found interlayered with both amphibolites and granites, suggesting the amphibolites are primarily sills and that the granites are dominantly syntectonic. Individual metasedimentary layers , as defined by bulk compositional similarity, average 500m in thickness, although individual units can be as thin as 2–3m or as thick as 1500m. Less common paragneissic varieties are rarely thicker than 5m.

The biotite-quartz-plagioclase gneisses tend to be light grayish in color but take on a more reddish hue with increasing garnet content and a more pinkish color where they have been partially digested by granitic material. Individual layers may grade from quartz rich zones to increasingly biotite rich and garnet bearing zones across the width of a layer, variations which perhaps represent original compositional differences in the sediments. Such units may represent original graded beds with biotite poor portions representing original sandy parts of the beds and biotite rich zones more shaley portions. Similar variations are observed in the high grade metasedimentary gneisses in northwestern Ontario (Van de Kamp and Beakhouse, 1979).

Individual layers can be traced for distances of several meters along strike without significant variation in band width, suggesting these layers may be functions of original compositional variations in the protolith, although no other more con-

clusive relict textures or structures are observable. No stratigraphic directions could be determined and the structural complexity of the area, along with the high metamorphic grade, make the determination of protoliths difficult. It is possible that these units may originally have been siliceous volcanic flows or falls, but the occurrence of beds unquestionably of sedimentary origin interbedded with the biotite-quartz-plagioclase gneisses and coexistent mineral phases such as biotite-garnet and biotite-sillimanite, which are uncommon in meta-felsic volcanics, argue more strongly for a sedimentary precursor. Most felsic volcanics do not have the amount of Fe, Mg, or Al needed to form the metamorphic assemblages observed in the paragneisses. Additionally, the geochemical trends these rocks display are similar to the chemical signatures displayed by sedimentary rocks, not igneous ones.

Petrography

Biotite-quartz-plagioclase gneisses show some minor mineralogic variations but overall are fairly consistent in their mineralogic make-up. Biotite is always present, may constitute anywhere from 5–35% of the rock and is commonly 1mm by 0.3mm in size, although some can be as large as 2mm. The biotites are almost always idioblastic and tend to impart a lepidoblastic texture to the rock. Quartz is always present, representing anywhere from 20–40% of the rock, tends to be xenoblastic, and commonly shows undulatory extinction. Feldspars consistently are a major mineral, both as plagioclase (usually oligoclase) and occasionally K-feldspar (usually as orthoclase). Plagioclase may constitute anywhere from 10–50% of the thin section and usually has an average diameter of 0.4mm, but can be as large as 2mm. It tends to be hypidioblastic, commonly has bent twin lamellae, and myrmikitic textures are common where oligoclase is in contact with orthoclase. K-feldspar tends to be xenoblastic, ranges anywhere from 0.6mm in diameter to 4mm, and tends to occur as an accessory mineral, although rarely it can constitute as much as 40% of the rock.

Garnet, generally almandine, is common but not always present, tends to be hypidioblastic, ranges in size from 0.2mm to as large as 2mm, and can constitute as much as 10% of the rock. When present, it imparts a poikiloblastic, "honeycomb" texture to the rock due to the coalescence of atoll garnets. This coalescence, in turn, imparts an idiomorphic aspect to the garnets in hand specimen.

Other paragneissic varieties are uncommon but are important in understanding the metasedimentary package. Sample LHS-30 is a quartz-microcline-biotite-sillimanite gneiss, 40%, 30%, 15%, and 15% of the rock respectively, with minor magnetite (2%, $\leq$ 0.4mm). The biotite (1mm by 0.4mm), quartz, and microcline

Sample	LMT-30	LWC-9	LMT-23	LHS-30	LMT-11	LMT-53
SiO_2	74.39	79.79	75.97	78.27	62.64	70.31
TiO_2	0.03	0.09	0.15	0.59	0.98	0.44
Al_2O_3	15.31	10.82	13.00	11.08	17.00	14.07
Fe_2O_3-T	1.30	0.85	1.65	3.93	6.27	4.19
MgO	0.35	1.75	0.56	1.12	1.96	1.50
CaO	4.05	1.05	1.73	0.22	4.20	1.73
Na_2O	4.78	4.70	4.22	0.98	4.98	3.58
K_2O	0.62	0.91	2.63	3.17	2.24	3.60
MnO	BD	BD	BD	0.01	0.06	0.15
P_2O_5	0.03	0.03	0.04	0.06	0.38	0.14
LOI	0.02	0.29	0.09	0.52	0.15	0.31
Σ	100.87	100.28	100.03	99.95	100.86	100.01
Rb	BD	19.3	33.1	111.8	58.0	81.4
Ba	763	298	1334	809	1179	1632
Cs	BD	0.5	0.1	1.6	0.6	0.7
Sr	381.2	44.4	226.2	112.2	615.8	86.4
Pb	15.1	15.8	13.6	32.0	12.2	58.9
Th	1.1	6.7	0.4	12.4	3.2	6.1
U	0.2	3.1	0.5	2.3	0.5	1.5
Sc	0.9	1.5	1.2	11.4	8.3	12.9
V	9.1	BD	8.4	70.6	69.5	76.4
Cr	0.9	0.5	1.0	73.4	23.7	8.6
Co	BD	0.6	2.4	9.4	13.2	7.6
Ni	BD	BD	0.7	16.0	8.0	6.0
Y	2.5	45.4	6.7	28.8	14.6	33.9
Zr	38.5	268.9	161.6	258.7	325.4	173.6
Nb	0.8	12.6	3.3	8.1	19.4	9.9
Hf	2.0	8.9	6.1	8.3	10.3	6.0
Ta	BD	1.55	BD	0.64	1.13	0.72
La	8.5	25.0	18.0	40.8	67.9	30.6
Ce	14.1	56.7	29.1	90.9	149.1	68.3
Sm	0.58	4.95	1.22	7.36	8.27	5.72
Eu	1.02	0.66	0.78	1.38	2.29	1.28
Tb	BD	1.13	0.11	1.03	0.60	0.98
Yb	0.14	5.19	0.36	2.61	1.17	3.74
Lu	0.03	0.88	0.08	0.43	0.19	0.62

Table V: Geochemistry of paragneisses

Sample	LWC-5	LSG-6	LMT-43	LMT-33	LMT-6	LMT-41
SiO_2	81.32	74.02	76.16	76.55	62.52	68.17
TiO_2	0.08	0.26	0.17	0.17	0.23	0.64
Al_2O_3	9.70	14.20	11.26	12.43	20.83	14.25
Fe_2O_3-T	0.91	1.62	5.09	1.97	3.31	5.56
MgO	1.97	0.75	1.83	1.04	0.41	2.76
CaO	1.37	3.38	1.67	1.75	6.03	3.66
Na_2O	3.72	5.26	2.32	3.31	6.66	2.56
K_2O	0.90	0.80	1.62	3.52	0.54	1.98
MnO	BD	0.03	0.19	0.03	0.05	0.08
P_2O_5	0.03	0.09	0.04	0.04	0.04	0.21
LOI	0.28	0.11	0.16	0.30	0.13	0.36
Σ	100.26	100.52	100.49	101.10	100.75	100.23
Rb	16.5	0.5	27.5	54.1	BD	55.0
Ba	400	312	903	1482	177	719
Cs	0.6	BD	0.2	0.2	BD	0.6
Sr	163.2	329.4	93.0	136.9	396.3	223.5
Pb	15.1	11.8	19.0	45.6	16.4	50.0
Th	7.7	2.7	3.5	5.3	10.9	6.7
U	2.4	0.7	1.1	0.7	2.7	1.6
Sc	0.7	7.6	5.2	3.1	4.4	10.8
V	BD	7.0	9.5	7.6	16.2	94.9
Cr	BD	0.9	2.0	1.3	1.4	23.6
Co	0.5	0.8	4.4	3.4	BD	9.2
Ni	BD	2.0	8.0	4.2	BD	9.0
Y	40.8	26.9	64.7	16.2	47.4	31.3
Zr	308.0	165.2	371.4	188.2	412.7	175.2
Nb	14.2	8.5	7.9	9.0	8.0	14.0
Hf	7.5	6.2	12.1	6.1	10.3	4.2
Ta	0.83	0.64	0.43	0.19	0.58	0.66
La	7.3	25.2	34.5	23.3	51.6	31.7
Ce	14.6	60.1	72.5	47.7	118.0	68.0
Sm	1.30	5.74	5.51	3.06	11.84	6.12
Eu	0.61	1.42	1.52	0.51	2.40	1.15
Tb	0.73	0.91	1.42	0.33	1.85	0.98
Yb	3.73	3.18	9.26	1.48	4.22	2.55
Lu	0.63	0.54	1.49	0.28	0.73	0.40

Table VI: Geochemistry of paragneisses, con't.

in the sample tend to be idioblastic, quartz (0.2mm to 2mm) commonly shows an undulatory extinction, and microcline (1mm) generally shows good tartan twinning. Sillimanite occurs as elliptical fibrolite needles 0.1mm by 2mm long and often forms elongated segregations along foliation, grouping together to form clusters. It also tends to occur along biotite margins, possibly along points of ductile shear, and imparts a grano-nematoblastic texture to the rock. This rock type seems to have had a shale protolith; the low Na_2O content (0.98 ppm) versus K_2O (3.17 ppm) in the rock means that once sodium is used up in the formation of biotite, aluminum will begin to be used to form sillimanite. This is common in meta-pelites and similar relationships are seen in sample LMT-52, although it is composed almost exclusively of quartz and sillimanite.

Sample LRG2-1 is representative of the calc-silicate paragneisses, which are commonly banded in hand specimen and have a green color due to the presence of epidote. The banding, which is also evident in thin section (see Fig. 28), may be due to original compositional differences in the protolith. Mineralogically, the calc-silicates are composed of plagioclase, 20% and up to 0.8mm, diopside, 25% and 0.4mm, quartz, 20% and from 0.2mm to 2mm, epidote, 20% and up to 1mm, and sericite, 15%. Additionally, many of the plagioclases, diopsides, and quartz grains appear to be rounded, perhaps a relict texture preserved from the sedimentary protolith or perhaps a product of brittle shear. These rocks are dominantly granoblastic and heterogranular with hypidioblastic epidote, plagioclase, and diopside being commonly present. Quartz and sericite are most commonly xenoblastic.

The outcrop from which sample LRG2-1 was collected remains a consistent thickness of 1.5m over a distance of tens of meters. The plagioclase (An_{83}) rich zones in LRG2-1 always have abundant epidote associated with them, suggesting the original rock was extremely calcareous. Since the Ca:Al ratio in plagioclase is

Figure 28: Photomicrograph of LRG2-1 showing epidote matrix, diopside grains, and some plagioclase. Note rounded grains, this may be a tectonic fabric or pre-served, rounded grains. Scale 1cm=0.5mm, X-polz. light.

1:2, excess Ca will be used to form epidote and diopside. The protolith, therefore, may have been a calcareous sediment with shaley portions which provided a source of Al and Mg needed to form epidote and diopside.

Other minor paragneissic rock types include quartz-garnet-amphibole paragneisses. Sample LMT2-3 is (Fig. 29) is such a gneiss composed of quartz, 40% and 0.7mm, garnet, 30% and 0.4mm, hornblende, 20% and 0.4mm, and plagioclase, 10% and 0.3mm, and displaying a compositional layering defined by alternating bands of hornblende rich and garnet rich layers, each about 3cm thick. As with the calc-silicate gneisses, the field and hand specimens strongly suggest a sedimentary protolith since the textures and coexisting mineral assemblages are most consistent with sedimentary parentage. As in LRG2-1, a protolith would require a ready source of Ca to form hornblende and garnet (grossularite variety, index of refraction 1.74–1.76, yellowish-brown color), Al to form plagioclase (An_{62}) and garnet, and yet be siliceous to explain high quartz contents. The protolith may have been a calcareous siltstone.

Geochemistry

Table V shows the chemical compositions of paragneisses analyzed from the Wet Mountains. The majority of the paragneisses analyzed are extremely siliceous (SiO_2), arguing for a silica rich sedimentary protolith. Paragneisses with low silica contents ($<65\%$ SiO_2), such as LMT-11 and LMT-6, have chemical compositions and mineralogies commensurate with shale precursors.

The siliceous nature of the majority of the biotite-quartz-plagioclase gneisses raises some question as to whether these gneisses actually represent paragneisses or if they may actually be orthogneisses. Fig. 30, a major element sediment discrimi-
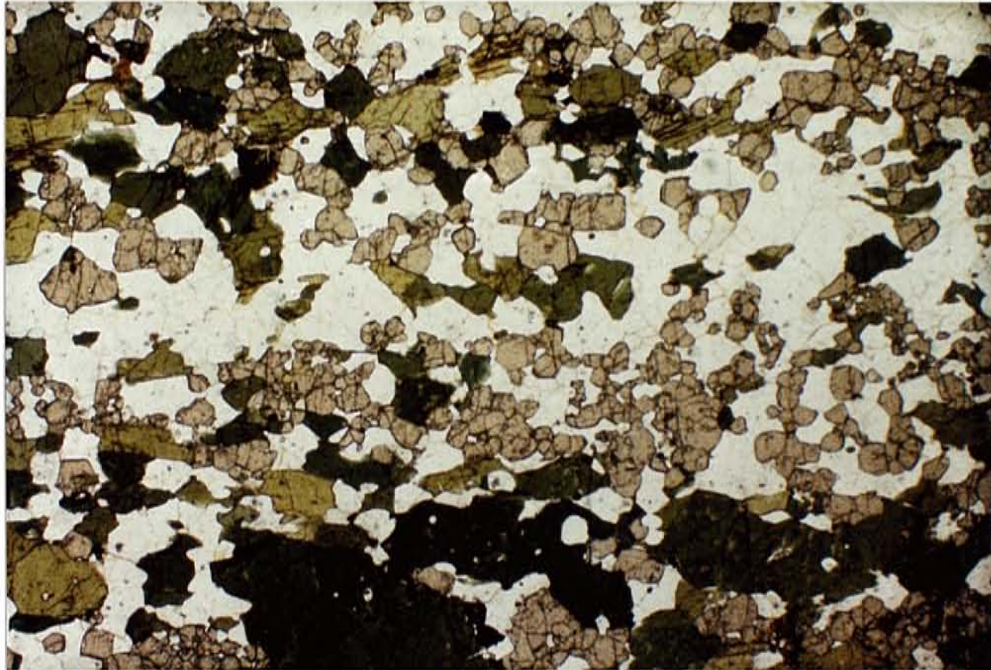
Figure 29: Photomicrograph of LMT2-3, a garnet (orange), diopside (light green), and hornblende (dark green) paragneiss. 1cm = 0.5mm, plain light.

nation diagram after De la Roche (1966) shows how similar the major element composition of these gneisses is to that of acid igneous rocks. The diagram shows fields of occurrence for certain major sediment types and also a line showing the chemical variation in common igneous rocks. The biotite-quartz-plagioclase gneisses plot slightly offset from the igneous trend line within the field of graywackes and arkoses but they do parallel the igneous trend very closely. Similarly, the average chemical composition of the Wet Mountains biotite-quartz-plagioclase gneisses shows similarities to the average composition of the meta-felsic volcanic rocks of the Sangre de Cristo range to the west (Table VII), although the standard deviations in element concentrations from the Wet Mountains are larger. Elements such as Hf, La, Zr, and Th in particular show significant scatter; elements which have been shown to be particularly sensitive to sedimentary processes (Bhatia and Taylor, 1981).

Mesonormal QFM plots have been used in metamorphic terranes in Canada, particularly by such workers as Van de Kamp (1979) and Sawyer (1987), in attempting to distinguish between ortho- and para-gneisses. The English River Gneiss belt, in Ontario, has similar biotite-quartz-plagioclase bearing gneisses to those in the Wet Mountains which are enigmatic as to progenitor rock types. Van de Kamp and Beakhouse (1979) proposed using mesonormal mineral assemblages (after Barth, 1959) since this method takes into account the metamorphic mineral assemblages. Van de Kamp and Beakhouse propose that QFM mesonormal plots (Fig. 31) can distinguish different compositional trends which will occur in orthogneisses versus paragneisses due to their different genetic histories. Although orthogneisses and paragneisses may have similar bulk composition, Van de Kamp and Beakhouse suggest that clastic sediments will show a trend of mesonormative quartz enrichment due to selective concentration of quartz and selective removal
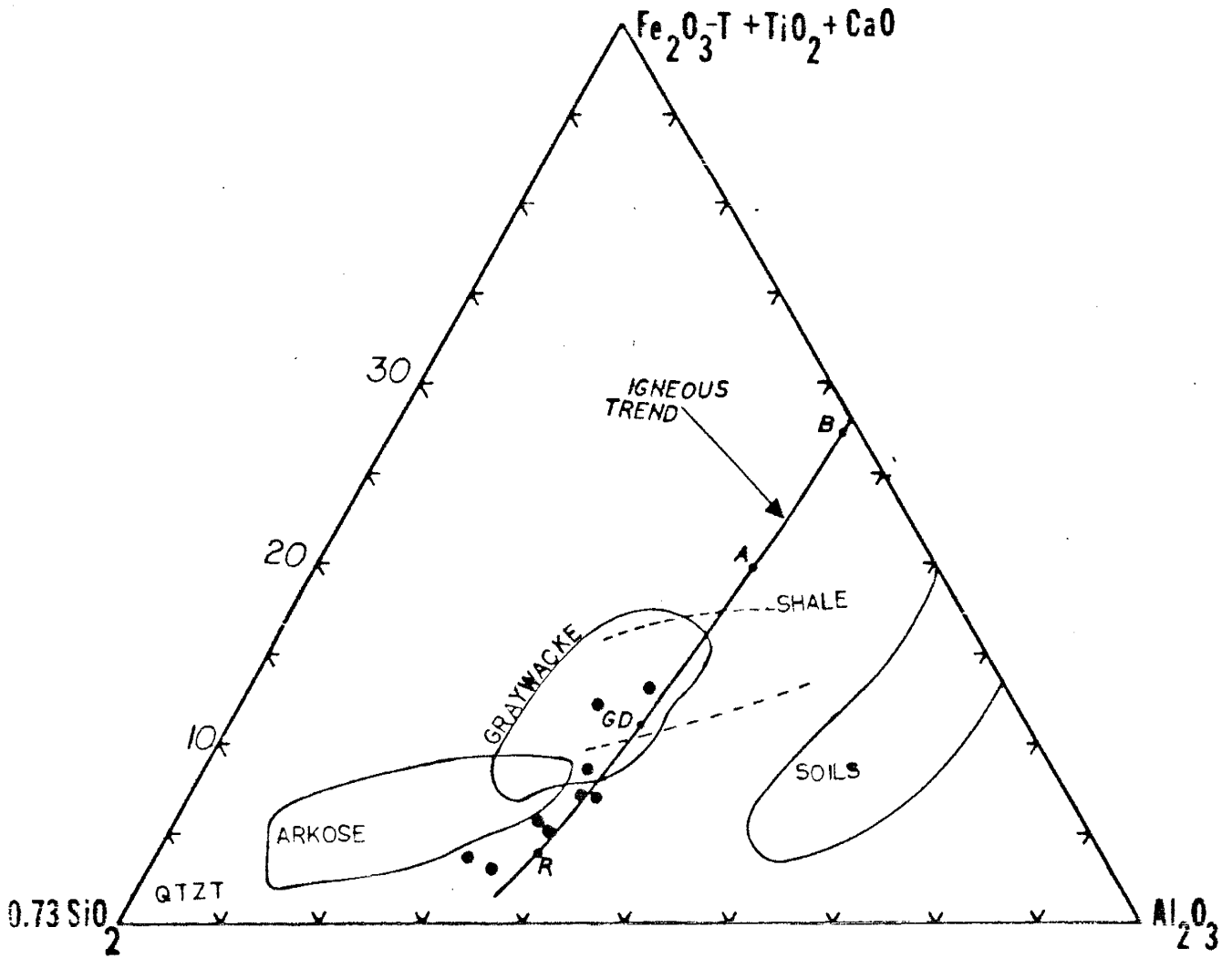
Figure 30: Triangular plot of Si-Al-Fe+Ti-Ca showing the fields of various sedimentary rocks together with the typical igneous trend (after De la Roche, 1966). Points B, A, GD, and R represent average compositions of basalt, andesite, granodiorite, and rhyolite, respectively. Dots are Wet Mtns paragneisses.
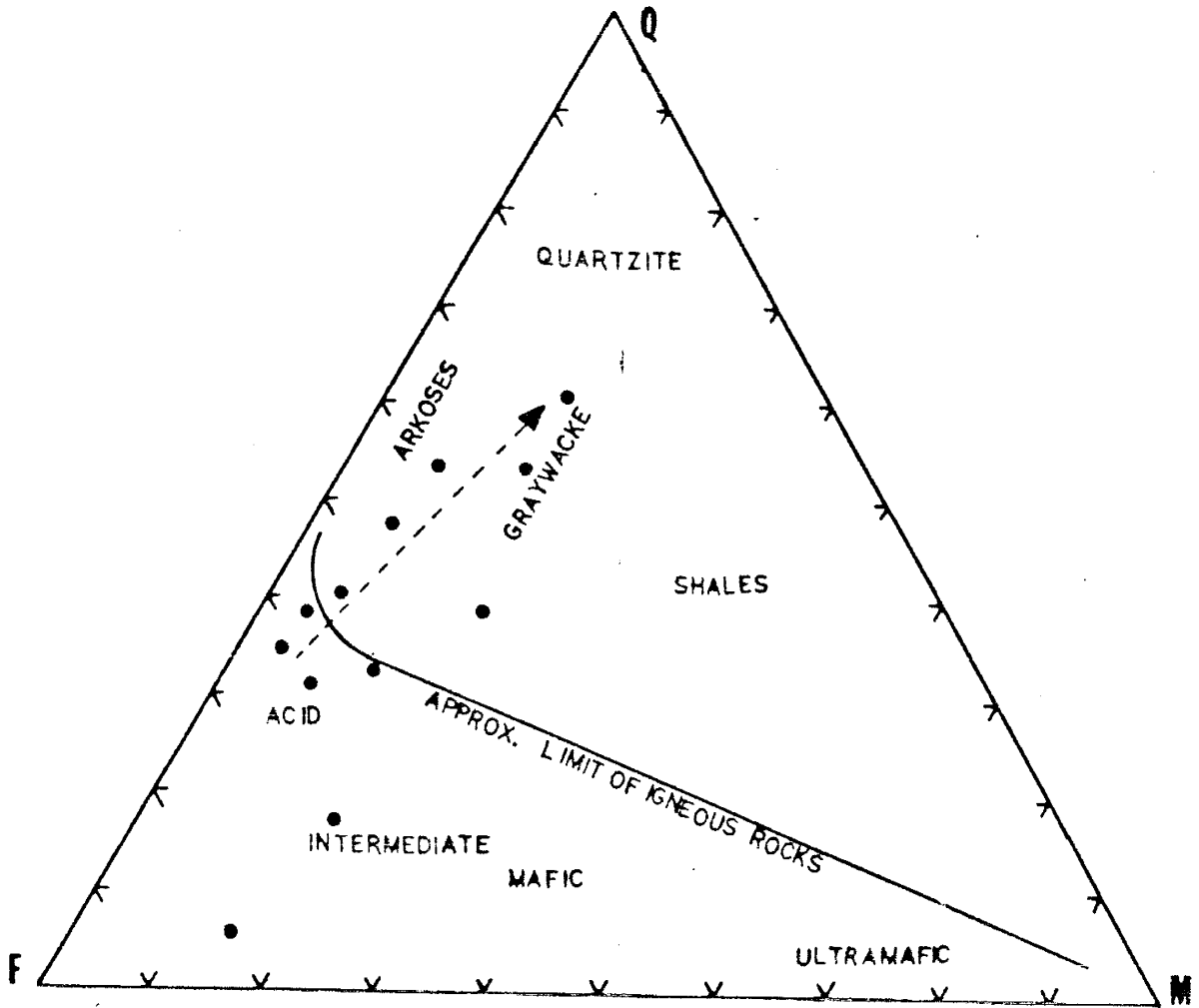
Figure 31: QFM mesonormal diagram showing where various sedimentary and igneous rock types plot. Solid circles are Wet Mtns paragneisses, arrow demonstrates how array of samples shows a quartz enrichment trend (after Van de Kamp and Beakhouse, 1979).

of feldspars and chain silicates. The Wet Mountains gneisses show a quartz enrichment trend, marked with the arrow, when plotted on a QFM diagram, and show chemical affinities to acid igneous rocks and arkoses and graywackes.

Other normative based diagrams show similar relationships, such as the Niggli number based si vs mg diagram (Fig. 32, Van de Kamp and Beakhouse, 1979). Again, samples show a sedimentary trend resultant from increasing normative si, possibly a reflection of the potential for quartz preservation relative to normative mg in magnesium bearing minerals during sedimentary processes. The geochemical similarity the Wet Mountains paragneisses bear to volcanic rocks, particularly on a De la Roche (Fig. 30) or a QFM mesonormal plot (Fig. 31), may imply that the sediments are derived from volcanic sources and may have inherited much of their geochemistry.
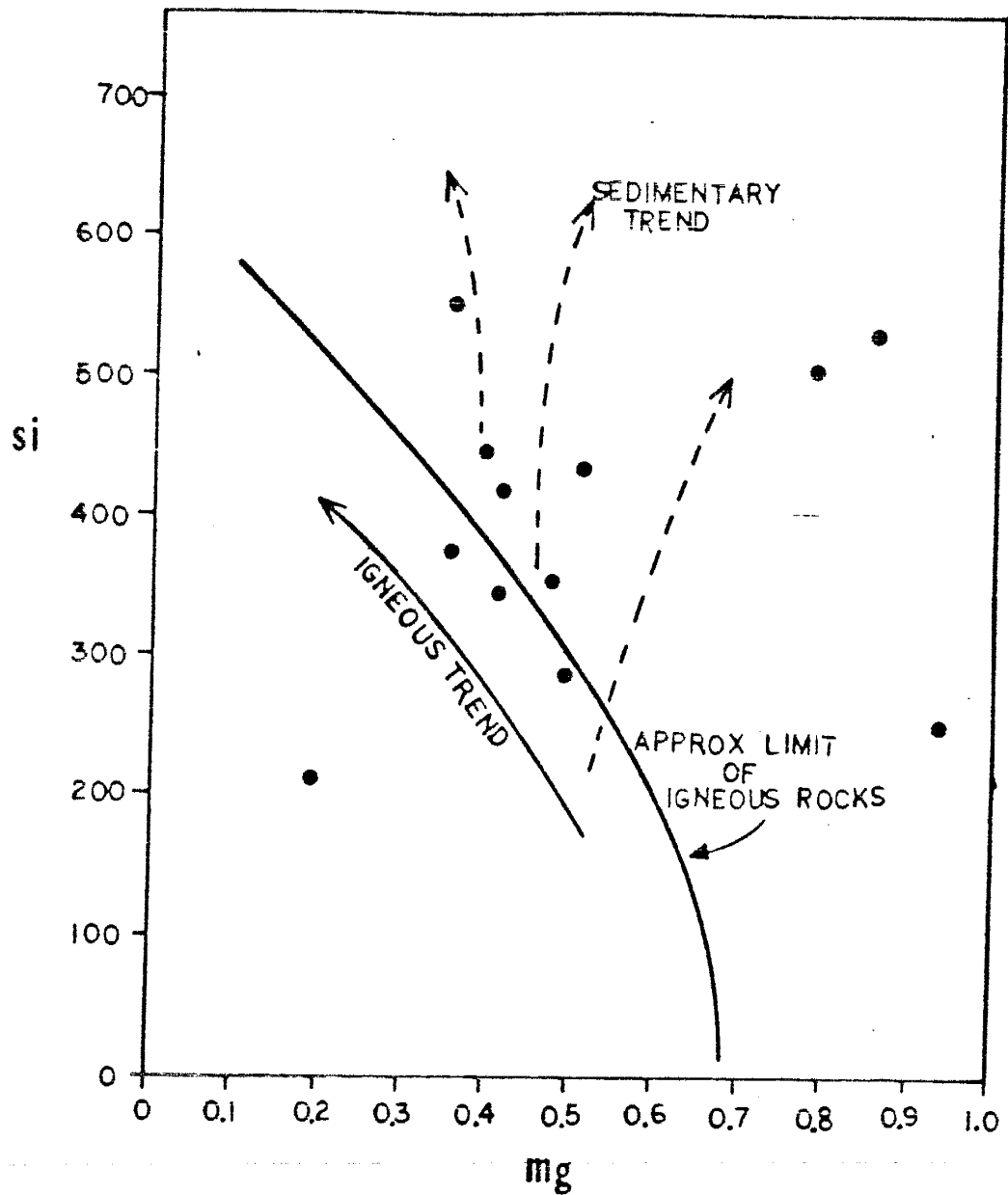
Figure 32: Plot of Niggli si vs mg showing the high-si character of the Wet Mtns paragneisses and demonstrating their affinity to sedimentary rock compositions. Arrows show trends followed by typical sedimentary rocks (after Van de Kamp and Beakhouse, 1979).

Sedimentary Protoliths

As discussed, paragneisses with probable shale, calc-silicate, and quartzite pro-
toliths can be recognized, but the biotite-quartz-plagioclase gneisses, however, are
more difficult to characterize in terms of precursor rock types and must rely pri-
marily upon chemical constraints to distinguish protoliths due to the high degree
of recrystallization. Table VIII is a table of the major element compositions of
some common sedimentary rock types in comparison to the average composition
of the biotite-quartz-plagioclase gneisses. Arkoses have neither the high Fe nor the
high Mg contents of the Wet Mountains gneisses and tend to be too high in K to
accommodate the Wet Mountains samples. The gneisses also don't seem to fit with
average analyses of either shales or graywackes; they are too high in Si and too low
in Al, Fe, Mg, and Ca to be either of these rock types. Table IX shows chemical
analyses from quartz-poor, quartz-intermediate, and quartz-rich graywackes from
Australia (Taylor and McClennan, 1985) compared to the average composition of
the Wet Mountains paragneisses and shows that the Wet Mountains paragneisses
display major element similarities to quartz-rich graywackes (quartzwackes). Com-
paring the Wet Mountains paragneisses to other Proterozoic gneisses from the
southwestern U. S. which have been classified as quartzwackes on both the basis
of chemistry and relict textures (Table X) shows that the quartzwackes from Pro-
terozoic terranes such as the Big Thompson Canyon area in Colorado, the Mazatzal
and Pinal sequences in Arizona, and the Isaleta and Moyos areas in New Mexico
are chemically similar. Additionally, comparing chondrite normalized REE pat-
terns for Phanerozoic quartzwackes to patterns from the Wet Mountains gneisses
(Fig. 33) shows that the REE patterns compare very favorably.

	Wet Mtns		Sangre de Cristo	
	Average	Std. Dev.	Average	Std. Dev.
SiO_2	76.31	3.28	75.02	3.03
TiO_2	0.32	0.23	0.18	0.04
Al_2O_3	12.43	1.57	12.67	1.23
Fe_2O_3	3.05	1.92	2.72	1.18
MgO	1.21	0.59	1.63	0.62
CaO	1.88	1.16	0.82	0.37
Na_2O	3.99	0.95	4.48	1.46
K_2O	1.83	1.25	2.12	1.90
MnO	0.10	0.08	0.07	0.08
P_2O_5	0.06	0.04	0.04	0.46
Th	4.19	2.68	8.34	1.90
U	1.28	1.01	3.39	0.83
Sc	4.14	4.29	5.54	2.05
Cr	2.17	2.87	1.43	1.56
Co	2.81	2.59	2.17	1.43
Y	29.64	20.95	57.51	16.15
Zr	209.4	103.3	297.07	32.42
Nb	8.28	4.44	16.69	3.89
Hf	6.86	2.88	8.71	1.20
La	21.55	9.74	37.91	11.72
Ce	45.39	23.31	84.93	27.26

Table VII: Chemistry of Wet Mtns and Sangre de Cristo quartzofeldspathic gneisses

[Data: Thacker, unpub.]
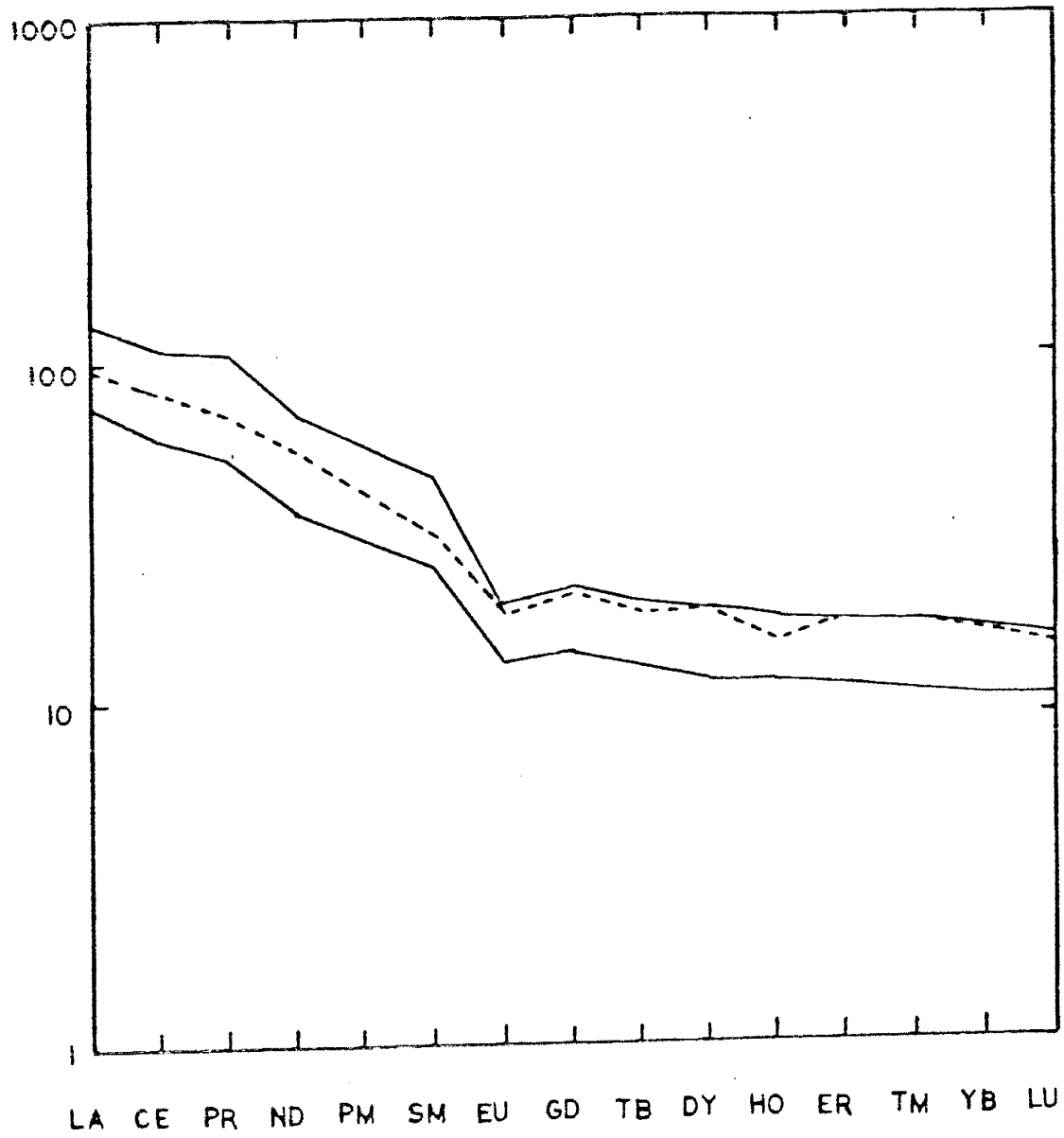
Figure 33: Chondrite normalized REE diagram showing envelope of occurrence of graywackes (range of 6 samples). Dashed line represents NASC. After Taylor and McClennan (1985).
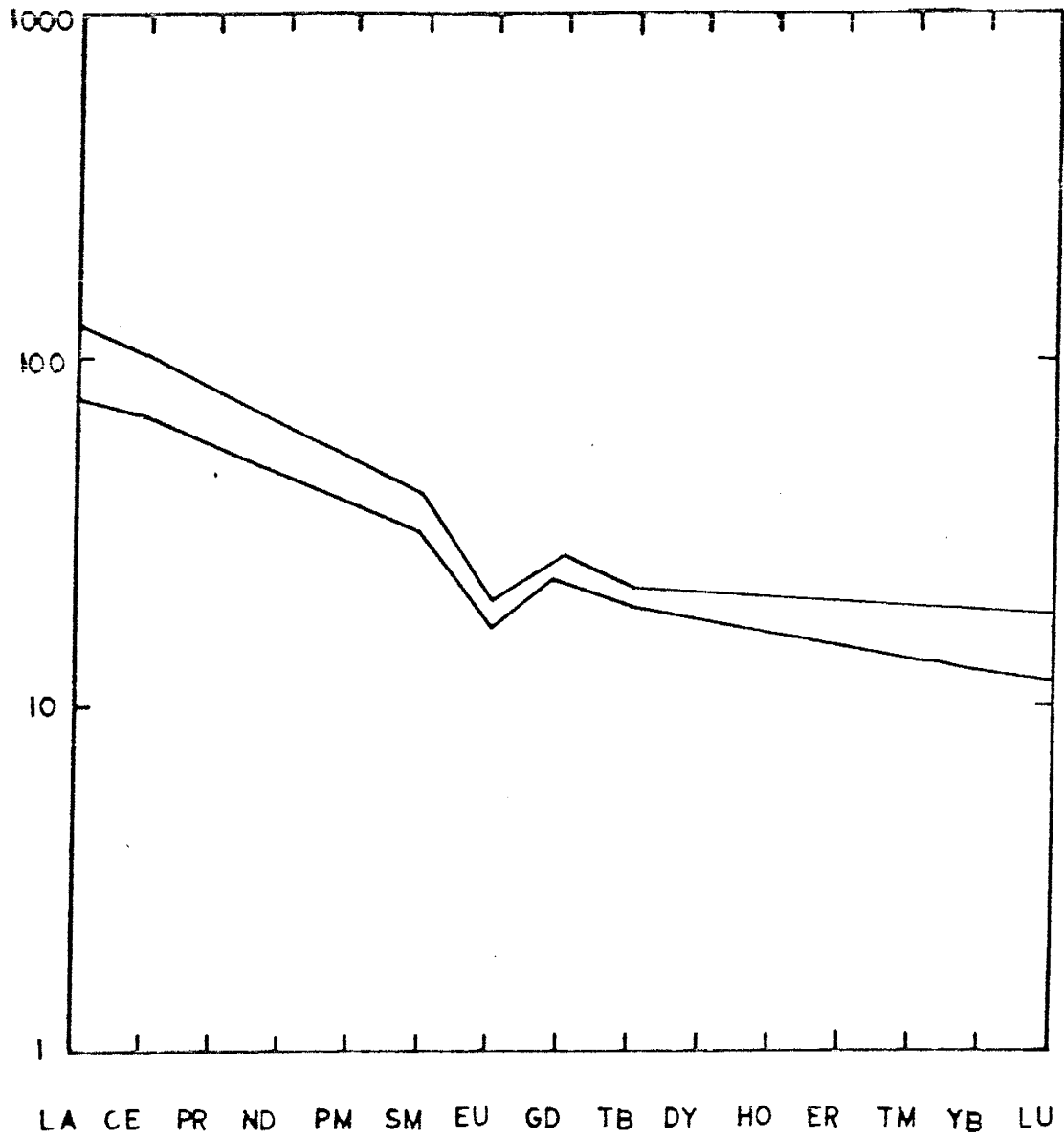
Figure 34: Chondrite normalized REE diagram of the Wet Mtns paragneisses. Envelope represents range of 7 samples.

Tectonic Affinities

Bhatia has proposed several diagrams based upon chemistry which seem to delineate tectonic settings (Bhatia,1983 and Bhatia and Crook, 1983) for sedimentary rock types. Most of his diagrams were constructed for use with graywackes and when quartzwackes are plotted on such diagrams it usually results in scatter. This may be due to high trace element contents in minor phases such as zircon, which would tend to be more concentrated in more siliceous rock types such as quartzwackes.

Bhatia suggests (Bhatia and Taylor, 1981) that sediments derived from arc material tend to be low in La, Th, Hf, and U (La$\approx$9.2, Th$\approx$1.4, U$\approx$0.52, and Hf$\approx$2.1), whereas those derived from granitic and sedimentary source rocks tend to have higher values (La$\approx$39, Th$\approx$16, U$\approx$3.4, Hf$\approx$7.9). The high values for these trace elements in paragneisses from the Wet Mountains may indicate a more granitic provenance for the sedimentary protoliths.

The highly siliceous nature of the metasediments may allow accurate discrimination of tectonic setting by using a discriminant function diagram based upon major element compositions in sandstones in relation to their tectonic settings (Bhatia, 1983). Bhatia's discriminant function is defined thus:

$$D_i = a_i x_1 + b_i x_2 + c_i x_3 + \ldots + p_i x_p + C \tag{1}$$

where D is the discriminant function, a, b, and c are the elemental coefficients which the elemental concentrations (x) are multiplied by, and C is a constant of proportionality. The coefficients have values which correspond to how sensitive an element is in determining a particular tectonic setting. When the Wet Mountains paragneisses are plotted on this diagram (Fig. 35) they appear to have affinities
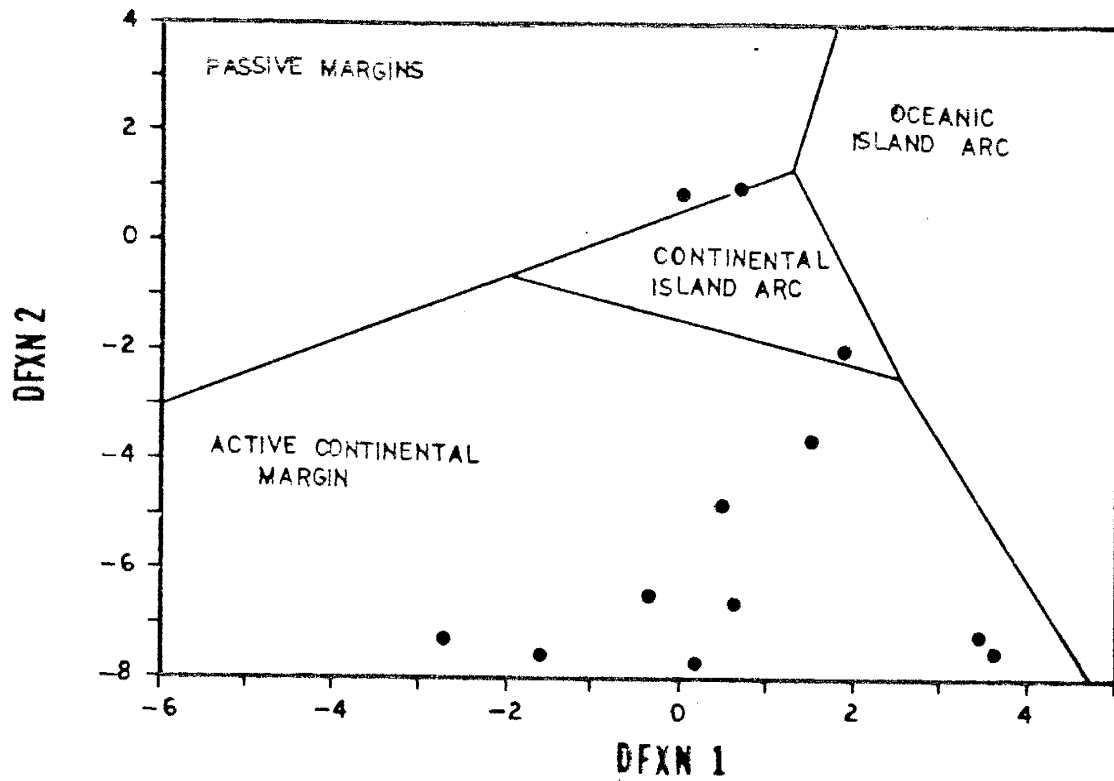
Figure 35: Plot of Wet Mountains metasediments on a major element discrimination function diagram for sandstones relative to tectonic environment of deposition (after Bhatia, 1983). DFXN are discriminant functions (see text for Explanation).

to active continental margin sediments, implying deposition in a basin associated with a continental margin arc.

Interestingly, most Phanerozoic quartzwackes are from dominantly sedimentary or granitic provenances whereas graywackes, quartz-poor or quartz-intermediate, are generally from more volcanic or mixed provenances (Potter, et. al., 1972). Therefore, the tectonically active continental margin setting the discriminant function diagram suggests is consistent with the mineralogy of the protolith. This may explain why the Wet Mountains paragneisses resemble acidic volcanic rocks in major element composition.

Fig. 36 shows a La/Th vs Hf diagram (Floyd and Leveridge, 1987) in which sediments derived from acid-dominated arcs have low and uniform La/Th ratios and Hf contents of about 3–7 ppm. With progressive dissection of the arc and erosion of its plutonic roots and metasedimentary basement, the Hf content increases as a result of increased liberation and recycling of zircon. The La/Th vs Hf plot allows discrimination of both source composition and tectonic setting and suggests that the Wet Mountains metasediments are derived from an acidic arc type source which is incorporating significantly increasing amounts of old sediment component.
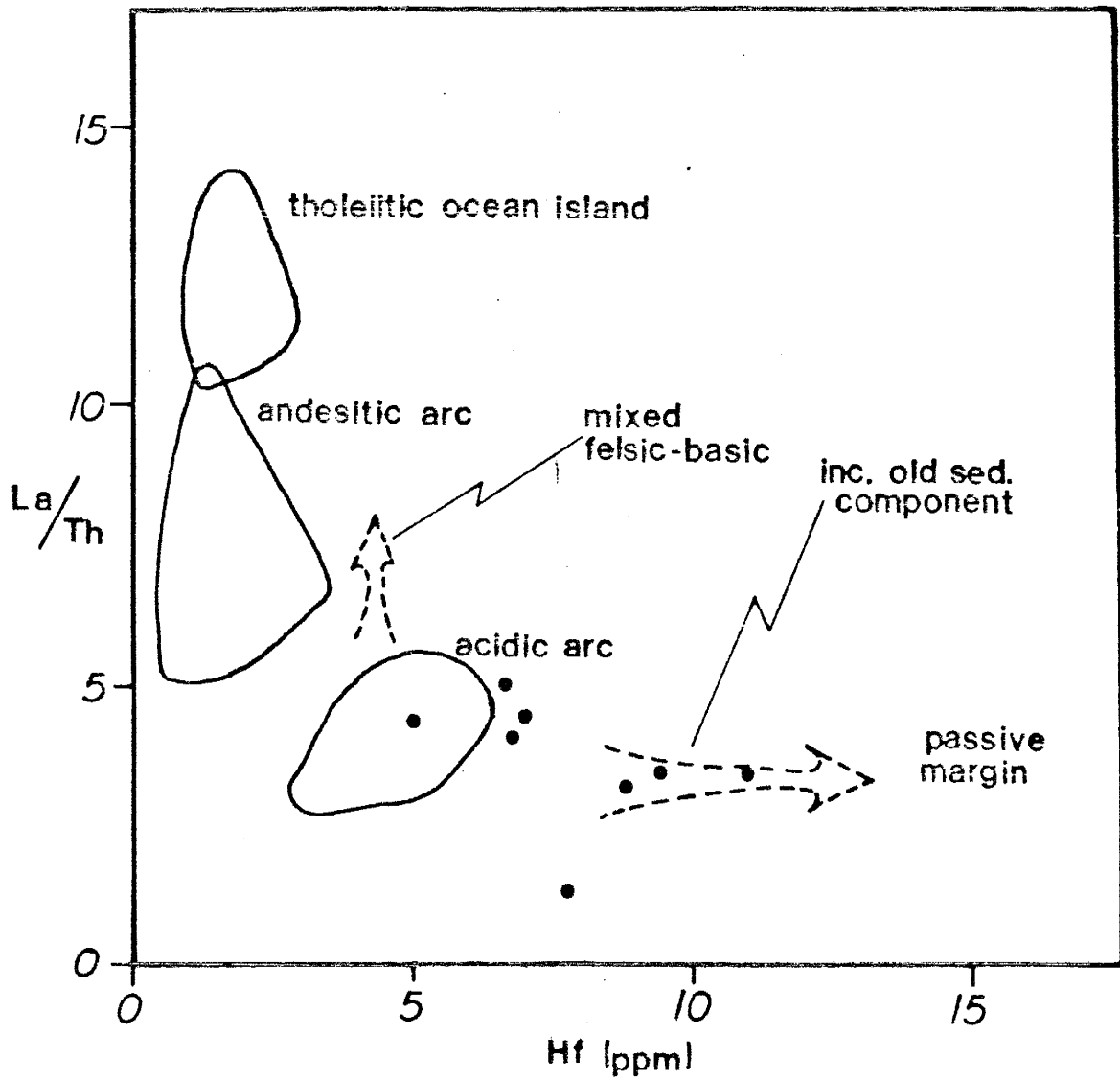
Figure 36: Hf vs La/Th source and composition discrimination diagram for sediments. Dots represent Wet Mtns metasediments, arrows show transitions into mixed felsic/basic sources and sources with increasing old sediment component (after Floyd and Leveridge, 1987).

	Shale	Graywacke	Arkose	Wet Mtns
SiO_2	62.8	70.1	79.3	76.31
TiO_2	1.0	0.5	0.22	0.32
Al_2O_3	18.9	14.0	9.94	12.43
Fe_2O_3	7.22	4.7	1.80	3.05
MgO	2.2	2.3	0.56	1.21
CaO	1.3	2.5	0.38	1.88
Na_2O	1.2	3.7	2.21	3.99
K_2O	3.7	1.8	4.32	1.83
MnO	0.11		0.02	0.10
P_2O_5	0.16	0.15	0.05	0.06

Table VIII: Chemistry of modern sediments and Wet Mtns. paragneisses
[Data: Pettijohn, Potter, and Siever, 1973]

	Wet Mtns.	Graywackes		
		Quartz-poor	Quartz-inter	Quartz-rich
SiO$_2$	76.31	58.57	68.95	78.39
TiO$_2$	0.32	1.11	0.78	0.70
Al$_2$O$_3$	12.43	16.85	14.74	11.04
FeO	2.75	8.70	5.23	3.48
MnO	0.10	0.15	0.17	0.03
MgO	1.21	3.26	2.37	1.82
CaO	1.88	5.37	2.54	0.29
Na$_2$O	3.99	5.17	2.57	1.87
K$_2$O	1.83	0.65	2.24	2.25
P$_2$O$_5$	0.06	0.20	0.15	0.16
Th	4.19	1.14	10.29	14.6
U	1.28	0.58	1.57	3.21
Sc	4	31	19	10
Cr	2	34	80	57
Co	3	24	11	12
Y	30	17	22	32
Zr	209	87	142	384
Nb	8.3	0.8	10.2	11
Hf	6.9	1.5	3.4	8.2
La	21.6	8.4	28.5	39.4
Ce	45	17	62	76
La/Sc	5.21	0.27	1.63	3.90
Th/Sc	1.01	0.04	0.44	1.45

Table IX: Chemistry of Phanerozoic quartz-poor to -rich graywackes and Wet Mtns. paragneisses

[Data: Taylor and McClennan, 1985]

	Idaho Spgs. Colo.	Pinal Shst. Ariz.	Moyos Fm. New Mex.	Los Pinos New Mex.	Wet Mtns. Colo.
SiO_2	76.9	78.4	77.5	76.3	76.3
TiO_2	0.48	0.49	0.48	0.39	0.32
Al_2O_3	10.8	10.2	10.2	12.6	12.4
Fe_2O_3	3.4	3.6	3.9	3.1	3.1
MgO	1.82	0.76	0.89	0.66	1.21
CaO	1.54	0.72	0.23	1.54	1.88
Na_2O	1.55	1.97	2.53	1.80	3.99
K_2O	2.12	2.39	1.58	2.94	1.83
Hf	6.4	8.3	6.9		6.9
Th	11.1	13.3	9.1		4.2
Sc	9.0	7.6	8.2		4.0
Zr	188	259	252	276	209
La	28.4	29.8	31.0	45.7	21.6
Ce	56.8	61.7	64.5	72.3	45
Sm	5.2	5.6	5.8	8.4	4.4
Eu	1.02	1.14	1.08	1.18	1.02
Tb	0.86	1.16	0.89	1.35	0.83
Yb	2.48	3.17	3.30	5.32	3.39
Lu	0.44	0.58	0.51	0.91	0.55
La/Sc	3.15	3.92	3.78		5.21
Th/Sc	1.23	1.75	1.11		1.01

Table X: Chemistry of Proterozoic quartzwackes and Wet Mountains paragneisses

[Data: Condie, Bowling, and Vance, 1985, Condie and DeMalas, 1985, Condie and Martell, 1983, Copeland and Condie, 1986, Condie, unpub.]

Granites

Lithology

Several granitic types are evident in the Wet Mountains but alaskitic granite gneiss is by far the most abundant and will be the primary rock type of interest in this section, since it is intimately associated with the supracrustals of the central Wet Mountains. This study will not deal with the larger granitic batholiths surrounding the area, since detailed studies by other workers is much more extensive, but a review some of the data available on these batholiths may aid in placing the alaskitic units in their proper regional perspective.

Cullers and Wobus (1986) state that most of the plutons in the northern Wet Mountains are granitic in composition (tonalite to granite) and this is also true of the plutons in central Wet Mountains. They also suggest that the Proterozoic plutons were emplaced during three major intrusive events, an early syn- to late-tectonic event and two post-tectonic and basically anorogenic events. The Crampton Mountain-Twin Mountain batholith (Fig. 2) is found north of the study area and is representative of the syn-tectonic granitic plutons. U-Pb zircon dating on the pluton yields ages of 1705 Ma (Cullers and Bickford, 1983), which is a common age found in the syn-tectonic granitoids. The batholith is calc-alkaline, generally well foliated, and compositionally course-grained tonalite and granodiorite. The Cotopaxi-Garrels Peak batholith, northwest of the study area, is similar in composition to the Crampton Mountain-Twin Mountain batholith, tends to be metaluminous to paraluminous, and yields U-Pb dates ages of 1650 Ma (Bickford and Cullers, unpub. data).

Anorogenic granites are represented by two plutons, the San Isabel batholith to the south and the West McCoy Gulch stock to the northwest. Both bodies tend to show no foliation, except at their margins, are not observed to be folded, and were probably emplaced as mesozonal granites post-tectonically. The San Isabel batholith has been dated at 1360 Ma and the West McCoy Gulch stock at 1460 Ma (Bickford, 1986).

Alaskites cover about 30% of the study area, are generally light pink in color, medium to fine grained, and equigranular and are almost always observed as concordant, tabular bodies interlayered within the supracrustal terrane parallel to the regional foliation. They commonly display a *lit-par-lit* texture in outcrop and occasionally cross-cut supracrustal units. Individual layers may be as thin as 0.5m but can reach thicknesses of 160m in thickness. Alaskitic bodies are commonly folded along with the supracrustal rocks and, when ferro-magnesian minerals are present, the rock takes on a strong foliation. Also, pegmatites are often associated with the alaskites and migmatites are common along boundaries between granitic and metasedimentary gneisses. Brock and Singewald (1968) note that scattered layers of leucogranite occasionally contain relict garnet and, although rarely, sillimanite and that portions of the biotite gneisses are intimately associated with leucogranitic sills, suggesting a genetic relationship.

Petrography

The alaskitic granites have, as major constituents, microcline (40%), quartz (35%), oligoclase (20%), and usually anywhere from 1 to 5% biotite and, as minor phases, magnetite, apatite, zircon, and hornblende. The microcline is commonly microperthitic and commonly shows myrmekitic textures when found in contact

with oligoclase. Quartz and microcline both tend to be xenoblastic whereas biotite and plagioclase are more commonly hypidioblastic. Quartz commonly displays an undulatory extinction and both plagioclase and microcline commonly have bent twin lamellae, suggesting they have been strained. The texture in thin section is generally granoblastic, but when enough biotite is present it may actually take on a grano-lepidoblastic texture (Fig. 37).

Geochemistry

The alaskites (Table XI) are generally siliceous (74–77% SiO_2) and alkali rich, ($Na_2O \approx$ 3% and $K_2O \approx$ 6%) but tend to be low in Fe (FeO-T$\approx$ 2%). The general absence of magnetite and biotite suggest that the granites crystallized under very reducing or low f_{O_2} conditions (Clemens and Wall, 1988). The felsic intrusives display bulk chemical similarities to granitic and tonalitic magmas when plotted on the An-An-Or normative system (Fig. 38) and, on the Al-Na+K-Ca diagram (Fig. 39), show peraluminous nature, a characteristic also suggested by the occasional presence of phases more aluminous than biotite. However, the intrusives with tonalitic compositions, representing the quartz diorites discussed in the BDH section, do not seem to be genetically related to the alaskites and thus are not included with them in analysis. Granitic norms for the alaskitic granites are anorthite poor, $An \leq$ 5%, and thus can be accurately plotted on the Q–Ab–Or portion of the Q–Ab–An–Or (+H_2O) tetrahedron (Fig. 40). On the tetrahedron the leucogranites plot very close to the 1 kbar P_{H_2O} cotectic, perhaps implying that they have been emplaced at low water pressures, omitting fractionation effects or volatile loss during crystallization.

The strongly peraluminous nature of the alaskitic granites, the low Na/K ratio, and predominance of metasedimentary xenoliths suggest that these may be S-type
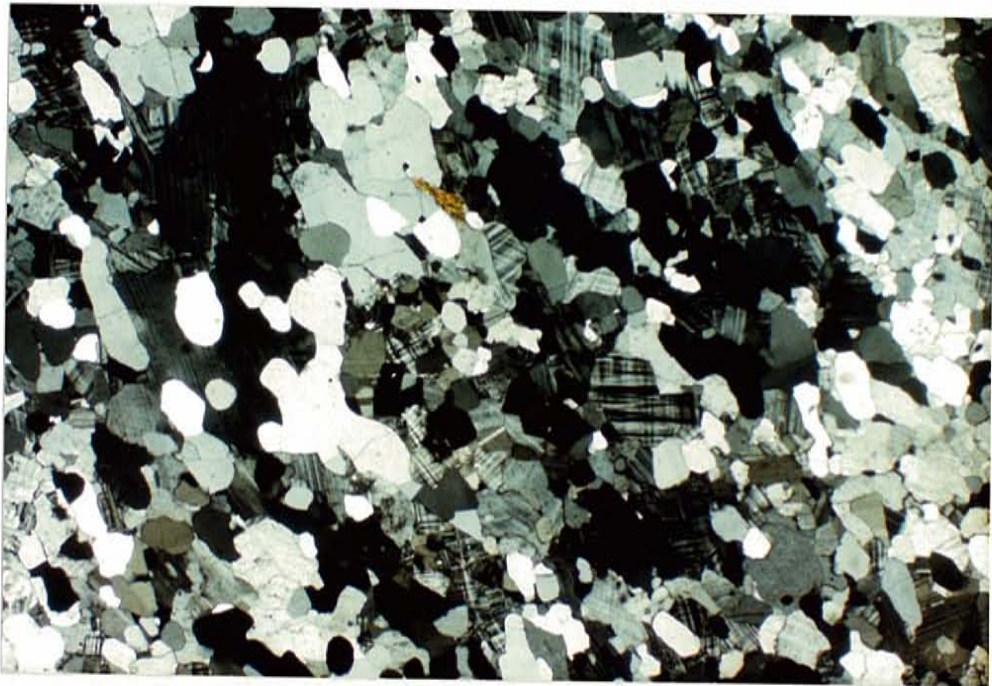
Figure 37: Photomicrograph LMT-20, alaskitic gneiss/leucogranite, with micro-cline, plagioclase and quartz. Note one small piece of biotite in sample. Scale 1cm=0.5mm, X-polarized light.
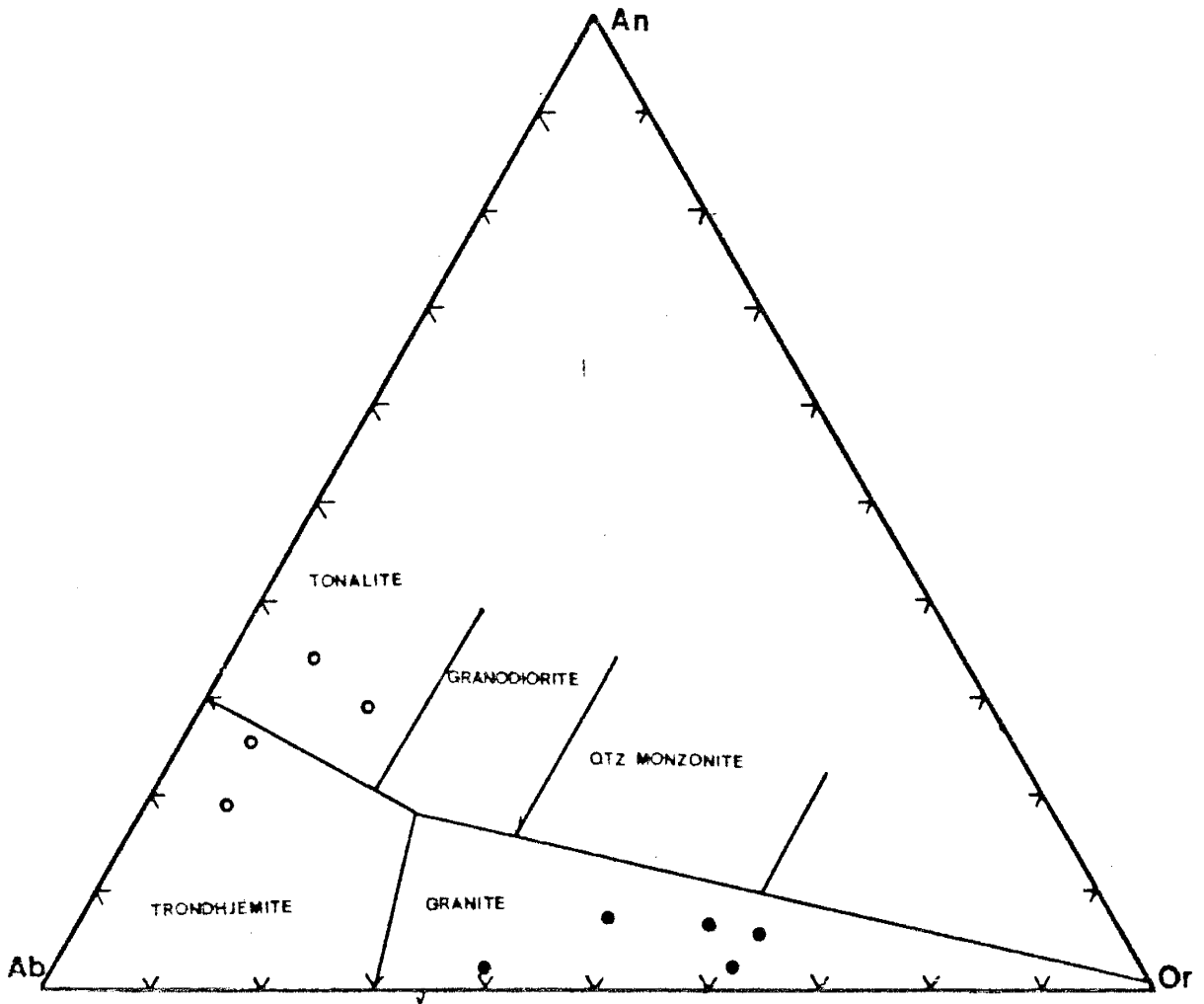
Figure 38: Triangular plot of normative Ab-An-Or in the granite system showing field, of various granitic rock types. Open circles represent quartz diorites and solid circles leucogranites (after Barker, 1979). Leucogranites are moderately to strongly peraluminous.
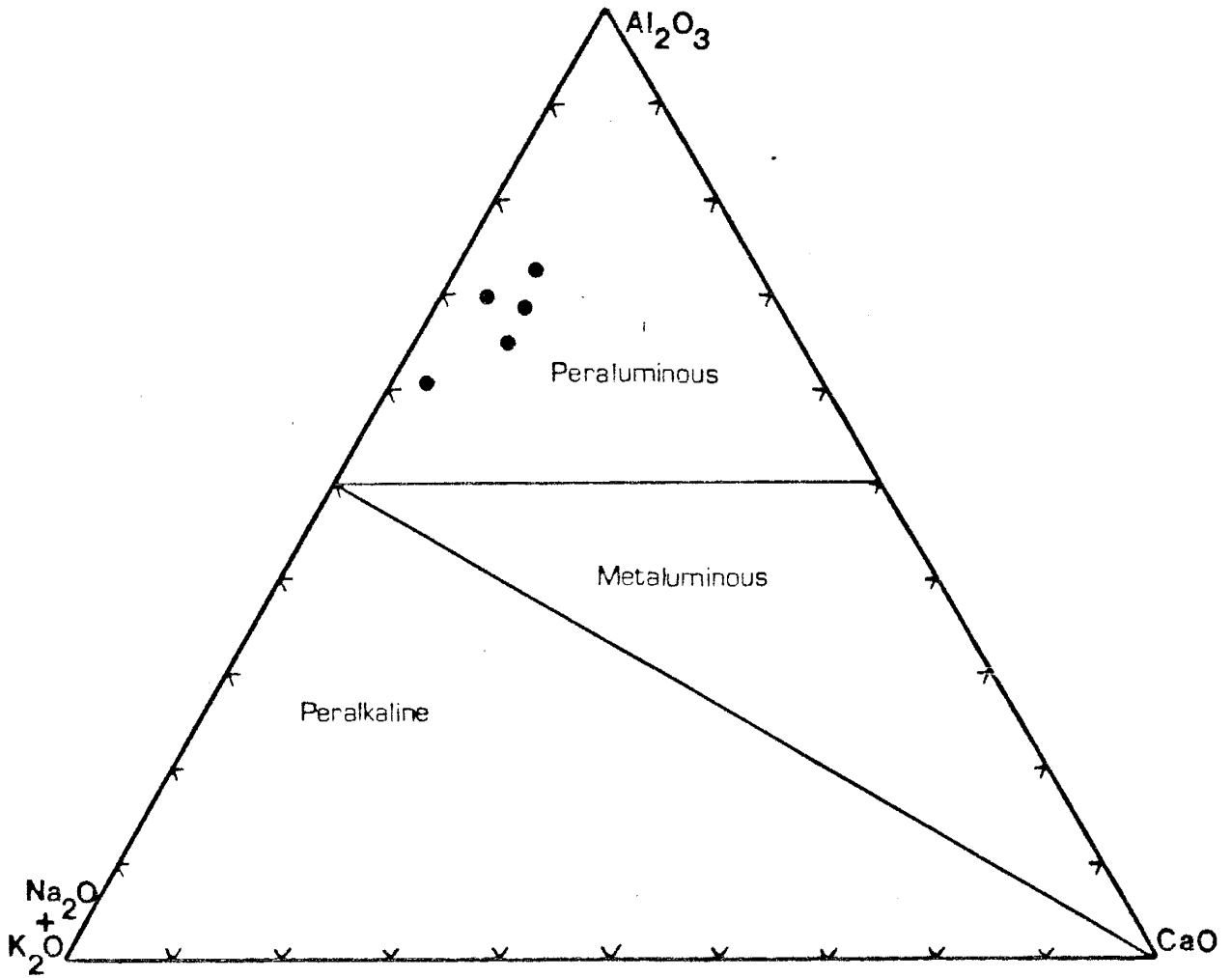
Figure 39: Molar plot in the ternary system Al_2O_3-Na_2O+K_2O-CaO for igneous rocks. Solid circles represent leucogranites.
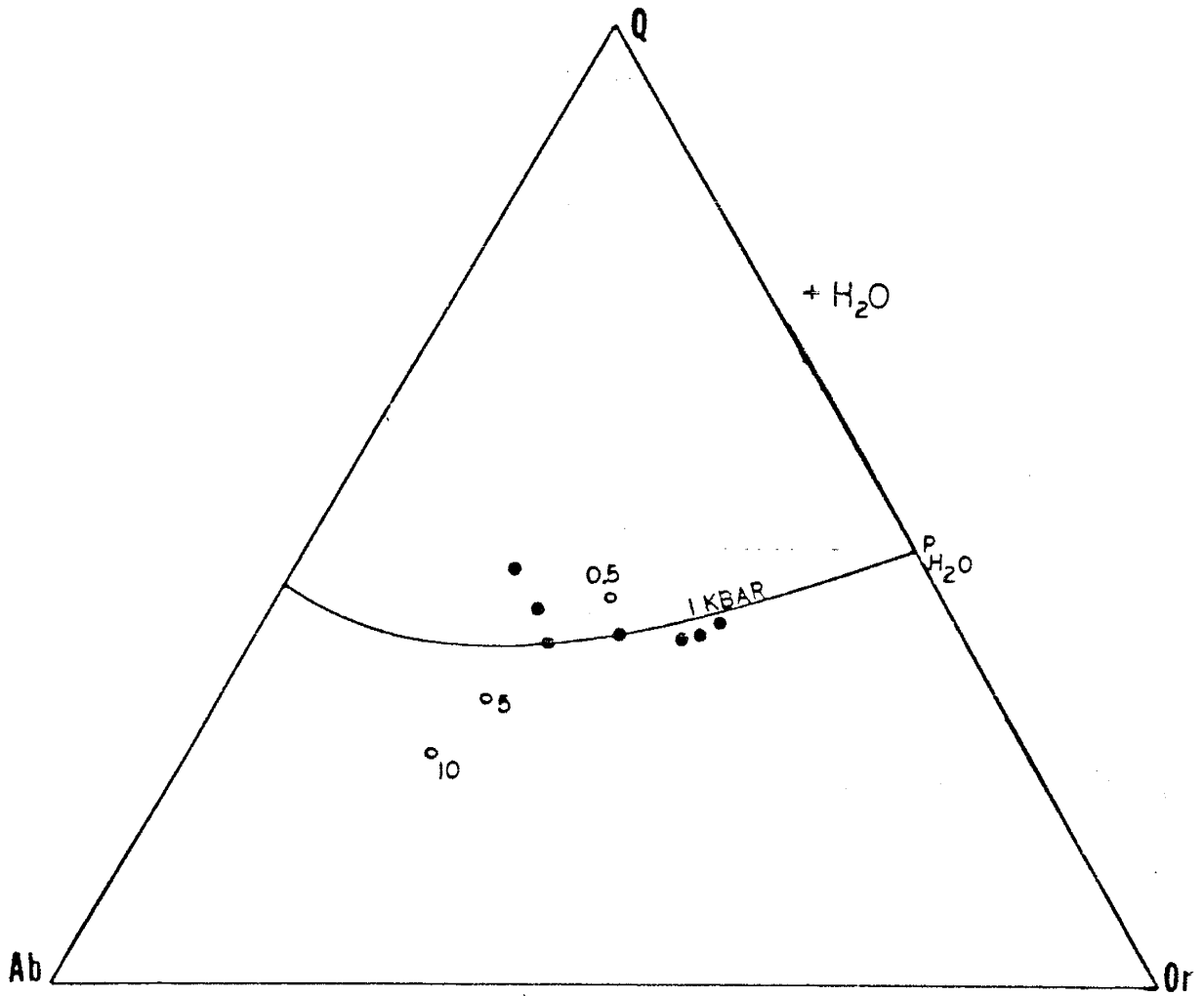
Figure 40: Ternary Ab-Or-Q +H₂O system at various water pressures. Open circles represent 0.5, 1, 5, and 10kbar water pressure eutectics, solid line is 0.5kbar cotectic, solid circles are Wet Mtns leucogranites (after Huang and Wyllie, 1975).

granitoids (White and Chappell, 1977). The occasional presence of garnet and sillimanite in the leucogranites also suggests derivation from a metasedimentary parent while the mafic-poor, low volatile compositions may suggest they represent minimum melts.

When plotted on a chondrite normalized REE diagram the leucogranites (Fig. 41) display a strongly enriched LREE pattern relative to the HREE (La/Yb$\geq$15) and a strongly negative Eu anomaly (Eu$\leq$1.5).

On Pearce's (1984) Yb + Nb vs Rb discriminant diagram for granitic rocks (Fig. 42) the leucogranites of the Wet Mountains display affinities to granitic rocks derived from within-plate settings. Within-plate granites, as described by Pearce, imply granites derived from an incompatible enriched mantle and intruded into crust, either continental or oceanic. Field relationships suggest, however, that the leucogranites (LCG) are derived from anatexis of the metasedimentary gneisses, thus making them crustally derived. Thus, to avoid confusion, the within-plate setting in this study is taken to only imply that the granites are crustal melts. Pearce suggests that post-collisional granites can fall in the within-plate field and the folded nature of the LCG is suggestive of granites emplaced during periods of crustal shortening. Although the Y + Nb vs Rb diagram is often used to constrain tectonic settings, the boundaries on the diagram are almost entirely constrained by chemical differences in the source. On Fig. 42, WMS and TS represent averages of most probable sources for the Wet Mountains and Himalayan leucogranites, respectively, the metasediments of the Wet Mountains and the gneisses of the Tibetan Slab. In both cases, simple partial melting of these sources cannot yield the high-Rb magmas observed unless a volatile component is added which can mobilise the LIL elements. The primary chemical difference between the collisional leucogranites of the Himalayas and those of the Wet Mountains is that the
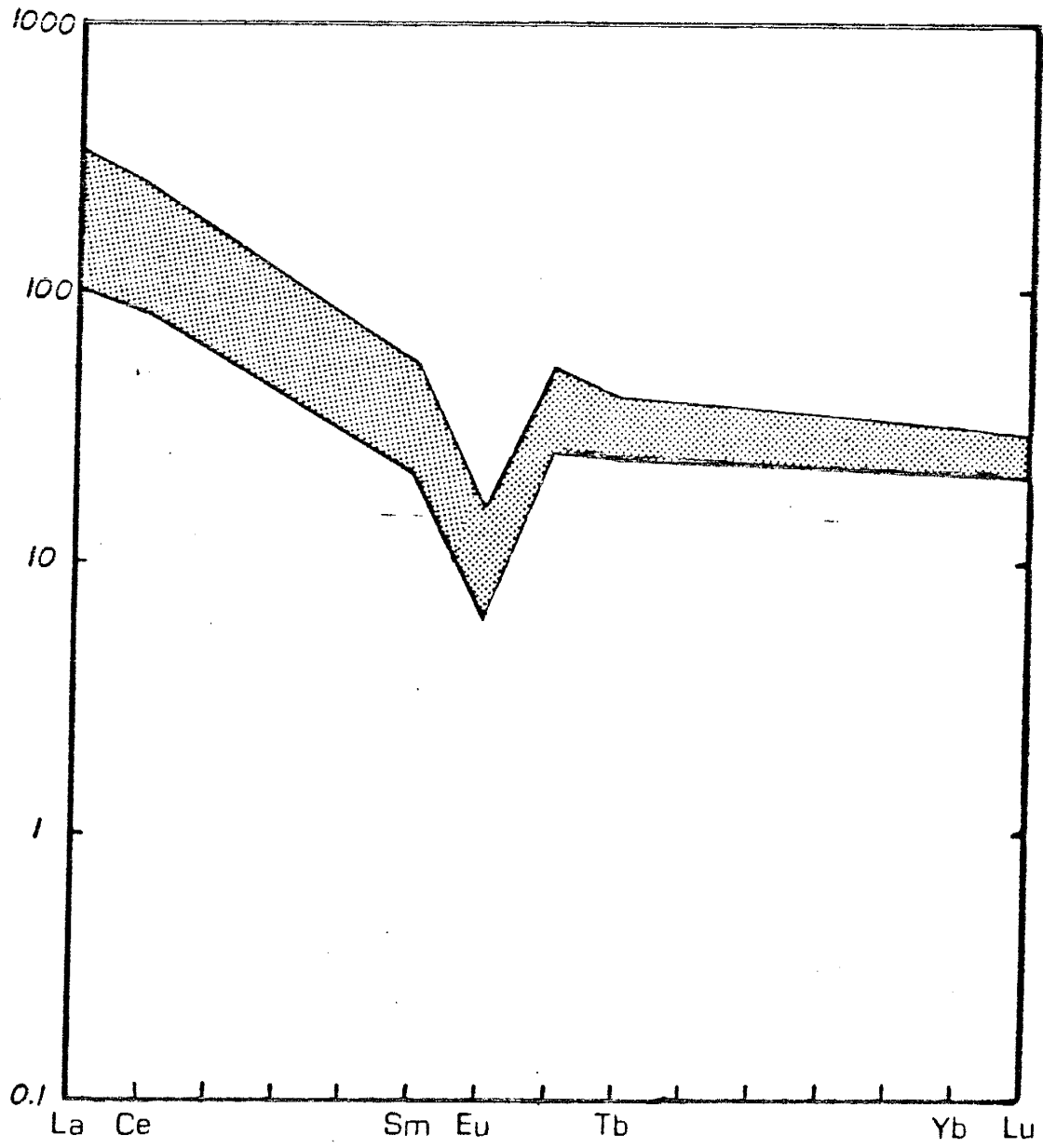
Figure 41: Chondrite normalized REE diagram of the Wet Mountains leucogranites (stippled pattern, range of 5 samples).
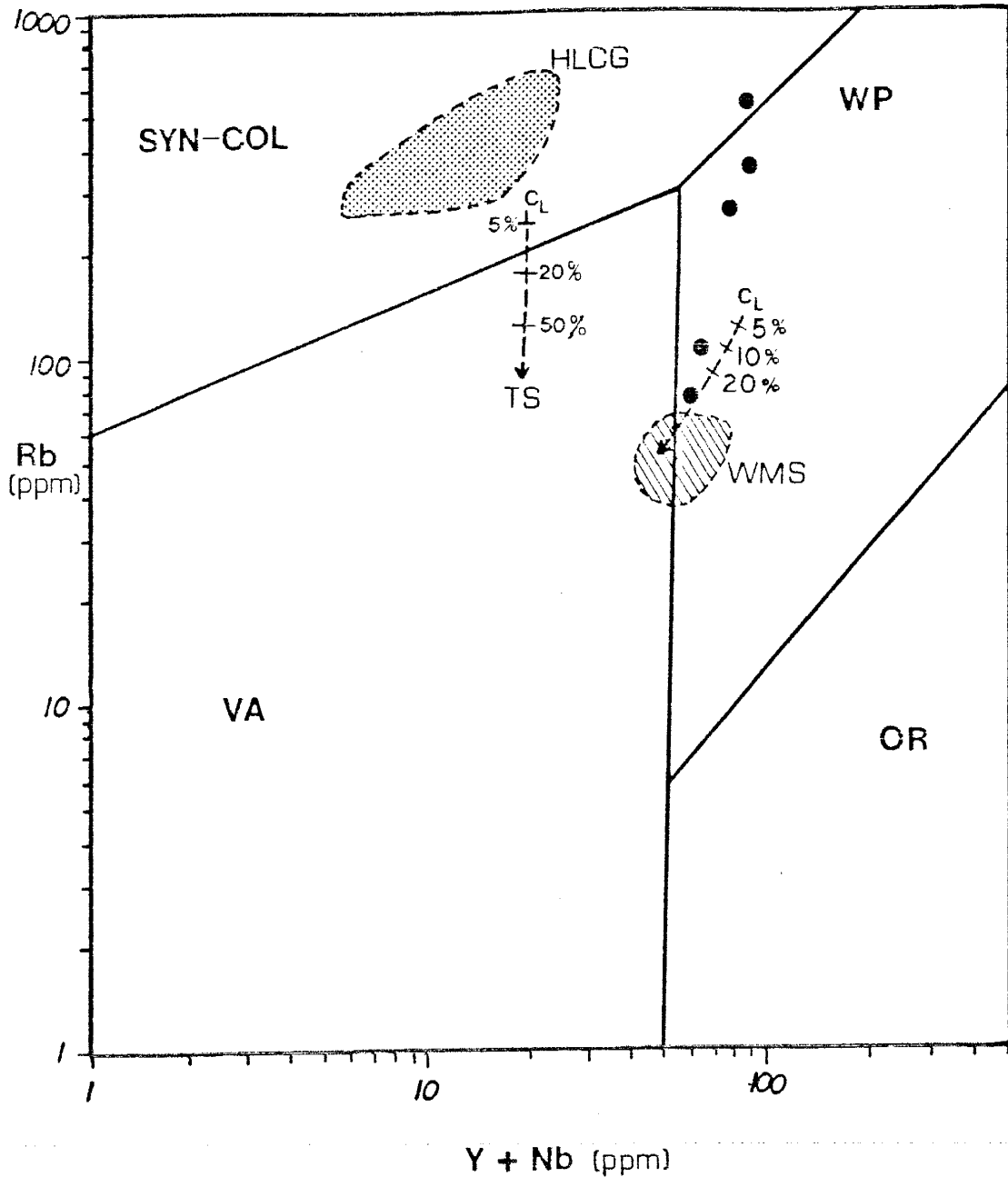
Figure 42: Tectonic discrimination diagram of Rb versus Y+Nb for granites (after Pearce et. al., 1984). Stippled field is for leucogranites from the Bhutan Himalayas (data from Gannser, 1983), TS is average Himalayan leucogranite source material (data from Le Fort, 1981, and Gannser, 1983), WMS is average Wet Mountains paragneisses (diagonal field), solid circles are Wet Mountains leucogranites. Shown are composition of liquids given batch melting of TS and WMS. See text for detailed Explanation.

metasediments of the Wet Mountains are much more enriched in Y and Nb than the gneisses of the Tibetan Slab. Both leucogranites are best explained by volatile induced melting, either from introduced volatile phases or from fluid-absent, dehydration melting (Clemens and Vielzeuf, 1987). It must be kept in mind, however, that "the lower boundary of the syn-collisional granite group is a purely arbitrary one and that collisional granites can plot outside this field if derived from Rb-poor or Nb/Y-rich crust or if the fluid component is small" (Pearce et. al., 1984).

Also, Hall (1987) points out that the greatest intensity of granitic magmatism in collisional zones occurs at the culmination of orogeny, when suturing is complete. This may explain why many of the granites in the Wet Mountains and vicinity show geochemical affinities to "within-plate" granites (Noblett et. al., 1987), and yet appear to be syn-tectonic.

Origin

There are several localities worldwide where similar associations of leucogranites conformably interlayered with high-grade gneisses can be observed. The pink granites of Sri Lanka (Pereara, 1983) form conformable layers within associated metasediments, are folded along with the supracrustal units, similarly to the leucogranites of the Wet Mountains, and layers have an average thickness ranging from a few centimeters to tens of meters.

Gannser (1983) states that the leucogranites of the Bhutan Himalayas are probably derived as anatectic melts from the underlying gneissic-migmatite terrane. As in the Wet Mountains, the leucogranites of the Bhutan Himalayas show a very consistent petrology and chemistry over a wide area, commonly occur as sills that are regionally concordant to sedimentary bedding, and are strikingly uniform

in composition and size, irrespective of thickness, which varies from a fraction of a meter to over one meter. The Manaslu leucogranite, in the Himalayas of Nepal and Tibet, also shows remarkably similar character. Le Fort (1981) has done extensive chemical sampling of the Manaslu pluton and states that these leucocratic rocks are of medium grain size, have a planar disposition defining foliation, and are composed of quartz (30%), plagioclase (35%), potassium feldspar, usually as microcline (30%), and some biotite (3%). The Manaslu leucogranite tends to be aluminum and alkali rich with Q-Ab-An-Or normal compositions close to that of minimum melts at about 2 kbars water pressure and low An contents ($\leq$ 4%). The Manaslu units also show LREE enriched patterns compared to the HREE (La/Yb$\geq$10) and have a clear negative Eu anomaly, a pattern which seems to be characteristic of granitoids of anatectic origin (Cocherie, 1978). The source of the Manaslu leucogranite is most often given as being biotite-garnet bearing metasediments exposed in the Tibetan slab. It's interesting to note that the Wet Mountains also have a preponderance of biotite-bearing paragneisses with similar bulk chemical compositions. Similar relationships are seen in leucogranites from the western European Hercynian complex, the Sveconorwegian complex, and others. Table XII shows some of the occurrences of leucogranites worldwide which seem to show similar associations to those seen in the Wet Mountains.

What all these areas have in common, other than being areas dominated with leucocratic granitic material in association with high-grade metasedimentary gneisses, is that they rely upon collisional tectonic models for the production of the alaskitic granites. In fact, they all fit into what has been referred to as a Himalayan-type, orogenic, granitic association (Middlemost, 1985). During crustal collision, pieces of the overriding plate, usually characterized by sedimentary units, become partially subducted and, during the ensuing crustal thickening, the over-

riden sedimentary package begins to undergo anatectic melting. However, the temperatures and pressures never reach the hypersolvus state and thus only allow for the melting of felsic minerals, resulting in the production of alaskitic magmas. Temperatures and pressures in these zones generally get up to about 730°C and between 5 and 8 kbars pressure. Le Fort (1981) recognized that "such a production of leucogranites seems to be a symptom of *post-collisional* basement thrusting."

A model in which anatectic melting of the metasedimentary gneisses in the Wet Mountains ensues following a collisional event would be a viable model to account for the production of the leucogranites in the Wet Mountains and their genetic association with deformed metasedimentary gneisses. There is evidence of extensive migmatization throughout the area and in some localities restite is exposed, although there are probably great amounts of restite at depth. This model for production of the alaskites also agrees with metamorphic data which suggests that metamorphic temperatures were as high as 900°C.

Jover and Bouchez (1986) provide some suggestions on the origins of the leucogranites of the French Western Massif Central complex which provide some understanding as to why leucogranites in collisional terranes are commonly seen interbedded with paragneisses. In the Massif Central the metamorphic infrastructure is internally "sheared" due to crustal shortening. Leucogranitic magmas would require low degrees of partial melting and the disjunctions along metamorphic or lithologic breaks provide avenues for water loss. In turn, the movement of hydrous fluids along such breaks promotes and restricts anatexis along these zones. The loss of water would tend to promote low degrees of melting even at elevated temperatures, an observation consistent with the anhydrous nature of fluid inclusions observed in the Wet Mountains' granulites. Thus the leucogranites would be issued from the infrastructure, primarily from the biotite-quartz-plagioclase

gneisses due to the low relative solidi of their component phases, and be variously deformed and transposed parallel to bedding.

Zwart (1967) points out that the abundance and composition of granitic rocks in collisional settings will vary as a function of the geothermal gradients of the terrane. Areas with low geothermal gradients would be characterized by high pressure metamorphic facies series, low abundances of granite, and have granites of very low Q and high Ab compositions, such as in the Alps. Belts with medium geothermal gradients, such as the Caledonides, would be associated with medium pressure metamorphic series and have fair amounts of granitic material being produced with low Q and high Ab compositions. In the Variscides of the Hercynian complex, however, a high geothermal gradient predominates, characterized by low pressure metamorphic facies series and abundant granitic magmatism with high Q but low Ab compositions.

Some of these compositional differences are shown on an Ab-Or-Q diagram in Fig. 43. Shown on the diagram are cotectic curves for 0.5 and 10 kbars water pressure and fields of occurrence for granites from Caledonian, Variscan, and Alpine belts and samples from the Wet Mountains. Note that the Wet Mountains samples bear the closest similarity to granites of the Variscan complex and, if the leucogranites of the Wet Mountains are indeed developed in collisional settings, perhaps this may imply they were formed in a collisional setting of high geothermal gradient. Like the Variscan complex, the Wet Mountains contains an abundance of granitic material, most of which tends to be very felsic in composition. This is generally speculation and what these ideas may imply is unclear, but perhaps a high geothermal gradient would be consistent with accretion of an oceanic arc with a continental margin arc, where high geothermal gradients already exist. Alternatively, it may be that the high geothermal gradients are a product of high

concentrations of felsic crust involved in the accretion, with correspondingly high amounts of radiogenic minerals.
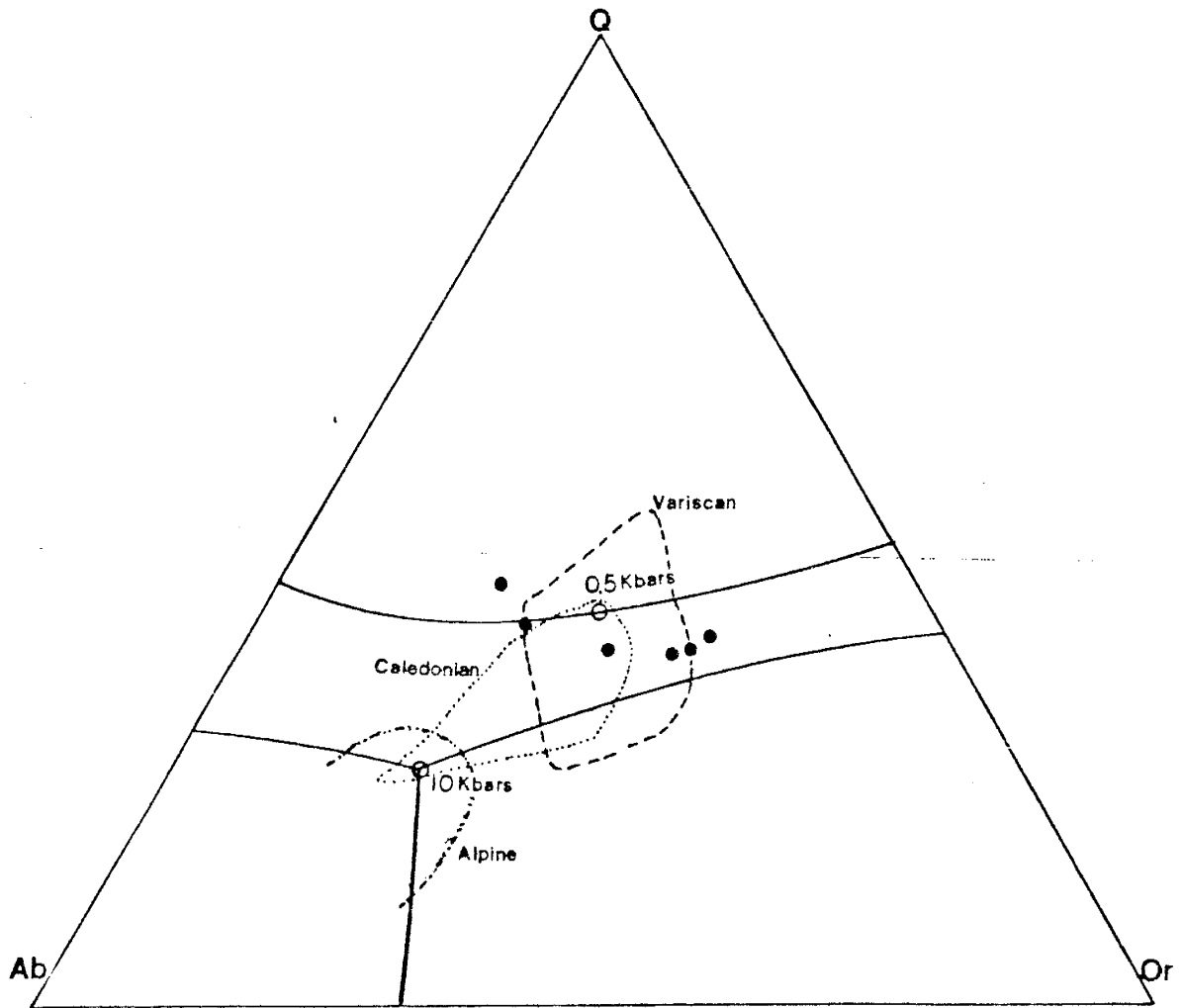
Figure 43: Ab-Or-Q plot of Wet Mountains leucogranites (solid circles) relative to 0.5 and 10kbar (H_2O) cotectics and collisional granites of the Variscan (dashed field), Caledonian (dotted field), and Alpine (dot-dash field) orogenic belts (after Hall, 1987).

Sample	LMT-20	LOC-11	LMT-36	LHS-29	LBM-3	LWC-27
SiO_2	74.92	77.49	72.35	74.13	75.47	77.84
TiO_2	0.18	0.05	0.36	0.37	0.07	0.10
Al_2O_3	13.27	11.99	14.71	13.31	13.45	11.43
Fe_2O_3-T	1.57	0.95	2.08	2.00	1.28	2.14
MgO	0.43	0.38	1.11	0.64	0.36	0.30
CaO	0.91	0.41	3.16	0.75	0.97	0.35
Na_2O	2.71	2.71	5.66	2.27	3.35	4.15
K_2O	6.04	6.50	0.83	6.18	5.11	3.91
MnO			0.03			
P_2O_5	0.05	0.04	0.12	0.08	0.04	0.02
LOI	0.15	0.28	0.06	0.39	0.15	-0.12
Σ	100.21	100.79	100.45	100.12	100.27	100.12
Rb	205.8	117.7	1.2	146.9	120.0	53.3
Ba	607	674	390	1083	547	841
Cs	0.4	0.6		1.6	0.8	0.1
Sr	125.7	110.7	366.6	168.9	99.8	104.1
Pb	40.0	31.8	12.5	43.3	26.9	14.1
Th	30.9	13.1	2.9	15.7	14.4	7.1
U	1.6	1.2	0.8	1.5	3.4	2.5
Sc	3.9	0.7	7.3	3.1	1.9	0.3
V	6.4		16.8	24.8	1.2	
Cr		0.8	1.6	1.1	3.5	0.7
Co	0.6	0.4	1.0	1.3	1.4	1.3
Ni				3.3	1.8	
Y	55.3	9.1	28.6	64.6	16.3	46.5
Zr	206.9	89.7	171.4	363.2	103.1	349.8
Nb	23.1	0.5	10.5	15.7	4.5	17.5
Hf	6.5	4.1	4.9	12.0	5.0	11.5
Ta	1.39		0.77	1.53	0.15	1.28
La	111.1	34.9	21.1	102.3	15.3	12.1
Ce	221.5	74.9	50.5	245.0	27.9	51.5
Sm	10.02	3.86	4.82	15.12	2.36	4.98
Eu	1.12	0.42	1.03	1.32	0.61	0.42
Tb	1.28	0.41	0.67	1.92	0.33	1.14
Yb	4.42	0.22	2.92	6.28	0.80	6.07
Lu	0.71	0.06	0.51	0.90	0.14	0.95

Table XI: Geochemistry of granites

Table XII: Occurrences and natures of collisionally derived leucogranites worldwide

Intrusions	Locality	Nature	Association	Tectonic Setting	Age	Reference
Varberg Alaskites	SW Sweden	Granitic sills parallel foliation; from anatexis of surrounding gneiss	Quartzofeldspathic paragneisses, charnockites	Sveconorwegian continental collision	c. 900–1100Ma	Quensel, 1951; Hubbard, 1975
Vijayan Leucogranites	Sri Lanka	Conformable granitic sheets; from anatexis of paragneisses	Granulites, migmatites, biotite paragneisses	Vijayan complex continental collision	c. 1250Ma	Perera, 1983; Munashige & Dissanayake, 1980
Himalayan Leucogranites	Nepal	Lenticular sheets and concordant sills; from anatexis of paragneisses	Metasedimentary gneisses	Himalayan-Tibetan continental collision	c. 20Ma	Vidal et. al., 1982; Gansser, 1983; Le Fort, 1981
Hercynian Leucogranites Variscan Complex	France	Autochtonous and conformable lenses; from anatexis of metasediments	Metasediments, granulites	Hercynian continental collision	c. 300Ma	Vidal et. al., 1984; Jover and Bouchez, 1986; Matte, 1983
Leucogranites of the Main Range	Malaysia	Foliated leucogranites derived from anatexis of crust	Associated with isoclinally folded Paleozoic metasediments	Arc collision	c. 200Ma	Mitchell, 1978
Rössing Alaskite	Namibia	Alaskitic pods and dikes generally concordant to foliation; from anatexis of metasediments	Metasediments, migmatites, and occasional granulites	Pan-African continental collision (Damara mobile belt)	c. 500Ma	Berning et. al., 1976; Jacob, 1978
Erzgebirge Granites	SW England	Foliated leucogranites and alaskites; anatexis of metasediments	Associated with metamorphosed and deformed metasediments	Continent-continent collision	c. 350Ma	Mitchell, 1978; Mitchell, 1974
Kabbaldurga Leucogranites	S India	Foliated leucogranites; from migmatization of metasediments	Closely associated with charnockites and metasediments	Continent-continent interface	c. 2670Ma	Janardhan et. al., 1982
Rauer Isl. Leucogneiss	E Antarctica	Irregular and folded lenses; from partial melting of metapelites	Associated with metapelites and granulites	Continental collision	c. 1100Ma	Harley, 1987

Granulites

Field Relationships

The granulites of the Wet Mountains are generally confined to an area within the Mount Tyndall quadrangle, with some minor occurrences in the Westcliffe and Royal Gorge quadrangles. The most detailed work thus far on the granulite facies units in the Wet Mountains has been done by Brock and Singewald (1968), who referred to these units as charnockites. Although strict usage of the term charnockite refers to granulites of dominantly granitic composition, over the years the term has become more flexible and, as a consequence, is used here interchangeably with the term granulite when referring to this rock type. Admittedly, the granulites of the Wet Mountains are, for the most part, substantially granitic in composition (more specifically, tonalitic), but portions of the granulitic terrane can be mafic, intermediate, or even calcic.

The granulites occur as units parallel to the regional foliation, generally restricted to a ridge 2km wide which strikes from 470800mE-4225400mN to 477000mE-4231200mN, using the Universal Transverse Mercator (UTM) system. These units tend to be extremely contorted and Brock and Singewald (1968) note that the charnockites "form layers and erratically ramifying masses of indefinite shape." In hand specimen, the granulites can be identified by their dull brown color, medium grain size, and greasy luster. Although domminantly tonalitic in bulk composition, mafic, such as CH-5, and calcareous, such as LMT2-2, varieties also exist.

The relationship of the granulites to the surrounding amphibolite grade terrane is complex. Commonly the granulites are surrounded by granitic gneisses but the

possibility that the charnockites are xenoliths within granitic material seems low due to the similarity in structural fabric over the amphibolite-granulite boundary and the apparent continuous transition which is observable in some localities. In fact, the presence of varied lithologies in the granulite terrane commensurate with high-grade metabasic, metasedimentary, and calc-silicate rock types strongly suggest that the amphibolite and granulite zones are derived from the same protoliths and that the differences in grade are results of complex variations in metamorphism over the area.

U-Pb dating on the zircons from a charnockite sample (approximately at the location of LMT-1) yields an age of 1694 ± 25Ma (Bickford, 1986). Bickford states that the zircons from the sample are exceptionally clear and euhedral, suggestive of recrystallization during high-grade metamorphism, which is common at granulite grades. This may imply that the date may be representative of the age of granulite facies metamorphism.

Petrography

Metabasites typically contain plagioclase, hornblende, orthopyroxene, and magnetite whereas metasediments commonly contain plagioclase, K-feldspar, garnet, hornblende, and clinopyroxene. Plagioclase is generally sodic (An_{28}) except in metasediments which appear to have calcareous protoliths (such as CH-3). Similarly, garnet is generally almandine in non-calcareous rocks, but is grossular otherwise. Granoblastic textures are common and foliation, while always present, is generally more poorly developed than in the amphibolite grade gneisses. The granulites are typically medium grained, equigranular, and occasionally display partial segregation of dark minerals into small lenses or laminae, imparting a spotted nature to the rock. In thin section, well preserved symplectic and reaction textures

are observable which allow reasonable characterization of equilibrium reactions. Some of these assemblages appear to be retrogressive in origin and generally occur closer to the edge of the granulite facies terrane while samples closer to the axis of the granulite terrane are more characteristic of granulite facies mineralogies. Detailed petrologic descriptions are given in the section on metamorphism since the observed textures are critical in deciphering the nature of the regional metamorphism.

Fluid Inclusions

Polished wafers were made of samples LMT2-2 and CH-2 to study the fluid inclusions. Wafers were ground to about 0.3mm thickness and polished on both sides to a 0.3μm polish. Thermometric studies of the fluid inclusions were made on a Linkam TH600 heating-freezing stage on twenty inclusions which proved large enough for precise study. The inclusions are typically dark brown in color, almost exclusively monophase at room temperature, acicular or occasionally elliptical in form, and generally elongated in the direction of the host-crystal. Most commonly they are 0.05mm by 0.01mm in size but occasionally they are found as large as 0.1mm and it is generally these larger inclusions which were used in thermometric analysis (Fig. 44).

The inclusions were initially cooled to −150°C to freezing and then slowly heated[1]. Fig. 45 is a histogram showing melting temperatures of the solid phase in the inclusions (T_m), which averages −58°C. At this temperature the inclusions melt from a monophase solid to a liquid-rich, two-phase inclusion (liquid +

---

[1]It was necessary to cool this low since the nucleation of vapor and solid is commonly metastably suppressed, depending on the cooling rate and the size of the inclusion.
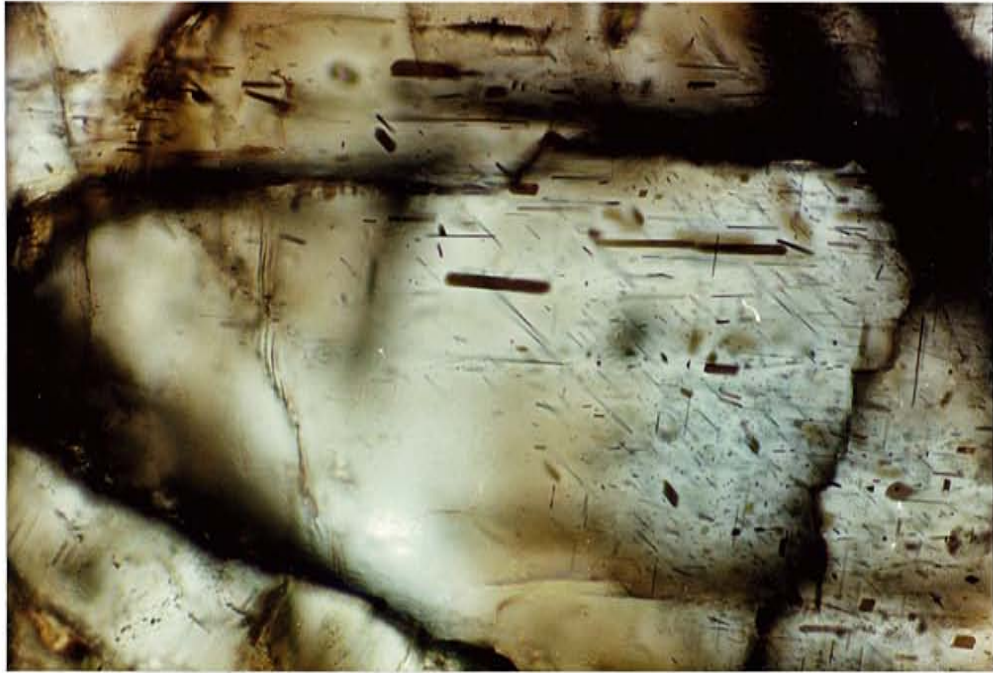
Figure 44: Photomicrograph of CH-5 showing dark, acicular, CO_2 rich fluid inclusions in quartz. Doubly polished wafer, scale 1cm=0.025mm, plain polz. light.

vapour). The triple point for pure CO_2, however, is $-56.6°C$ and it seems probable that methane may be complexed with the CO_2 in the inclusion. This is quite common in granulite terranes (Newton, 1986) and generally results in the lowering of the CO_2 triple point by about 1°C per 5mol% CH_4. Thus, an average T_m of $-58°C$ may imply that as much as 10mol% CH_4 may be complexed with CO_2 in the inclusions.

Upon further heating the two-phase (L+V) inclusions homogenize into monophase (L) inclusions at a temperature (T_h) of about $-38°C$. Assuming a pure CO_2 system to simplify calculations, since the systematics of the CO_2-CH_4 system are poorly known, it is possible to calculate the density of the fluid in the inclusions. Using the P-T diagram developed by Touret and Bottinga (1979) for phase boundaries of CO_2 and isochores (Fig. 46), a T_h of $-38°C$ implies a fluid density (ρ_{CO_2}) of about 1.10 g/cm^3. It is now possible to use the $\rho = 1.10 g/cm^3$ isochore to deduce an entrapment pressure for the fluid (P_e).

Since petrographic studies show that scapolite occurs as a prograde assemblage in the granulite facies, and since it is only stable above 875°C, it's possible to use this temperature in conjunction with the 1.1g/cm^3 isochore to deduce an entrapment pressure. A temperature of 875°C intersects the 1.1g/cm^3 isochore at a P_e of 9kb (Fig. 46). However, Newton (1986) cautions that neglecting 10mol% CH_4 in a CO_2-rich inclusion may result in an overestimation of P_e in a granulite by about 1kb. Thus it is probably most accurate to say that the metamorphic conditions under which these fluids were entrapped would have been about 850°C and about 8kb pressure, well within the conditions for granulite facies metamorphism.
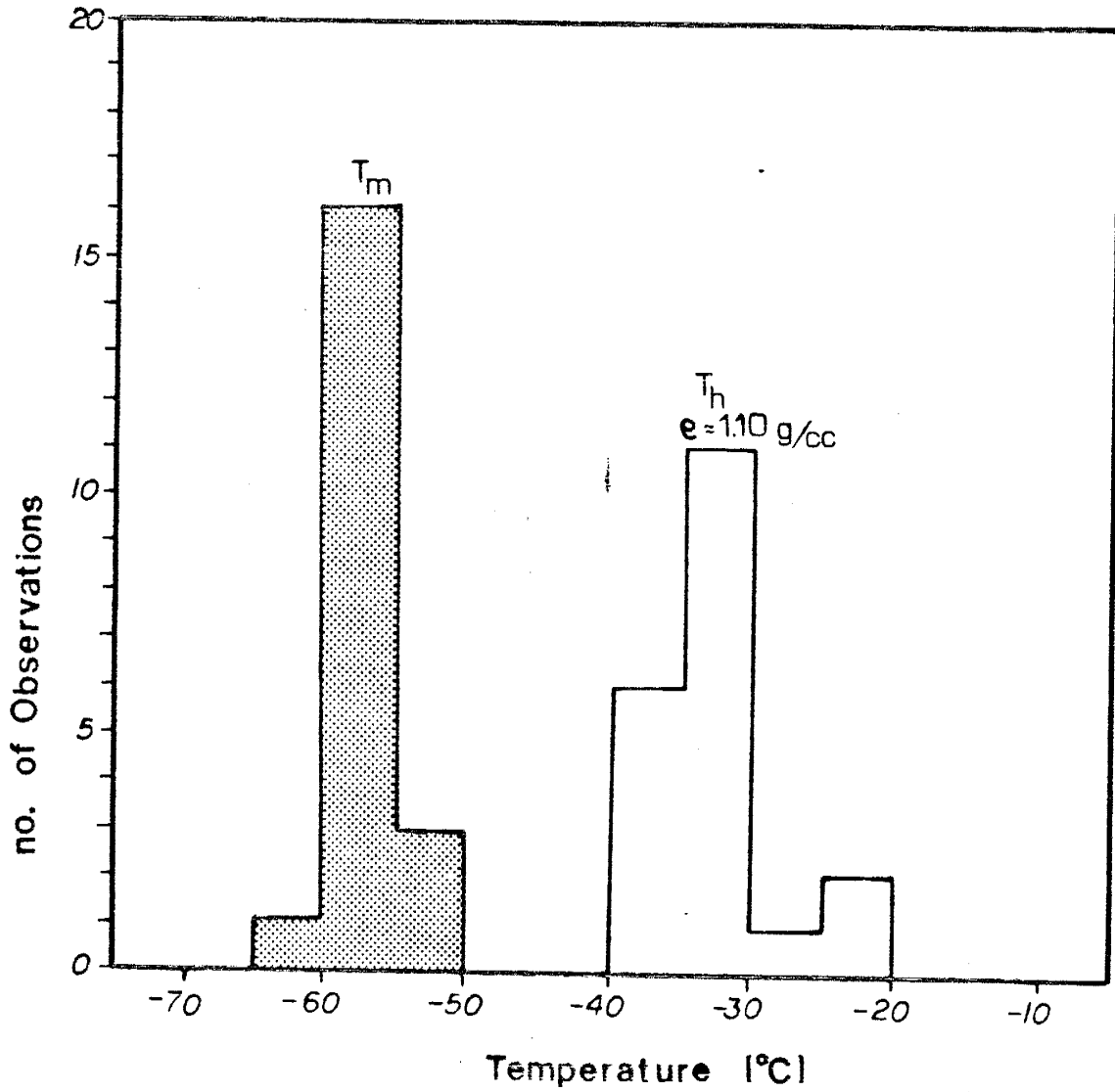
Figure 45: Histogram of fluid inclusion data. Stippled pattern is temperature of melting of the inclusion phase (T_m, $S \to L + V$), white pattern represents temperature of homogenization (T_h, $L + V \to L$) and deduced inclusion density (ρ).
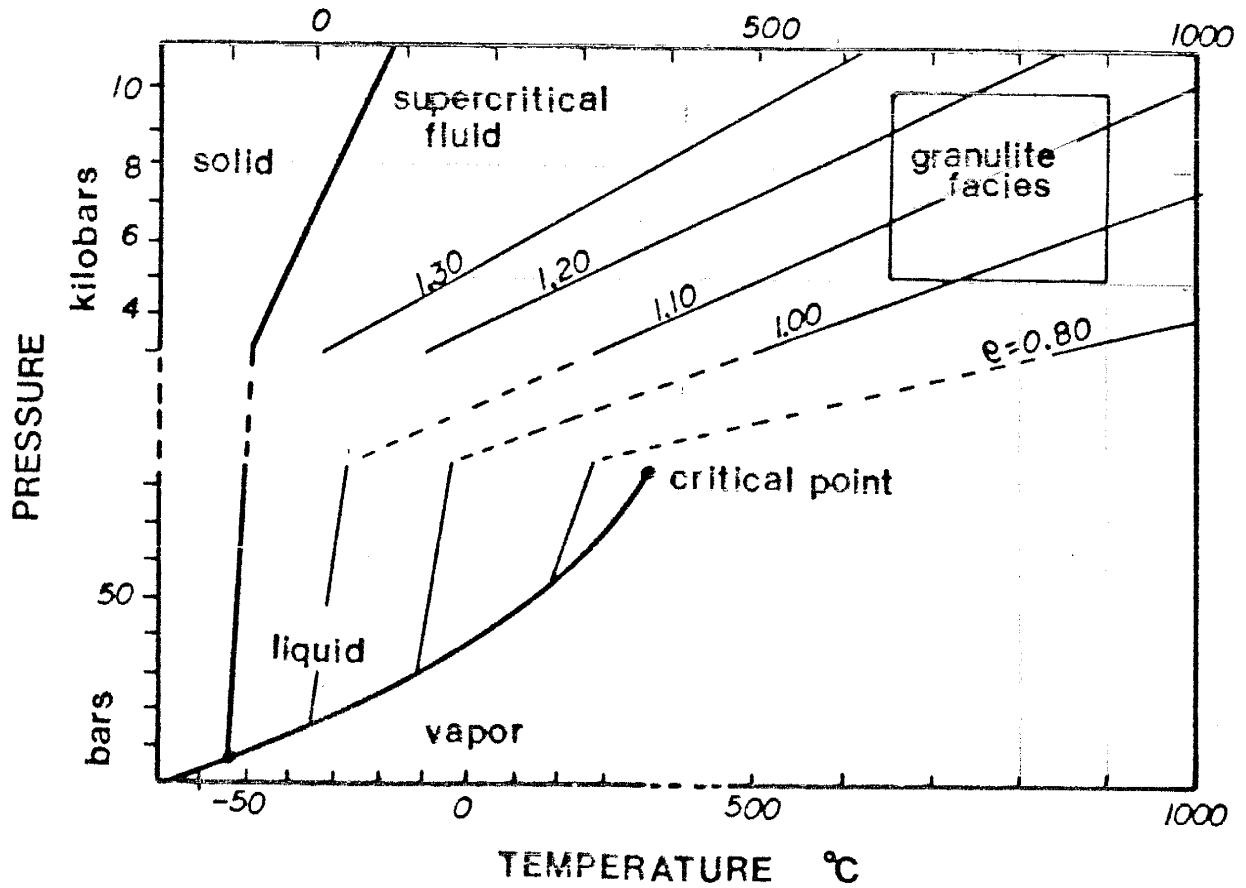
Figure 46: Phase boundaries of CO_2 and isochores from modified Rudlich-Kwong equation (after Newton, 1986). Box represents typical P-T conditions in granulite facies rocks. Shown are fields where solid, liquid, and vapor CO_2 are stable and the critical point above which liquid and vapor CO_2 coexist as a supercritical fluid. All isochores (unbold lines) are in g/cc.

Geochemistry

Only four samples of granulite have been analyzed chemically but samples were chosen to give a somewhat representative geochemical overview of the granulite facies terrane. Major elements were analyzed for LMT-1, CH-1, CH-5, and LMT2-2 and selected trace elements were analyzed for LMT-1, CH-1, and LMT2-2, shown in Table XIII. Samples CH-1 and CH-2 were microprobed at the University of Chicago's ARL fully automated EDS microprobe facility (Newton, personal comm., 1984), shown in Table XIV.

Samples CH-1 and LMT-1 are representative of the granulites with tonalitic bulk-compositions, sample CH-5 is representative of the metabasic varieties, and LMT2-2 of the calc-silicates. Table XIII shows bulk-chemical analyses of these granulites and Table XIV shows the microprobe data for CH-1 and CH-2.

As in the high-pressure granulites of India and Scotland, incompatible elements such as Rb, Pb, Cs, K, Th, and U are strongly depleted in the granulites in comparison to the amphibolite grade gneisses (Fig. 47). Condie and Allen (1984) suggest that these elements are very soluble in fluids with high CO_2/H_2O ratios in high pressure granulites only (8–10Kb). These fluids also raise the solidus temperatures of the granulites so as to prevent partial melting. The high pressure depletions in these elements agrees with fluid inclusion data which suggests that entrapment pressures were >8Kb. Interestingly, the diagram also points out that the leucogranites are strongly enriched in LILEs and may imply that these anatectic melts may play a role in mobilizing aqueous fluids in the surrounding gneisses and thus provide a pathway for depletion of these elements in the granulites.

The REE distributions in the Wet Mountain's granulites are similar to those reported in other granulites (Condie and Allen, 1984; Weaver and Tarney, 1980).
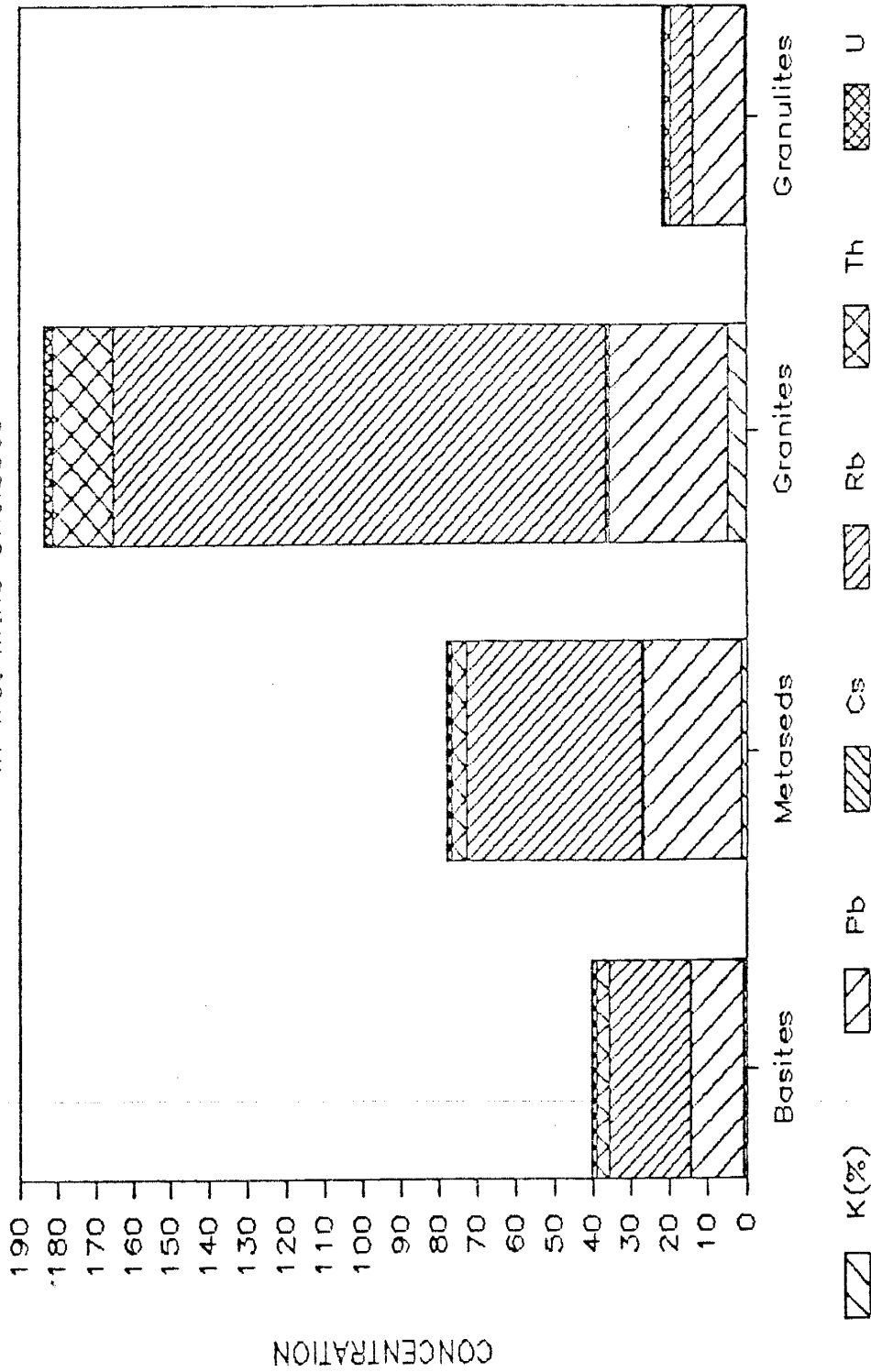
Figure 47: Histogram showing relative concentrations of large ion lithophile elements (LILEs) in metabasites (12 samples), metasediments (12 samples), leucogranites (5 samples), and granulites (2 samples). Note depletions in LILEs in granulites and enrichments in LILEs in leucogranites.

The granulites have light-REE enriched patterns (Fig. 48) with Eu anomalies that are slightly positive, except for LMT2-2.

The lack of extensive geochemical data for the granulites would make conclusions regarding element mobility somewhat premature but preliminary evidence does suggest that the granulites are geochemically similar to granulites from other high-grade terranes and have not seen significant mobilization of the REE and HFSE. The mineralogic variations in the granulites suggest the presence of varied protoliths, commensurate with a model in which the metasediments and amphibolites of the surrounding amphibolite facies terrane are metamorphically lower grade equivalents of the granulites. The metabasites may represent high-grade equivalents of the amphibolites, the tonalitic gneisses may be high-grade equivalents of the metasediments, and the calc-silicates high-grade equivalents of the calcareous units.

Microprobe Data

The microprobe data, Table XII, shows that the tonalitic varieties of granulite are composed of virtually unzoned, Fe-rich minerals, a conclusion verified by the petrographic studies. The orthopyroxene seems to be ferrohypersthene (En_{34}), the amphibole appears to be ferrohastingsite (SiO_2 43–37%, FeO/MgO> 2), and plagioclases tend to be andesine (An_{28}) in composition.
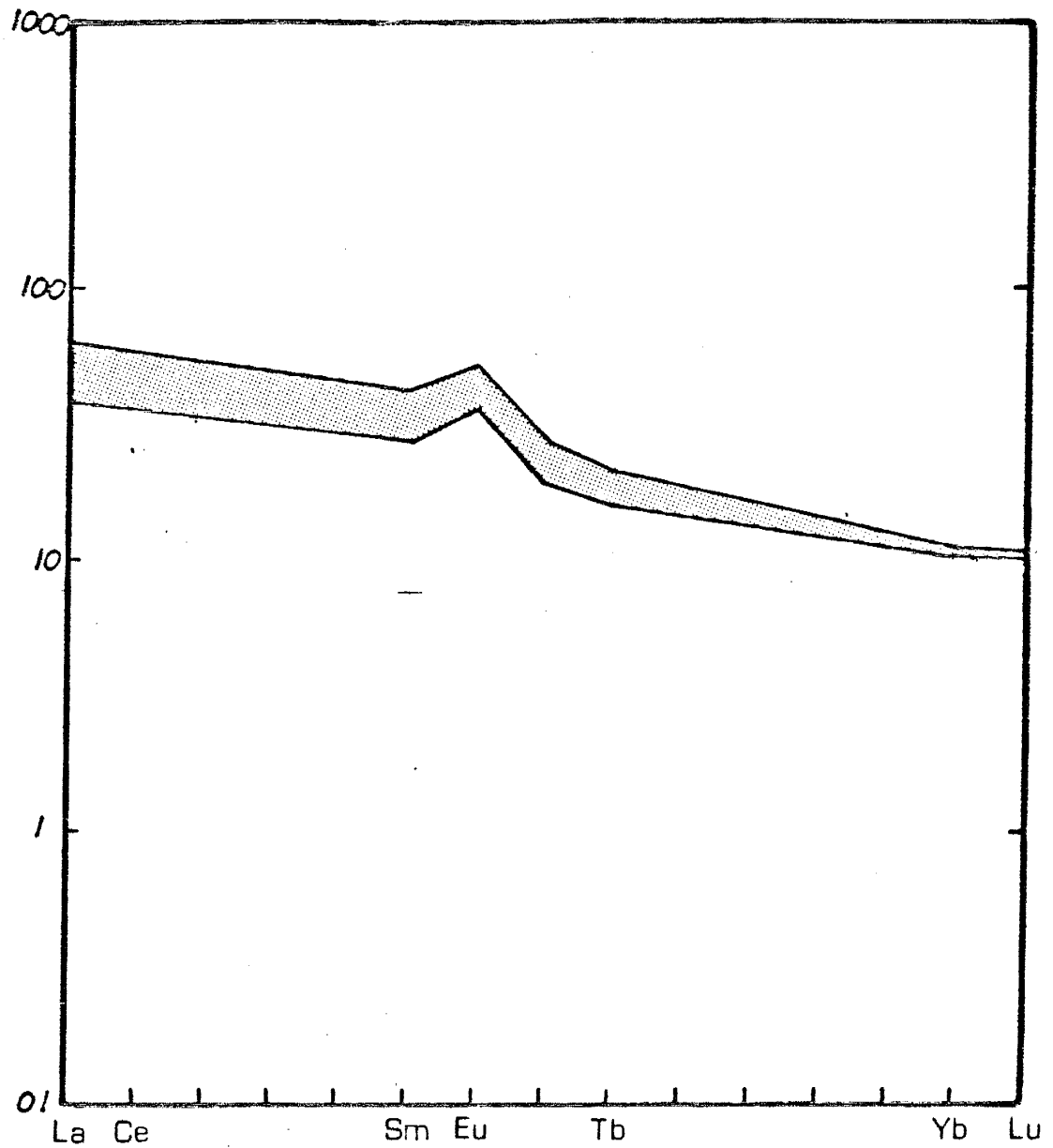
Figure 48: Chondrite normalized REE plot of granulite facies rocks from the Wet Mountains. Stippled pattern range of 2 samples.

Sample	LMT-1	CH-1	CH-5	LMT2-2
SiO_2	57.82	57.01	54.97	44.98
TiO_2	0.89	0.98	0.31	0.58
Al_2O_3	18.53	19.05	22.17	16.64
Fe_2O_3-T	8.31	9.52	5.48	6.51
MgO	1.63	1.69	1.03	1.96
CaO	4.68	5.13	11.00	19.64
Na_2O	6.30	4.83	5.95	1.73
K_2O	0.86	0.93	0.20	0.28
MnO	0.23	0.25	0.07	0.09
P_2O_5	0.23	0.27	0.04	0.49
LOI	-0.09	0.24	-0.49	2.12
Σ	99.39	99.90	100.73	95.02
Rb	1.1			10.4
Ba	950	952		32
Cs				0.33
Sr	535.1			535.0
Pb	13.4			
Th		0.1		3.1
U	0.2	0.3		0.7
Sc	16.4	26.0		13.11
V	29.0	24.2		
Cr	5.9	29.0		63.8
Co	5.0	8.0		15.3
Ni	2.0	33.0		69.0
Y	25.5			
Zr	338.6			200.0
Nb	5.1			
Hf	8.0	9.5		2.8
Ta	0.36	0.46		0.89
La	13.6	21.0		28.3
Ce	31.0	49.0		70.2
Sm	4.98	7.56		6.95
Eu	2.52	3.65		1.52
Tb	0.75	1.10		0.91
Yb	2.07	3.20		3.34
Lu	0.35	0.46		0.59

Table XIII: Geochemistry of granulites

Wt%	OPX		AMPH		BIOT		PLAG	
	CH1	CH2	CH1	CH2	CH1	CH2	CH1	CH2
SiO_2	50.56	50.05	40.78	40.21	35.52	34.68	61.07	61.42
TiO_2	0.00	0.00	2.35	2.29	6.14	6.50	0.00	0.00
Al_2O_3	0.74	0.61	11.66	11.11	14.57	14.24	24.11	23.82
FeO	30.76	31.99	20.29	20.48	20.07	21.75	0.00	0.00
MnO	2.43	1.86	0.00	0.00	0.00	0.00	0.00	0.00
CaO	0.75	0.67	12.70	12.36	0.00	0.00	5.68	6.09
Na_2O	0.00	0.00	1.13	1.18	0.00	0.00	7.55	8.36
K_2O	0.00	0.00	1.80	1.80	10.23	9.79	1.81	0.42
Cl	0.00	0.00	0.35	0.79	0.32	0.63	0.00	0.00
Σ	101.14	99.71	99.45	97.61	96.38	96.29	100.24	100.13
							An27.2	An29.0

Table XIV: Microprobe data for CH-1 and CH-2
[Data from Newton, pers. comm.]

Metamorphism

This section details some of the aspects of the regional metamorphism of the mafic, pelitic, and calcareous gneisses. The mineral parageneses found in the mafic lithologies are:

- hornblende + plagioclase

- hornblende + plagioclase + biotite

- orthopyroxene + plagioclase

- orthopyroxene + clinopyroxene + plagioclase.

The orthopyroxene bearing units are characteristic of the metabasites of the granulite facies terrane while those devoid of orthopyroxene are commonly amphibolite grade. These relationships are shown schematically in ACF projection on Fig. 49. Rock analyses plotted on the ACF diagrams show that amphibolite grade metabasites plot primarily along the plagioclase-hornblende tie-line while granulite facies metabasites plot close to the plagioclase-orthopyroxene tie.

Parageneses in the pelitic rocks include:

- biotite + plagioclase

- biotite + plagioclase + orthoclase

- biotite + plagioclase + sillimanite

- biotite + plagioclase + garnet

- plagioclase + garnet + hornblende

- plagioclase + clinopyroxene
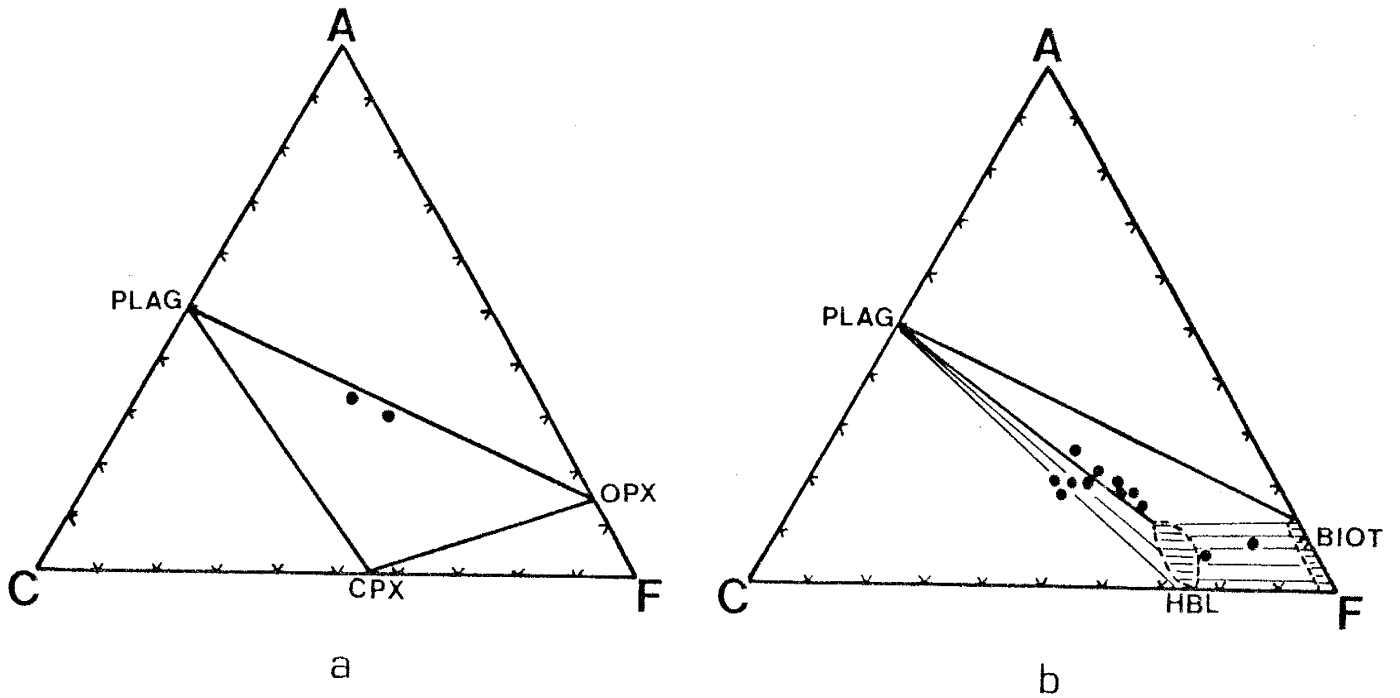
Figure 49: ACF projection of minerals found in the metabasites of granulite (a) and amphibolite (b) grade and rock analyses.

- plagioclase + clinopyroxene + garnet.

The metasedimentary gneisses in the granulite terrane commonly contain clinopyroxene whereas amphibolite grade metasediments generally are devoid of clinopyroxene. These assemblages are shown in ACF projection in Fig. 50. The amphibolite grade metasediments plot within garnet-biotite-plagioclase and plagioclase-biotite-sillimanite subtriangles but primarily along the plagioclase-biotite tie. Granulite facies metasediments lie in the garnet-clinopyroxene-plagioclase subtriangle, close to the plagioclase-clinopyroxene tie.

The calc-silicate gneisses have parageneses of:

- clinopyroxene + plagioclase + epidote

- scapolite + clinopyroxene + garnet.

The scapolite bearing varieties seem to be characteristic of granulite facies assemblages but only two calc-silicate gneisses were studied in any detail.

Some minerals, such as hornblende (Miyashiro, 1973) and biotite (Hyndman, 1972), are known to undergo changes in Z-absorption colors as a function of increasing metamorphic grade. With hornblende there seems to be a systematic change in the Z-absorption color from blue-green to green to brownish-green to brown as metamorphic grade increases, a phenomenon generally attributed to the increase in TiO_2 in hornblende as a function of increasing metamorphic grade. In the Wet Mountains the preliminary data seems to suggest a systematic change in the colors of hornblende moving east across the study area from the Beckwith Mountain quadrangle to the Mount Tyndall quadrangle. Hornblendes from the Westcliffe and Beckwith Mountain quadrangles are generally blue-green (LBM-2 and LWC-20) but become increasingly green (LWC-28 and LMT2-3) and then
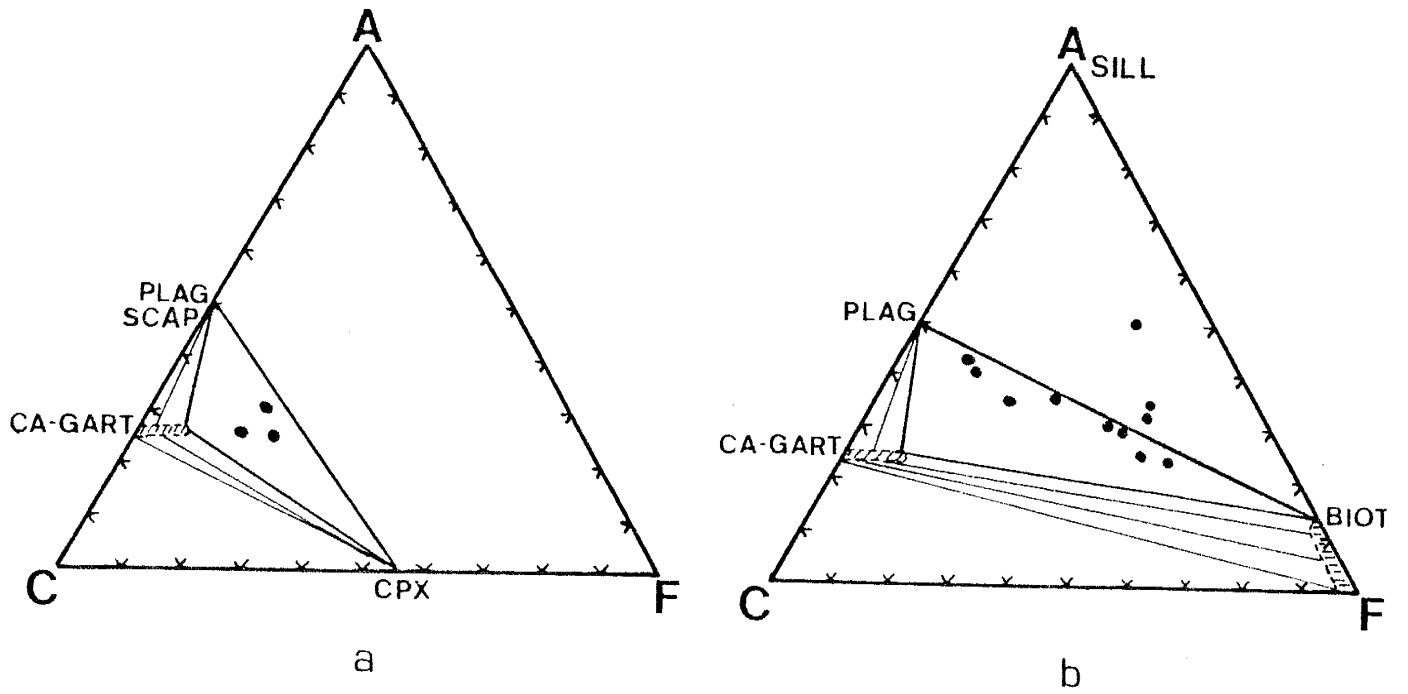
Figure 50: ACF projection of minerals found in metasediments of granulite (a) and amphibolite (b) grade and rock analyses.

brown closer to the granulite terrane (LMT-1 and CH-1). Similar relationships can be seen in biotite since in low grade metamorphic terranes this mineral has a green color and in higher grade areas it goes to brown and then deep red. The color change in biotite is a function of the increasing titanium content and $Mg/(Mg+Fe^{+2})$ ratio with increasing metamorphic grade. On the western edge of the study area the biotites are light brown (LWC-9 and LWC-5) but become dark brown (LMT-41 and LMT-53) and reddish-brown closer to the granulite terrane (CH-2). These relationships may suggest that the metamorphic grade increases from the western edge of the area east towards the granulite facies terrane. East of the granulite terrane, past the Ilse fault, hornblendes are green (LHS-36), biotites are brown (LHS-30), and mineral assemblages are commensurate with amphibolite metamorphic grades. To what degree these relationships represent prograde or retrograde effects is unclear. Certainly retrogression is occurring, but it is difficult to establish how large an area has been retrogressed from granulite to amphibolite grades.

Figs. 51, 52, and 53 represent the observed stability ranges of some important minerals in the metasedimentary, metabasic, and calc-silicate gneisses. The presence of green and brown hornblendes, plagioclase of intermediate composition ($> An_{20}$), almandine garnet, and occasional sillimanite and diopside suggest that the majority of the terrane is of the amphibolite grade. The occasional presence of sillimanite would imply, in a standard Barrovian pattern at moderate pressure, that the assemblages are in the upper portion of the amphibolite facies (higher temperature part). The occasional transition into migmatites seems to corroborate this viewpoint (implies that $P_{H_2O} = P_{lith}$).

The granulitic rocks, by comparison, tend to be coarser grained and lack micaceous minerals and hornblende, for the most part. It seems these units have

FACIES MINERALS	Amphibolite	Granulite
Plagioclase	An > 35	
K feldspar	Orthoclase	
Biotite		
Garnet		
Hornblende	grn	
Clinopxn		
Sillmanite		
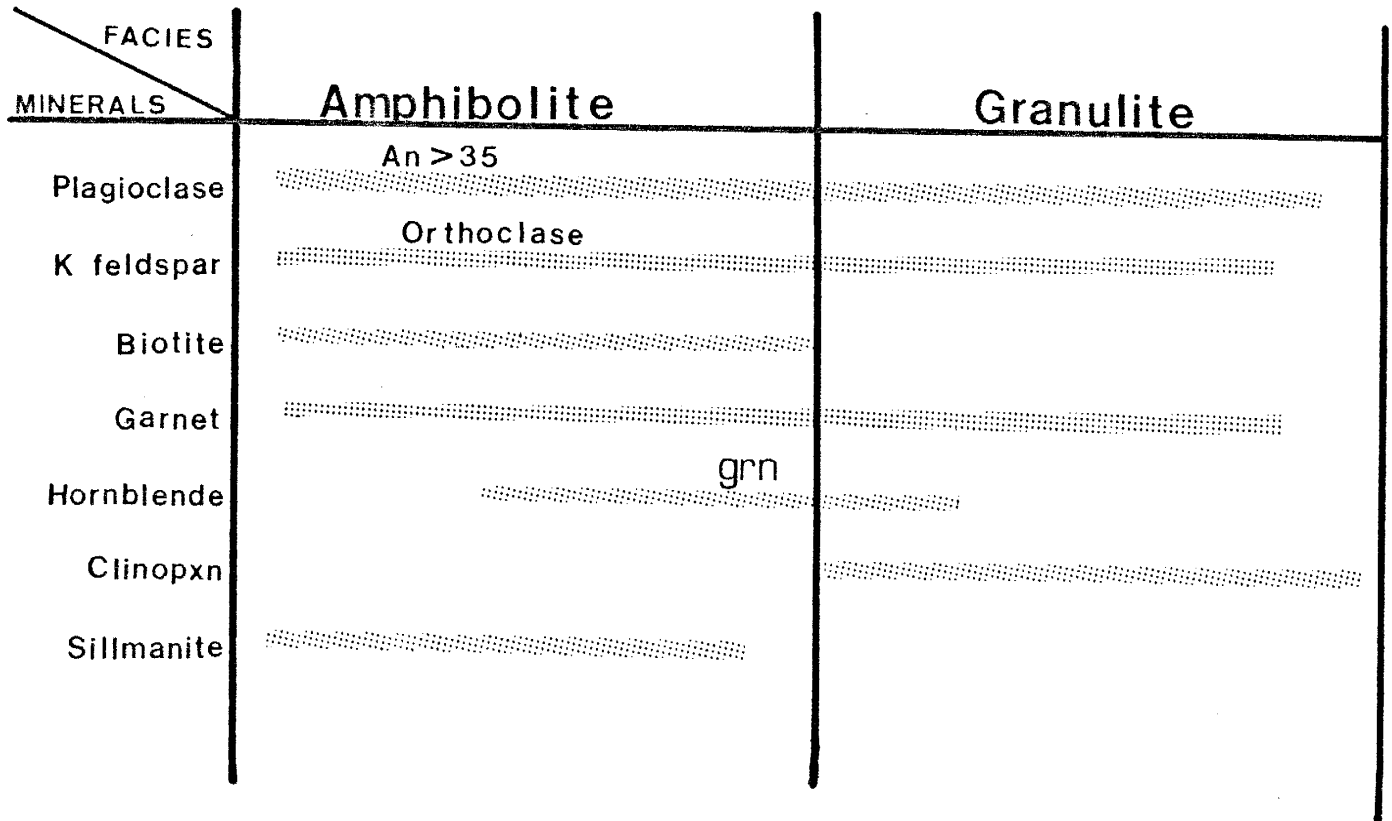
Figure 51: Paragenetic diagram showing the stability of various mineral phases in the metasedimentary gneisses at amphibolite and granulite grades. Also shown is hornblende color and anorthite composition.

112

FACIES MINERALS	Amphibolite		Granulite
Plagioclase	An>30		
Hornblende	blu-grn	grn	brwn
Magnetite			
Orthopyroxene			

Figure 52: Paragenesis of metabasic gneisses from amphibolite to granulite grades
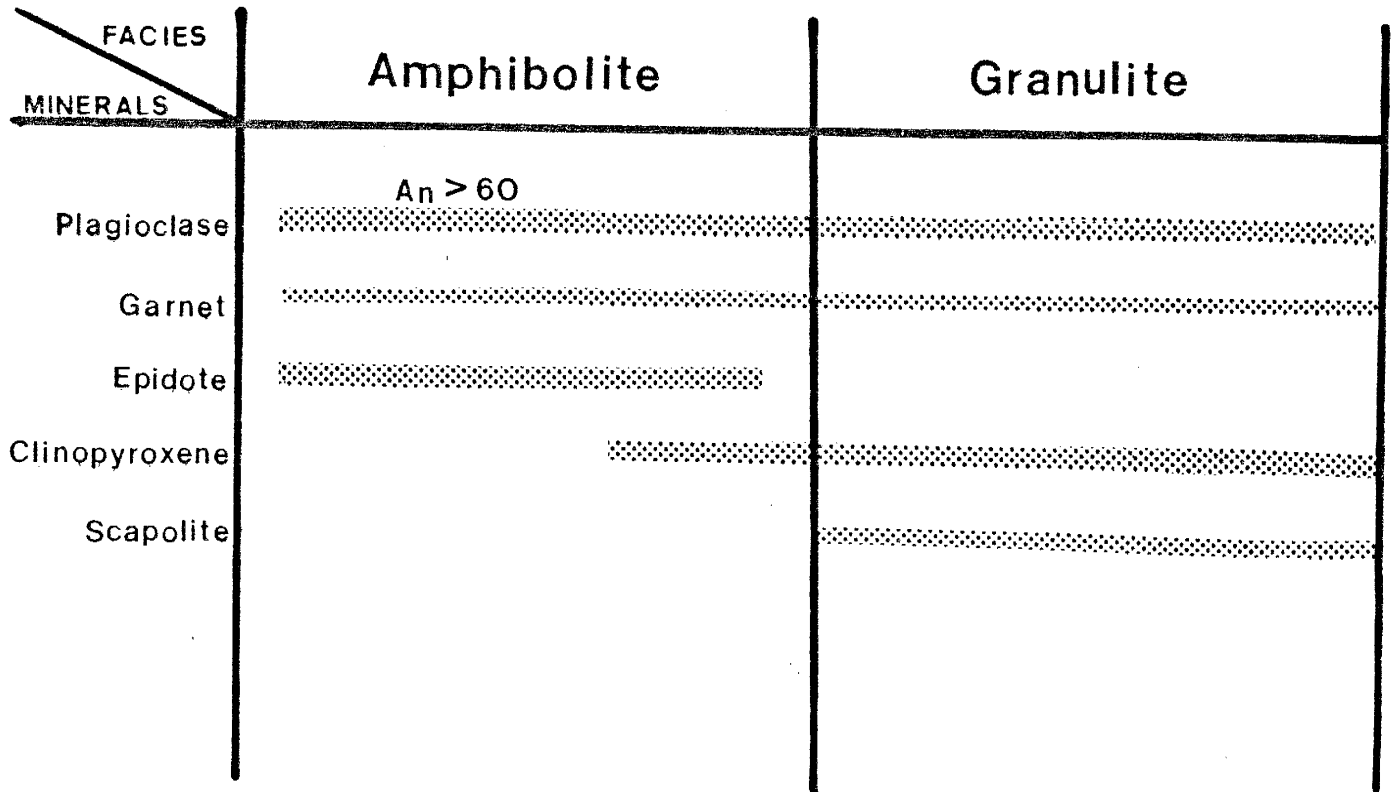
Figure 53: Paragenesis of calc-silicate gneisses from amphibolite to granulite grades

exceeded the P-T stability levels for biotite and hornblende and are essentially an-hydrous and clinopyroxene, and orthopyroxene, commonly as diopside, ferrosalite, and hypersthene-bearing, although garnet, as almandine, and scapolite also occasionally occur.

Determination of P-T relationships in the metamorphic rocks is generally restricted to petrographic observations. In the amphibolite grade gneisses the dominant aluminosilicate tends to be sillimanite and in some units (LHS-30) sillimanite is stable with biotite and aqueous inclusions. Furthermore, the amphibolite facies rocks, in particular the metasediments, are commonly migmatitic. The minimum melting curve for alkali feldspars (Ehlers and Blatt, 1983), $(K,Na)Si_3O_8$, where Al_2SiO_5 + biotite + H_2O is stable would be above $\sim 650°C$ and $\sim 4kb$ pressure (Fig. 54).

Fig. 55 is a schematic representation of a portion of Brock and Singewald's (1968) geologic map of Mount Tyndall with the geology and sample locations of the granulites superimposed. Samples closer to the center of the granulite terrane are much more characteristic of the granulite facies than those along the edge. Sample CH-2, for instance, is from the edge of the granulite terrane and in thin-section (Fig. 56) displays a characteristic granulite facies assemblage of orthopyroxene (10%), plagioclase (35%), quartz (20%), and magnetite (5%). The texture is dominantly heterogranular and granoblastic but minerals such as hornblende (20%) and biotite (10%) in the sample tend to display post-kinematic textures. The biotite in particular shows a nematoblastic "sheaf-like" texture, commonly perpendicular to the direction of schistosity, growing along cleavage planes, suggesting it has formed as a later, non-deformational, retrograde phase. The other minerals found in the assemblage are more characteristic of granulite facies mineralogies, are generally oriented within the schistosity plane, and appear to have
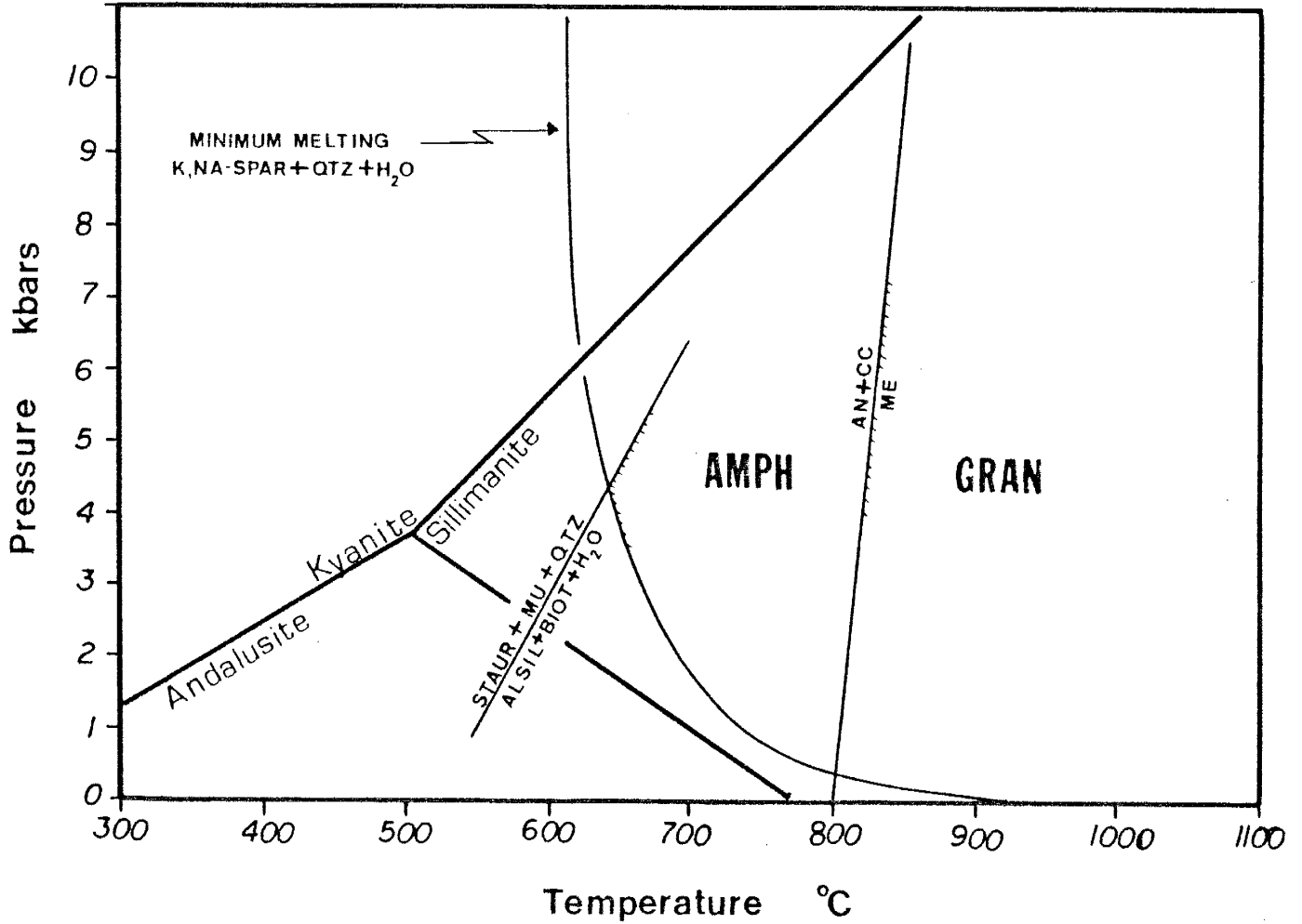
Figure 54: Stability limits of various minerals as a function of P and T. An = anorthite, CC = calcite, Me = meionite, BIOT = biotite, ALSIL = aluminosilicate, STAUR = staurolite, MU = muscovite, QTZ = quartz, -SPAR = feldspars, AMPH = amphibolite facies stability, GRAN = granulite facies stability (modified after Ehlers and Blatt, 1982, and Goldsmith and Newton, 1977). See text for interpretation.

Figure 55: Reproduction of a portion of Brock and Singewald's map (1968) showing the granulite terrane and sample locations. Note that moving away from the center of the terrane the samples contain more retrogressive phases. Samples beginning in L are LMT samples, otherwise they are CH samples.

Figure 56: Photomicrograph of CH-2 showing nematoblastic, retrogressive, crossed biotites (brown) and hornblendes (green) with plagioclase (clear) and orthopyroxene (yellow). Scale 1cm=0.5mm, plain polz. light.

formed during the thermal peak of granulite facies metamorphism.

Sample CH-1, a sample also marginal to the granulite terrane (Fig 57) contains orthopyroxene (15%), magnetite (10%), quartz (25%), and plagioclase (40%) and has a heterogranular, granoblastic texture with some symplectic reaction textures being observable. Hornblende (10%), although present, is dominantly controlled by pre-existing grain boundaries and has a tendency of replacing magnetite grains. These relationships, observable in thin-section, suggest that reactions such as the following are likely to have controlled the formation of these mineral phases [2]:

$$4H_2O + 5Fe_3O_4 + 6(Na, Ca)AlSi_3O_8 \rightleftharpoons 3NaCa_2Fe_5Si_6Al_2O_{22}(OH)_2 + H_2 \uparrow \quad (2)$$

$$Water + Magt + Plag \rightleftharpoons Hornbld + Hydrogen$$

or

$$3FeSiO_3 + KAlSi_3O_8 + H_2O \rightleftharpoons 3SiO_2 + KFe_3AlSi_3O_10(OH)_2 \quad (3)$$

$$Opx + Kspar + Water \rightleftharpoons Qtz + Biot$$
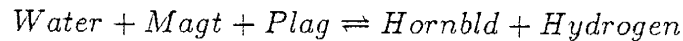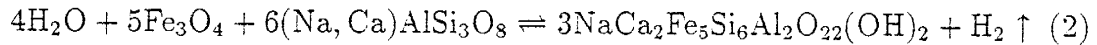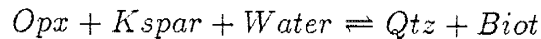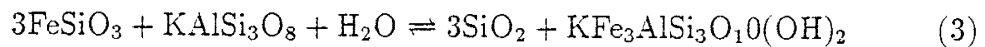
Such retrograde reactions require a hydration process which may have associated with it mobilized alkali elements (such as K_2O). Interestingly, hydrated phases are less common toward the axis of granulite terrane, where granulite assemblages dominate. Sample CH-3 is a granulite containing garnet (20%), plagioclase (60%), quartz(15%), and magnetite (2%) and some minor orthopyroxene (opx) and hornblende (hbl). The garnets (gar) show a "honeycomb texture" and epidote (epd) crystals (5%) show a remarkable symplectic, vermicular texture with respect to

---

[2] Reactions represent most probable mechanisms given the observed petrographic equilibrium assemblages. Detailed reactions will require microprobe data.
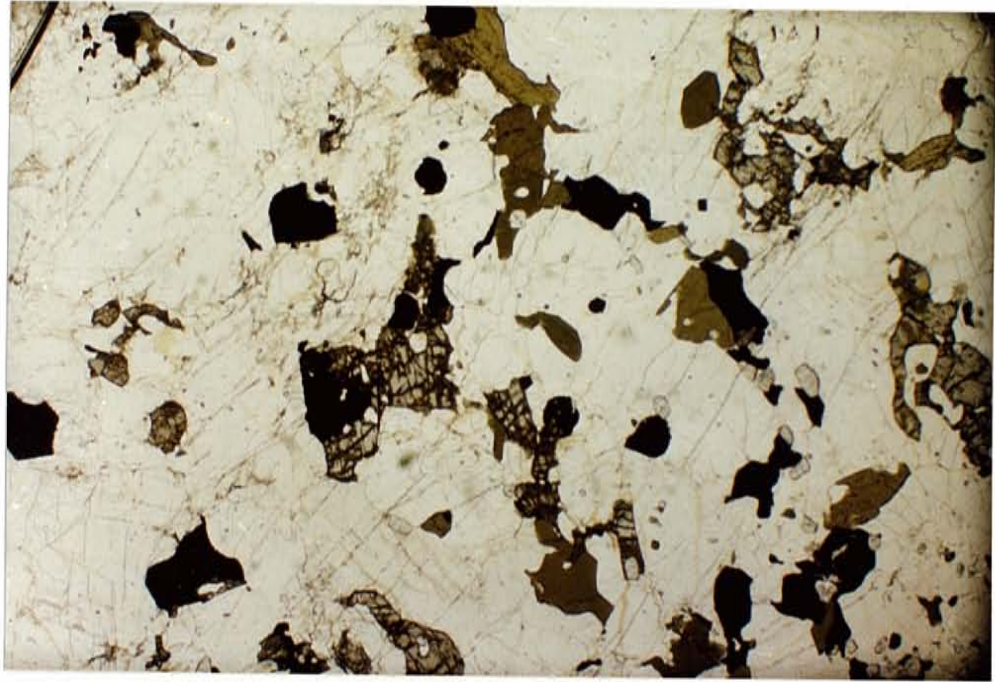
Figure 57: Photomicrograph of CH-1 showing plagioclase (clear), orthopyroxene (light green), and magnetite (opaque), and associated retrogressive phase hornblende (dark green). Scale 1cm=0.5mm, plain polz. light.

plagioclase. As with the hornblende and biotite (biot) in CH-1 and CH-2, the epidote shows no preferential mineralogic orientation, again suggesting that these phases are retrograde and post-kinematic (Fig. 58). Phase relationships suggest that epidote formed in a reaction such as:

$$H_2O + Ca_3Al_2Si_3O_{12} + 5CaAl_2Si_2O_8 \rightleftharpoons Ca_2Al_3Si_3O_{12}(OH) + SiO_2 \quad (4)$$

$$Water + Gar + Anor \rightleftharpoons Epid + Qtz$$
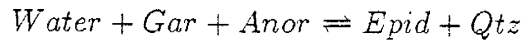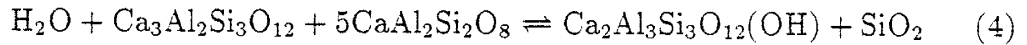
Sample CH-8B shows a more intermediate variety of granulite where the dominant pyroxene is clinopyroxene (cpx). Since the variation in the index of refraction (n_x) for clinopyroxenes as a function of their Fe/Mg ratio is distinctive , it is possible to determine the composition of the cpx by optical means. The n_γ for the cpx, measured from crushed grains in immersion oils, is 1.77 and implies that the cpx is the Fe-rich variety ferrosalite. The sample also contains plagioclase and quartz and minor biotite and microcline. Like the other granulites, CH-8B is granoblastic and contains significant amounts of opaques (Fig. 59), but the opaques here are dominantly ilmenite. The stability of a more Ti-rich rather than Fe-rich oxide as we approach the axis of the granulite terrane suggests a lower f_{O_2} (oxygen fugacity) for the metamorphic fluids involved in the formation of the opaque oxide phases (Newton, 1986). This is because magnetite-ilmenite solid solution is f_{O_2} dependent, as can be seen in the following reaction:

$$4[Fe_3O_4]_{ss}^{mt} + O_2 \rightleftharpoons 6[Fe_2O_3]_{ss}^{ilm} \quad (5)$$
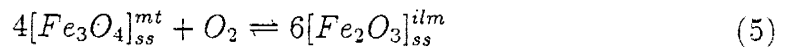
Thus, ilmenite is stable under more reducing conditions than magnetite (Essene, 1982). In the Monts du Lyonnais metabasites in the Massif Central section of the Hercynian complex (France) ilmenite is generally the dominant Fe-Ti oxide phase

Figure 58: Photomicrograph of CH-3 showing nematoblastic, retrogressive epidote with a symplectic texture (in plagioclase) and its relationship to garnet (orange). Scale 1cm=0.1mm, plain polz. light.
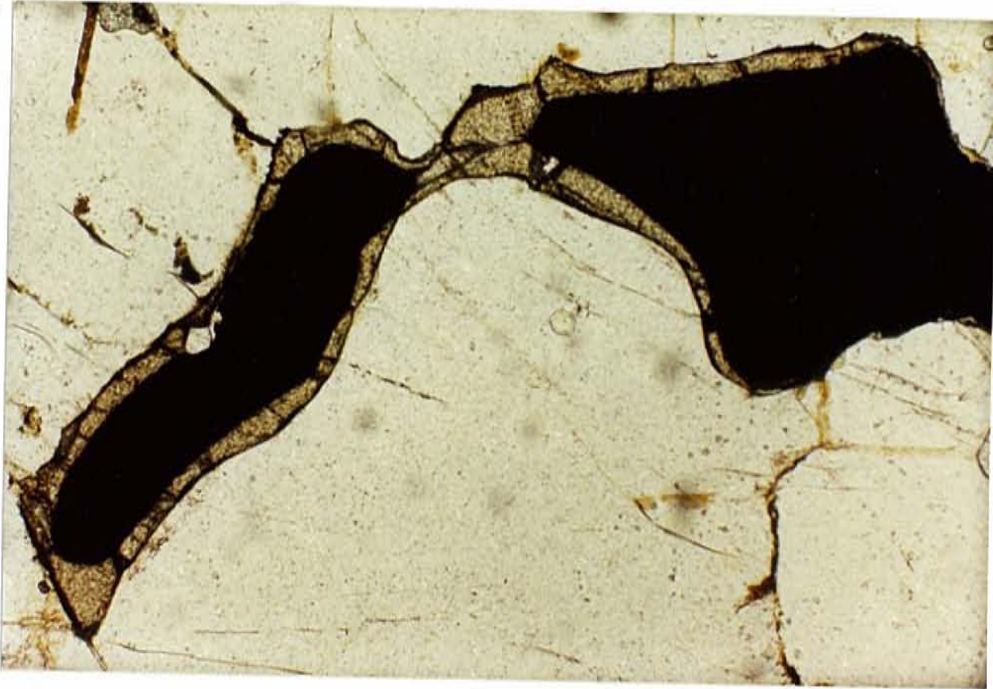
Figure 59: Photomicrograph of CH-8B showing ilmenite being replaced by sphene. Matrix is dominantly plagioclase. Scale 1cm=0.1mm, plain polz. light.

in the granulite terrane while magnetite dominates in the retrogressive assemblages (Dufour, 1985).

In fact, reflected light studies suggest that pyrrhotite occasionally occurs at the axis of the granulite terrane and pyrrhotite can only be stable under very reducing conditions, or very low f_{O_2} fluids. Similar relationship are observed in the granulites of southern Calabria (Schenk, 1984).

In CH-8B sphene occurs as pseudomorphs after ilmenite as a reaction corona, suggesting that ilmenite has become unstable and is retrogressing to sphene by the reaction:

$$3FeTiO_3 + 3CaAl_2Si_2O_8 \rightleftharpoons 3CaO \cdot TiO_2 \cdot SiO_2 + Fe_3O_4 + 6SiO_2 + O_2 \quad (6)$$

$$Ilm + Plag \rightleftharpoons Sphene + Mgt + Qtz + Oxy$$
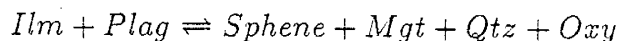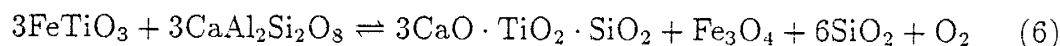
Sample CH-7, exhibiting similar textures is dominated by areas of differing mineralogy, one of ferrosalite and another of garnet. At the contact of the two zones the phases display granoblastic textures and appear to be in equilibrium (Fig. 60). This is interesting since Winkler (1967) suggests that orthopyroxene (opx) and anorthite (an) become unstable at high pressures (at constant temperature) to form cpx and gar by the reaction:

$$3Fe_2Si_2O_6 + 2CaAl_2Si_2O_8 \rightleftharpoons CaFeSi_2O_6 + 2Ca_{0.5}Fe_{2.5}Al_2(SiO_4)_3 + 2SiO_2 \quad (7)$$

$$Opx + Anor \rightleftharpoons Cpx + Gar + Qtz$$
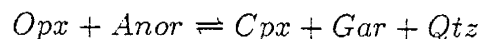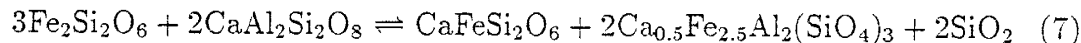
Winkler suggests that by extrapolation this reaction will proceed at about 9kb pressure and 750°C.

Scapolite bearing calc-silicates, of which LMT2-2 is representative, comprise only a small portion of the granulite terrane, but allow important thermal constraints on the granulite facies metamorphism. The scapolite in LMT2-2 (Fig. 61)
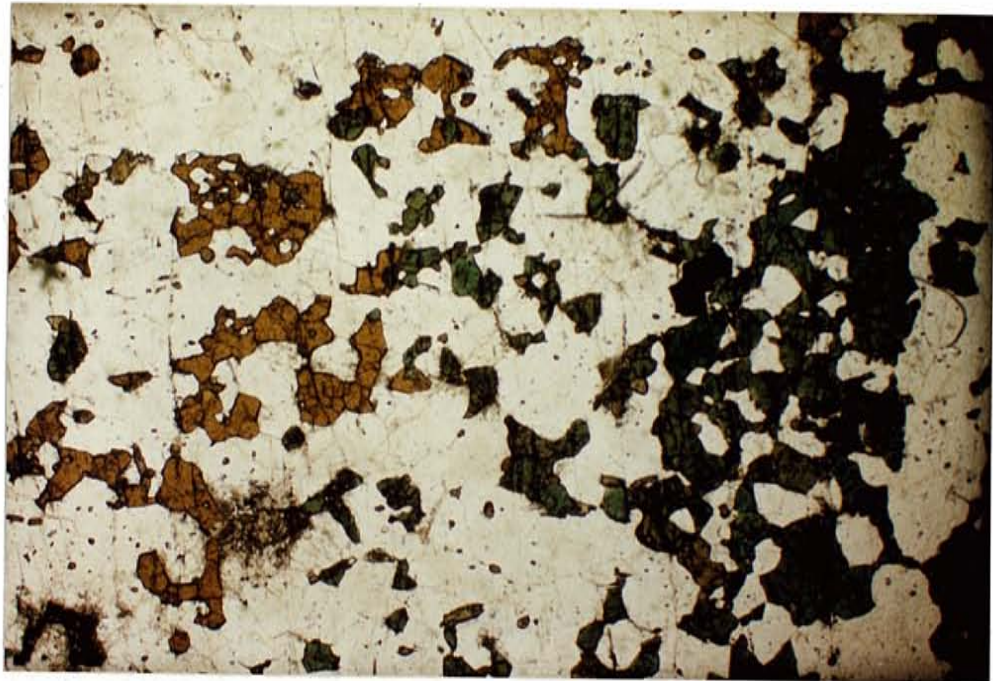
Figure 60: Photomicrograph of CH-7 showing a equilibrium boundary between ferrosalite (green) and garnet (orange). Matrix is plagioclase. Taken in plain polarized light at a scale of 1cm=0.5mm.

is porphyroblastic and can be as large as 1 or 2cm in diameter, imparting a grano-porphyroblastic texture to the thin-section. Poikiloblastically enclosed in the scapolite (65%) occurs ferrosalite (20%), garnet (10%), calcite (5%), and some minor K-feldspar and quartz. As in CH-7, the ferrosalite and garnet appear to be in equilibrium, an assemblage representative of the high-pressure/temperature regime of the medium-pressure sub-facies of the granulite facies (Miyashiro, 1973). The presence of calcite in association with the scapolite suggests that the scapolite is the variety *meionite*, $3CaAl_2Si_2O_8 \cdot CaCO_3$. Scapolite is becoming increasingly recognized as a prograde metamorphic mineral phase in the granulite facies (Goldsmith, 1975, Goldsmith and Newton, 1977, and Warren et. al. 1987) in which scapolite is most probably formed by the reaction:

$$3CaAl_2Si_2O_8 + CaCO_3 \rightleftharpoons 3CaAl_2Si_2O_8 \cdot CaCO_3 \qquad (8)$$

$$Anor + Calc \rightleftharpoons Meionite$$
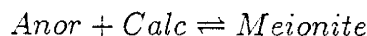
Goldsmith and Newton (1977) have calculated experimentally the stability relationships for this reaction and have determined that pure meionite is unstable at all temperatures below 875°C, independent of pressure[3].

The attributes of the amphibolite and granulite facies rocks seem to correspond most closely to Miyashiro's (1973) medium pressure baric type, that is to say rocks under a moderate geothermal curve. In particular, in the amphibolite facies terrane the metabasites are dominantly composed of plagioclase and hornblende, metapelites have biotite and almandine stable, and calcareous rocks contain Ca-rich garnet and diopside. In the granulites the metabasites have orthopyroxene and clinopyroxene formed from the decomposition of biotites and

---

[3]Due to the near zero volume change in the phases involved as the reaction proceeds.
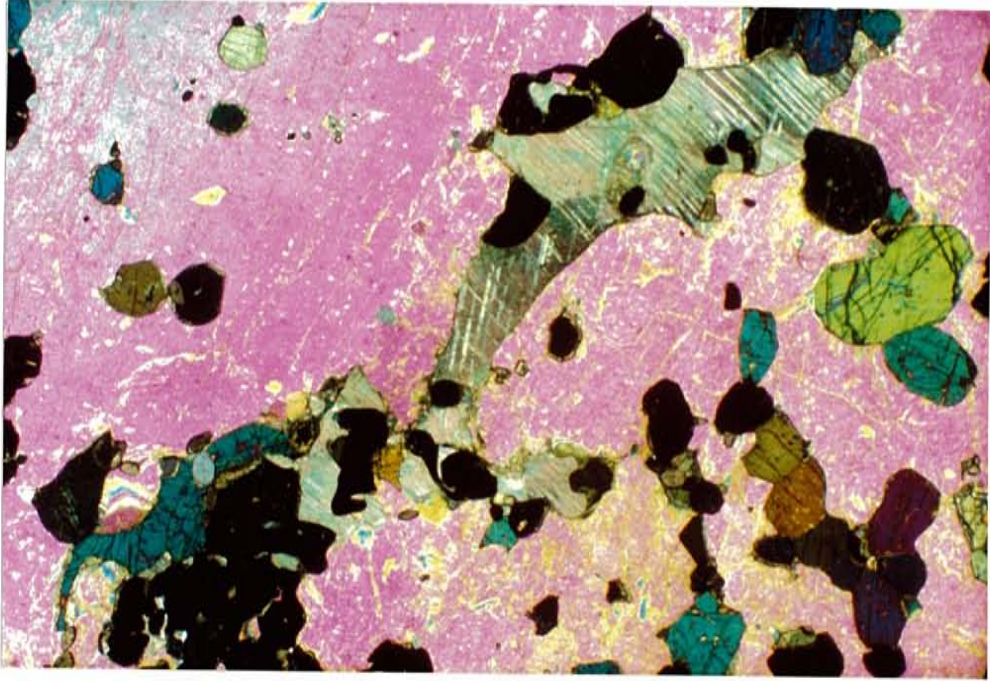
Figure 61: Photomicrograph of LMT2-2, a scapolite gneiss. Pink crystals are scapolite, green crystals are clinopyroxene, isotropic minerals are garnet, light green, twinned crystals are calcite. X-polz. light, 1cm=0.5mm.

hornblendes, plagioclase is common but decreases with increasing concentration of garnet (garnet forms at the expense of plagioclase), and the metapelites commonly contain quartz, plagioclase, garnet, and K-feldspar. In fact, the mineralogy of the granulites is consistent with Miyashiro's high-temperature subfacies of the medium-pressure baric type.

Structure

Although a detailed structural analysis is not the intent of this study, a review of some pre-existing data can provide some important insights into how the deformational history of the Wet Mountains fits into the general geochronology of the area. The central Wet Mountains are characterized by a dominantly northeast trending structural fabric and the foliation associated with this fabric is generally steeply dipping to the northwest and primarily defined by the alignment of biotites and gneissic banding. Foliation generally parallels the compositional layering, even around the hinges of fold axes and lineations tend to parallel, with some important exceptions, the axes of major folds. More complex patterns are observed in lineations which have been visibly affected by superimposed folding. The lineations are generally defined by elongate minerals, most commonly hornblende, and also by the fold axes of mesoscopic folds.

Folds in the area vary from close to isoclinal on a mesoscopic scale but tend to be tight, asymmetric folds on a megascopic scale. Axial planes tend to be moderately to steeply inclined and folds show gentle to moderate plunge with wavelengths as large as 3km. Most of these relationships are apparent on Brock and Singewald's (1968) detailed geologic map of Mount Tyndall.

Individual megascopic folds have been taken to define structural domains so as to localize deformational effects. This allows the analysis of structural data from the Mount Tyndall quadrangle (Brock and Singewald, 1968) in stereographic projection. Figs. 62, 63, 64, and 65 are lower hemisphere stereographic projections of poles to foliation and lineations from some major folds in the Mount Tyndall quadrangle. Poles to foliation were contoured using a counting net after Ragan (1973). Figs. 62, 63, and 64 represent stereonets for what are re-
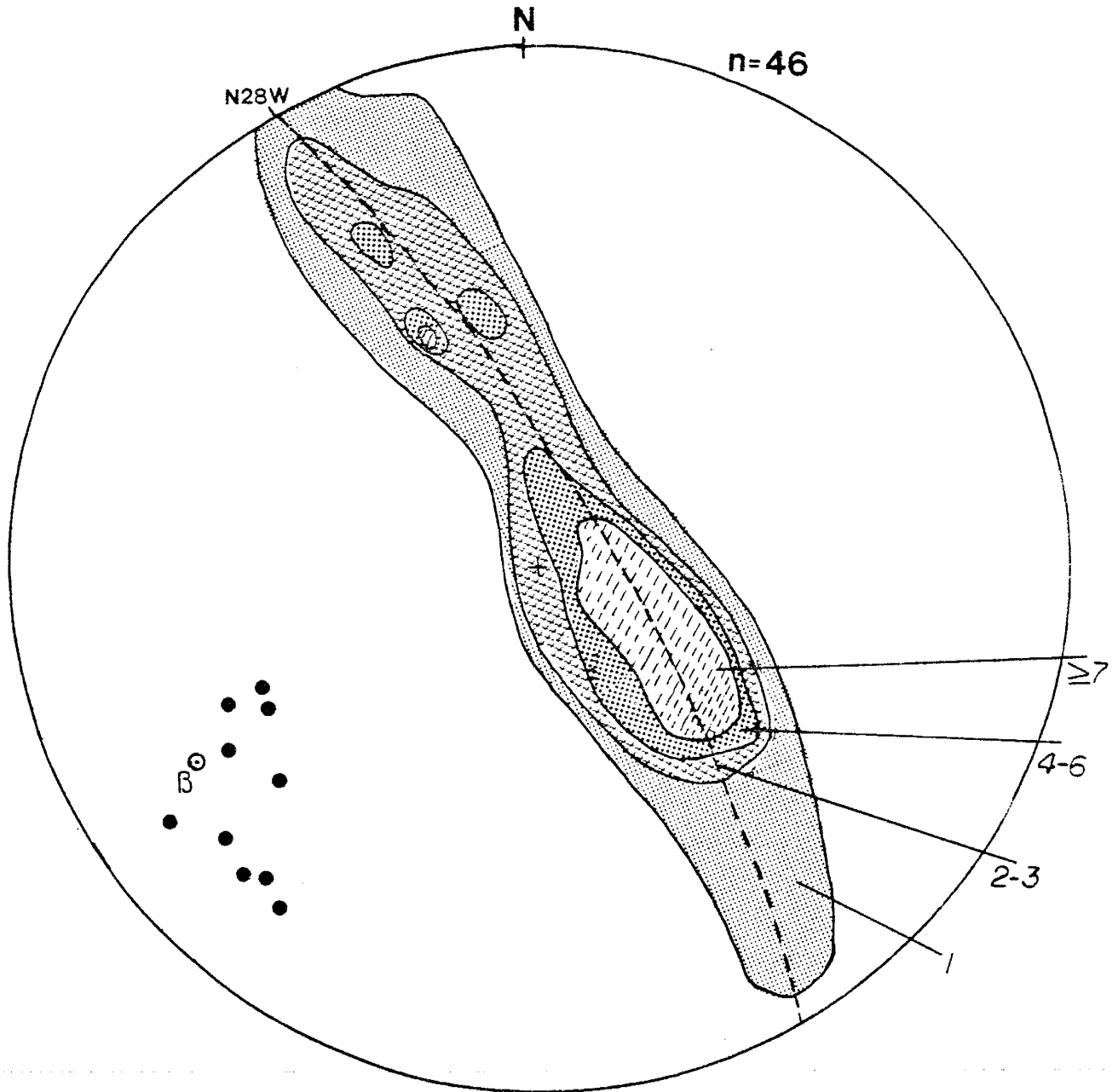
Figure 62: Contoured stereographic projection of poles to foliations from the fold in the Dead Mule Gulch area. Contouring was done on the number of points per 1% area of the stereonet. The "n" represents the total number of points. Solid circles are lineations, β is fold axis, plot is lower hemisphere projection (data from Brock and Singewald, 1968; method after Ragan, 1973).
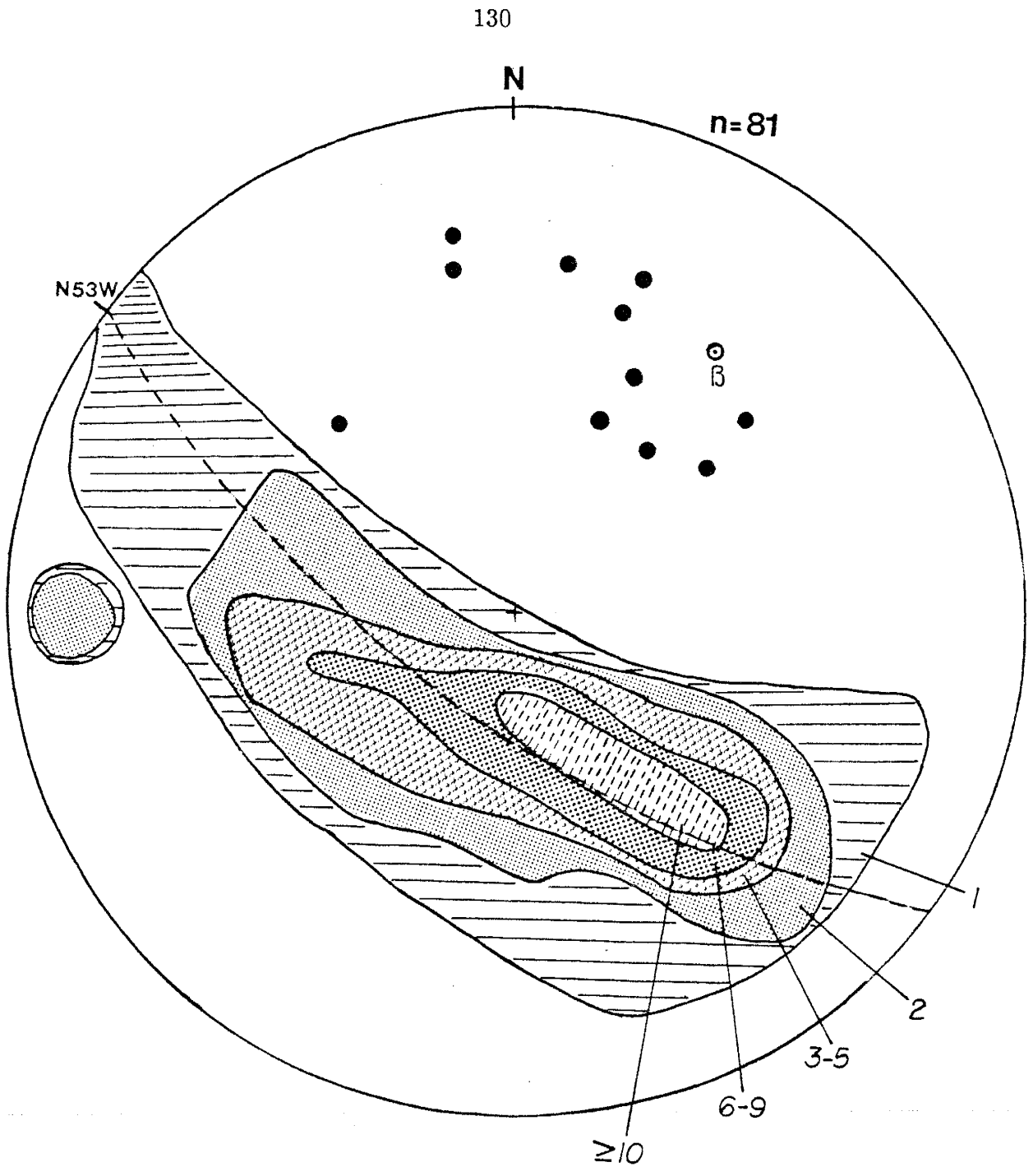
Figure 63: Contoured stereographic projection of fold in Querida Gulch area, data from Brock and Singewald, 1968. Symbols as in Fig. 62.
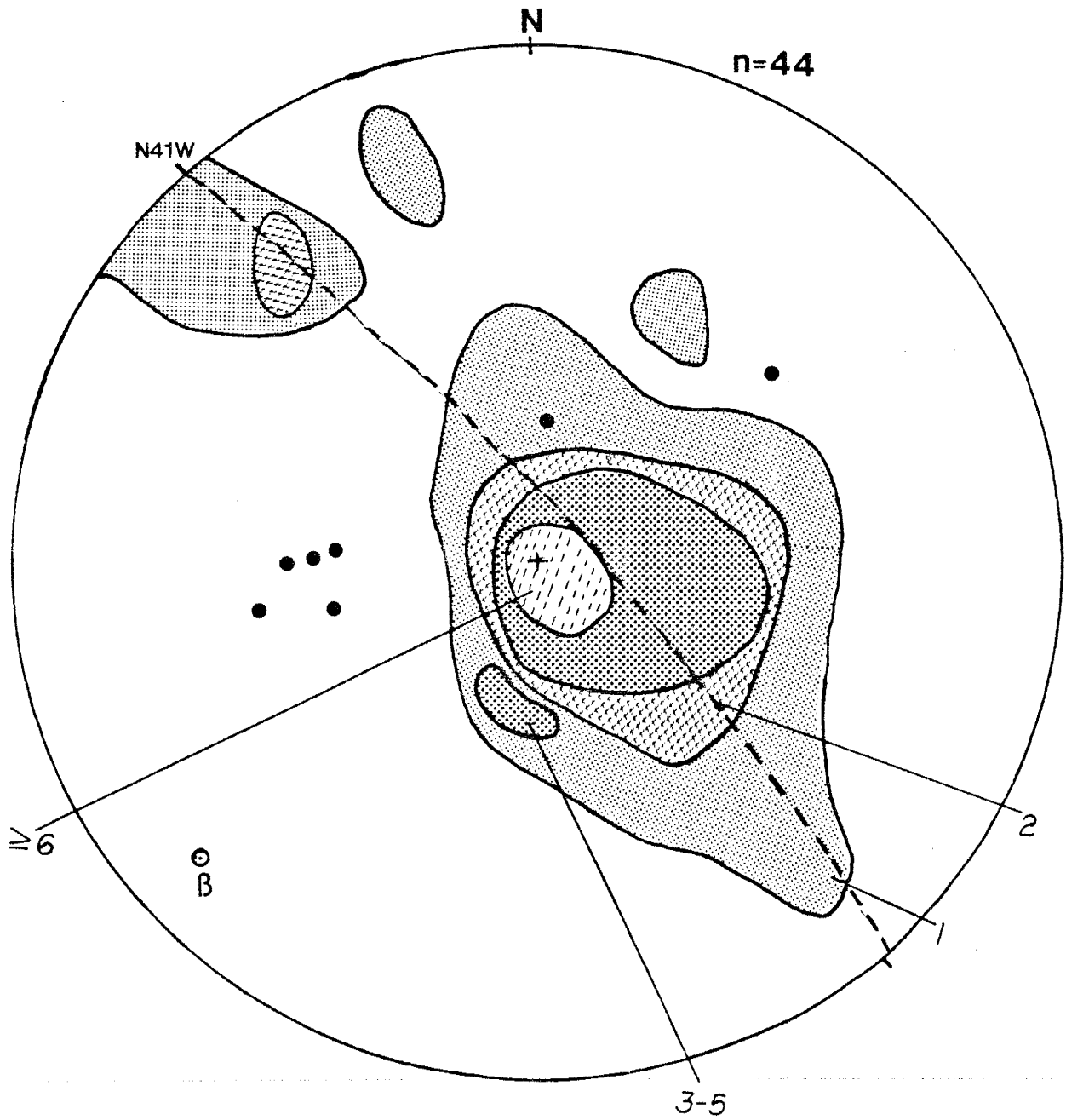
Figure 64: Contoured stereographic projection of fold in Tyndall Gulch area, data from Brock and Singewald, 1968. Symbols as in Fig. 62.
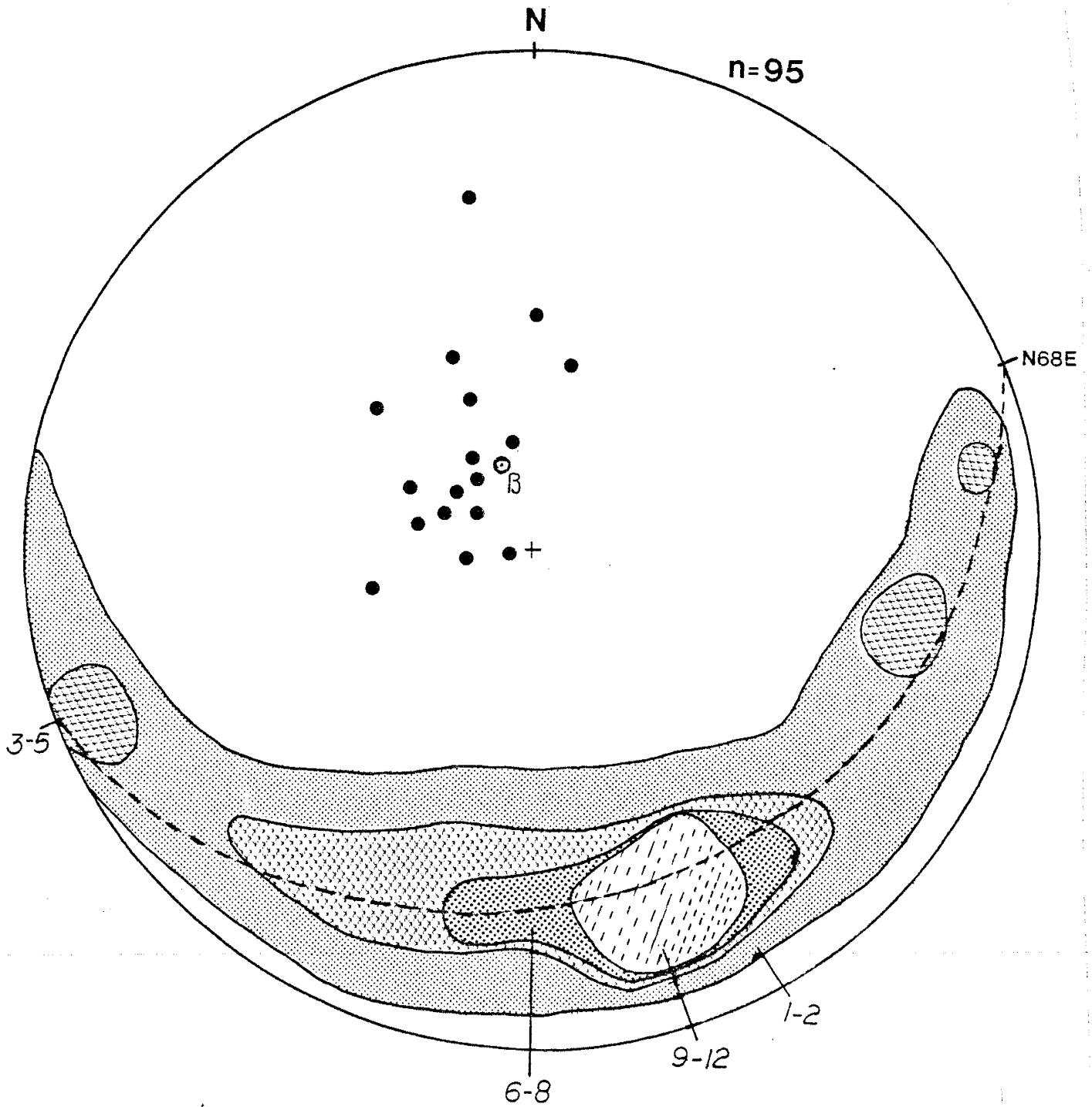
Figure 65: Contoured stereographic projection of fold in Sevenmile Gulch area, data from Brock and Singewald, 1968. Symbols as in Fig. 62.

ferred to here as the Dead Mule Gulch (468000mE-4231000mN), Querida Gulch (469000mE-4223000mN), and Tyndall Gulch (471000mE-4224000mN) folds, respectively. Figs. 66 and 67 are reproductions from Brock and Singewald (1968) showing maps of the Dead Mule Gulch and Querida and Tyndall Gulch domains. The stereonets show that that the fold axes of these three folds lie within the prevalent northeast trending fabric of the area, from N35E to N52E, and that the lineations associated with the folds generally correspond to the position of the fold axis (β), the Tyndall Gulch fold being the exception. The axial planes for the Dead Mule Gulch and Querida Gulch folds dip to the northwest, approximately 78° and 62° respectively, and the axial plane of the Tyndall Gulch fold also dips to the northwest approximately 62°.

Fig. 65 is a stereonet for the Sevenmile Gulch fold, where structural interference patterns suggest the presence of superposed folds. A first fold has been complexly refolded and rotated about a northeasterly trending fold axis, however it is still evident that the earlier fold appears to have opened in a generally easterly direction (Fig. 68), implying that the axis of the first fold had a westerly trend (NW to SW). Shown on Fig. 68 are the fold axes of the different folding episodes. In addition to the D_1 and D_2 folds, the axial traces of the D_2 folds appear to be "warped," suggesting that the Sevenmile Gulch fold may even have been subjected to a NW trending D_3 folding. On the stereonet the interference of the two fold patterns results in a great circle with an axis that trends north, although it seems from the geologic map that neither the first or second period fold appears to have a north trending axis. Thus, the second deformation may have been unable to completely reorient the foliations, the result being a south-dipping plane formed by the foliation poles.

If all the lineations available from the four structural domains are plotted on
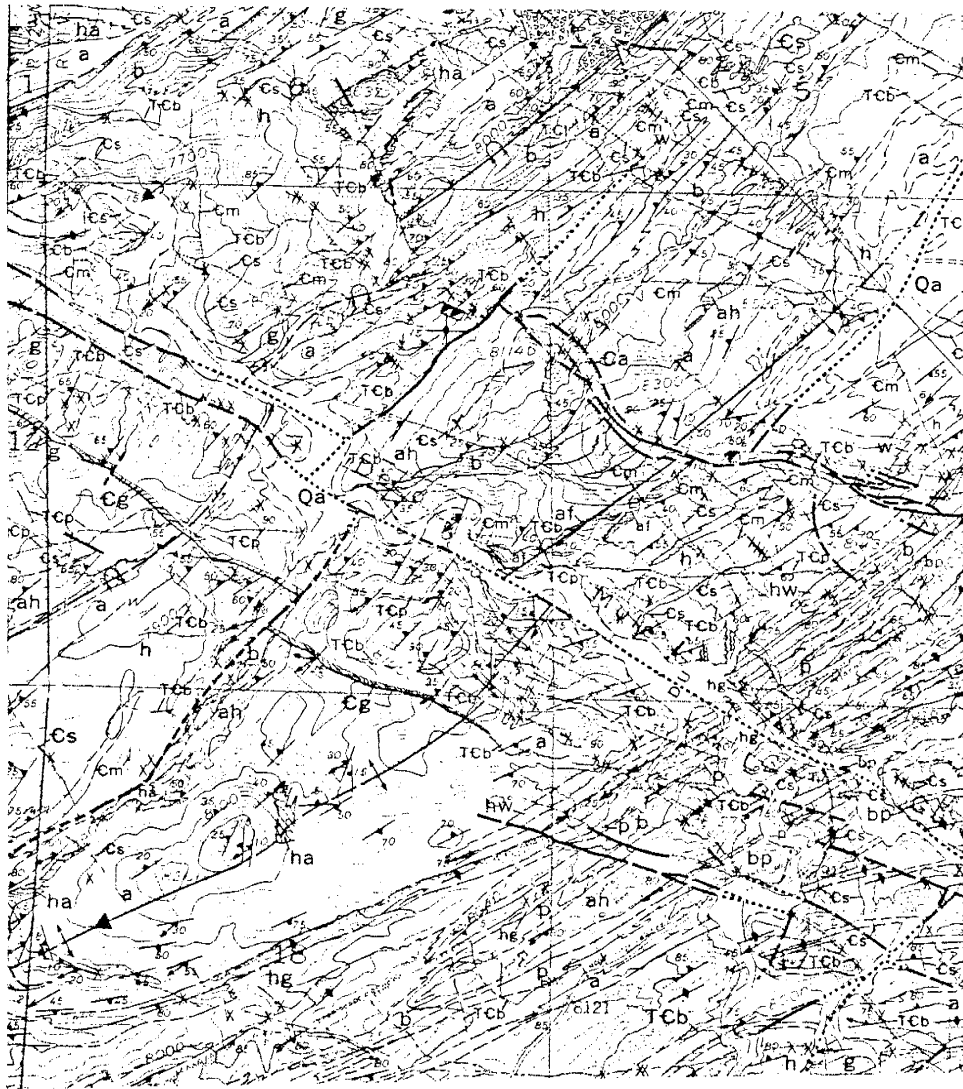
Figure 66: Portion of Brock and Singewald's (1968) geologic map of Dead Mule Gulch structural domain.

Figure 67: Portion of Brock and Singewald's (1968) geologic map of Querida and Tyndall Gulch structural domains.
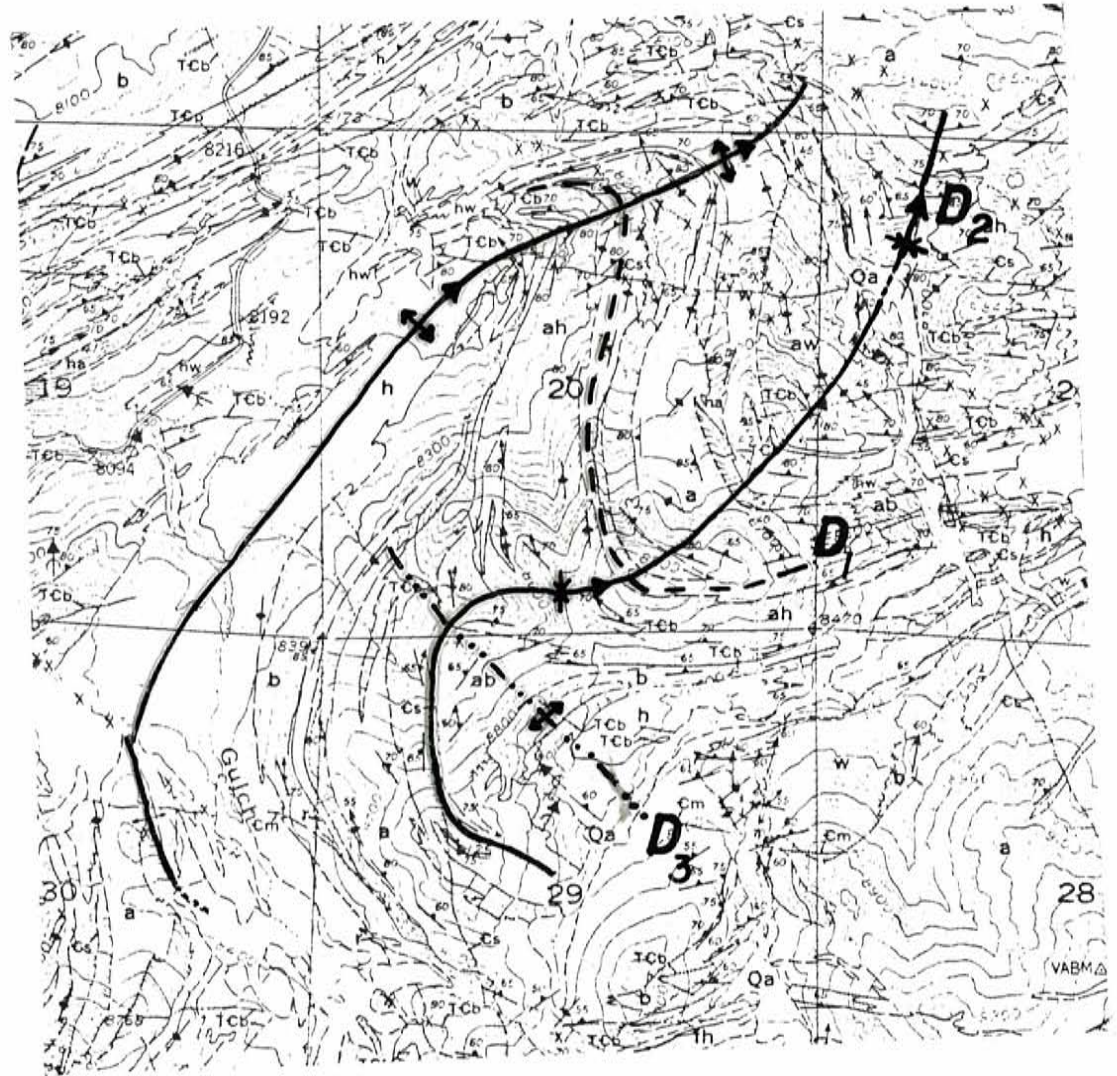
Figure 68: Portion of Brock and Singewald's (1968) geologic map of Mount Tyndall, showing detail of Sevenmile Gulch Fold. Note fold interference pattern, particularly the hook pattern. Also shown are what appears to be D_1, D_2, and D_3 fold axes.

one stereonet (Fig. 69) the lineations define a single great circle which dips to the northwest. The easiest way of explaining this pattern would be to suggest that the lineations were formed during an earlier deformation and that these lineations defined the fold axes of this earlier deformation. The deformation which formed the northeasterly fabric would have followed this event and would have scattered the lineations along a plane which this great circle defines. The northwesterly dip of the plane may suggest that the axes of the earlier folds trended northwest. However, since Brock and Singewald do not specify what lineations were from mineral lineations and which were from cleavage traces, the lineation data is extremely ambiguous but does point out the fact that the later folding affected and rotated a pre-existing lineation.

Since the second deformation appears to be the strongest event, it seems that it's this deformation which may be responsible for rotating the pre-existing lineations and the orientation of the lineations along a great circle rather than a small circle suggests that D_2 resulted in similar folding. In similar folding it's possible to use the plane of the lineation locus to compute the a direction of shear (Ramsay, 1968). Since the lineation locus (Fig. 69, dashed line) is controlled by the original lineation direction and a_2, a_2 will be the only line common to the lineation locus and the axial surface of the second folds (Fig. 69, dotted line). Given this scenario the a_2 direction is quite steep ($\sim 70°$), suggesting that the stress directions of D_2 were almost horizontal.

There are studies which make use of two dimensional fold interference patterns to infer orientations of structural forces relative to each other (Ramsay 1967, Thiessen and Means 1980, Odonne 1987) and in the Wet Mountains there are several interference patterns visible, including sinusoidal waves, hook patterns, and linear patterns. Ramsay (1967) has shown that the kinematic superposition of
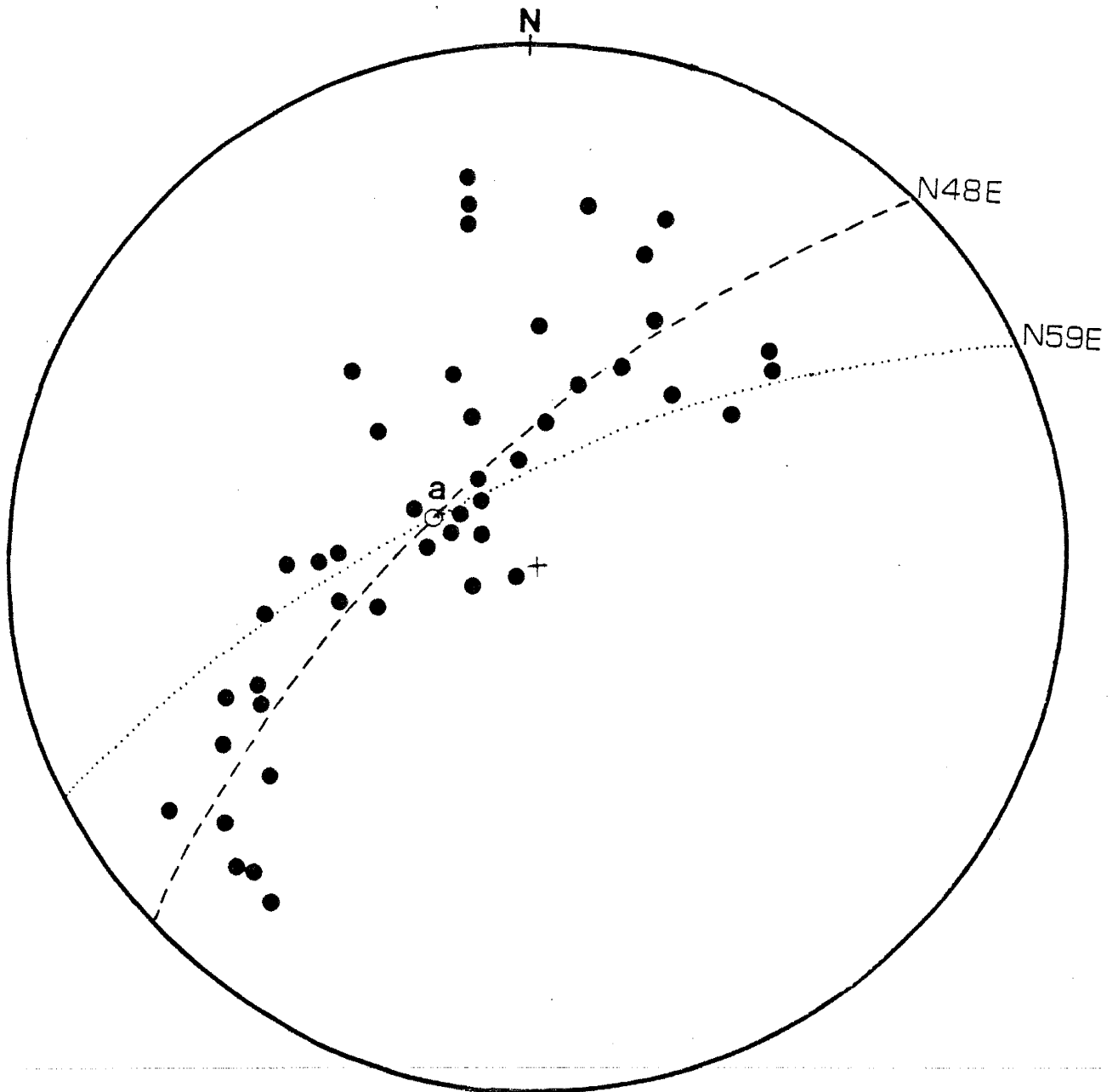
Figure 69: Stereographic projection of lineations from throughout the Mount Tyndall quadrangle. Dashed line is great circle for lineations, dotted line is axial surface of second folds, and *a* is slip direction (data from Brock and Singewald, 1968).

two phases of a fold forming deformation produces a three dimensional geometric pattern termed a fold interference pattern. The identification of such patterns provides a simple way of determining the kinematic features of each fold-forming deformation. Thiessen and Means (1980) provide a detailed, computer generated study of the effects of a deformation orientation on interference pattern formation. However, Ramsay's approach is a much simpler classification scheme which groups interference patterns into four types (0, 1, 2, and 3) which are functions of the orientation between the first axial plane, the displacement direction of the second deformation (a_2), and the axial orientation of that second deformation (b_2). The hook patterns, which are common throughout the Mount Tyndall quadrangle, are diagnostic of a type 3, divergent-convergent pattern, where the flow direction of the superimposed folding (a_2) is oriented at a high angle ($\sim 90°$) to the axial surface of the first folds but the axis of the first folds is close to the b_2 direction. A type 3 pattern basically implies that there has been a shift in compressional direction of about 90° about the fold axis or, in the Wet Mountains, a shift from a northeast-southwest to a northwest-southeast compression. This agrees roughly with the stereographic plots which suggest that two deformational fabrics are present, one trending northeast and one trending west-northwest.

Tweto (1980a) states that in the central and southern Front Range there are large early folds with a west to northwest trend which have been refolded during a second period of deformation about north-northwest to north-northeast trending axes. He also states that this second period of deformation was accompanied in its later stages by intrusions of granite of the 1700Ma group which accommmodated to and slightly distorted the fabric into which they were intruded. There may be a similarity in the deformational patterns seen in the southern Front Range in comparison to those seen in the Wet Mountains.

Two deformational directions are also observable in the microfabrics. Figs. 70 and 71 are photomicrographs of samples LOT-1 and WIL-2, from the Wilson Park area, a lower metamorphic grade terrane, just below muscovite breakdown, just north of the study area. Sample LOT-1, a cordierite schist, shows a deformational direction (S_1) preserved by the inclusions in the prekinematic cordierite porphyroblasts and a postkinematic schistosity at about 90° to S_1 and defined by muscovite growth. A similar relationship is seen in WIL-2, a biotite schist where the cleavage in a postkinematic porphyroblast of biotite defines an S_1 direction while later, postkinematic biotites define an S_2.

The Twin Mountain-Crampton Mountain batholith, a 1705Ma pluton, is generally concordant to the surrounding gneisses and is itself well foliated throughout. Although it's true, as Reed, et. al., (1987) pointed out, that whether a pluton is syn- or post-tectonic may depend more on its level of emplacement in the crust rather than on its placement relative to a regional tectonic event, in this case either argument can be used without consequence. The relationship is such that a pre-existing structural fabric seems to control the intrusive character of the batholith. This being the case, either the Twin Mountain-Crampton Mountain batholith was intruded during, but close to the end of, the second period of deformation or it was intruded post-tectonically to the deformational episode. In either case the deformation would have to have occurred prior to 1700Ma.

Although the dominant structural fabric is to the northeast, most of the Precambrian faults trend northwest, the most extensive of which is the Ilse fault. The Ilse fault is a wide, complex, essentially vertical fault zone along which Tweto (1980a) suggests the earliest movement predates emplacement of the 1700Ma granites. In many places along the fault, segments of gneiss between fissures exhibit sharp flexures and contortions which Singewald (1966) suggests implies folding
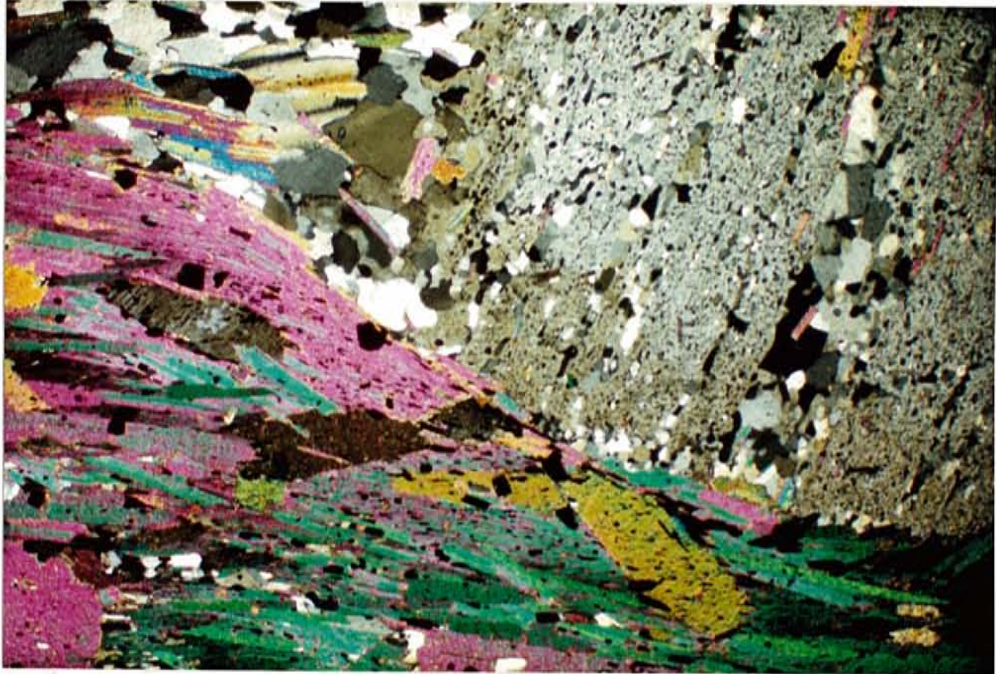
Figure 70: Photomicrograph of cordierite schist LOT-1 showing microfabrics S_1, in cordierite inclusions, and S_2, in muscovite and biotite, at $\sim 90°$.
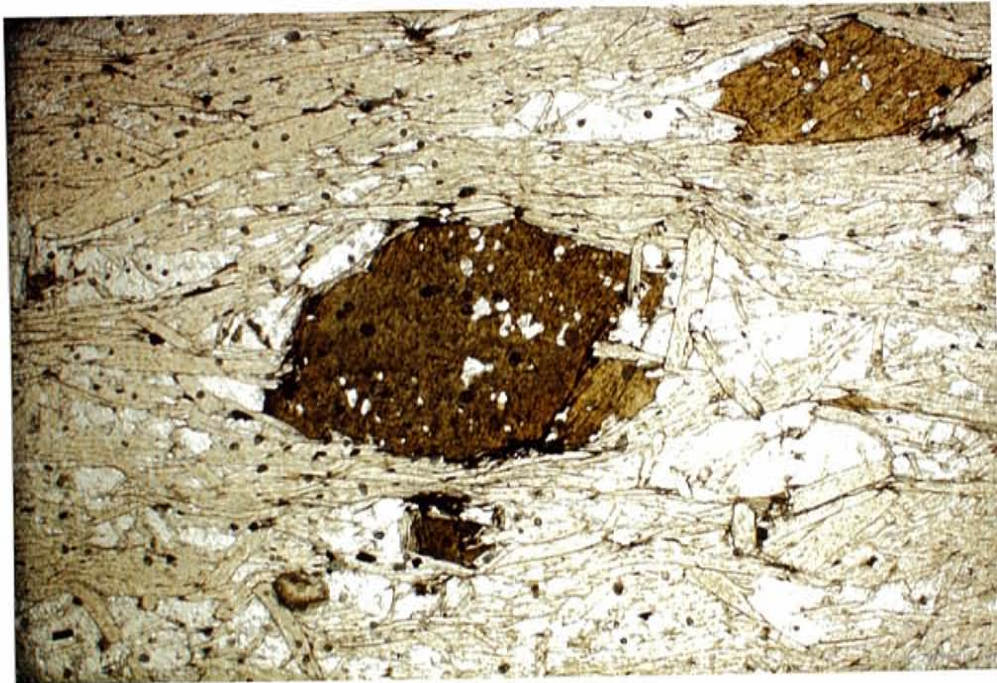
Figure 71: Photomicrograph of biotite schist WIL-2 showing microfabrics S_1, in biotite porphyroblast, and S_2, in later biotites, at $\sim 90°$.

while the rock was still plastic enough not to break. Tweto (1987) notes, correctly, that the Precambrian terranes on either side of the fault differ. The eastern side contains upper amphibolite facies gneisses with a north to northwest fabric while the western side contains granulite facies rocks, is generally more migmatitic, and has a northeasterly fabric which has seen multiple periods of deformation. However, 1700 Ma plutons on both sides of the fault are similar in character and were evidently emplaced at approximately the same depth, suggesting that displacement along the fault predates their intrusion.

Conclusions

Recapitulation

The primary objective of this study is to attempt to constrain the tectonic evolution of the Wet Mountains terrane during the early Proterozoic. What geochronologic data is available seems to suggest that the sediments and basaltic units which intrude them were emplaced, deformed, and metamorphosed prior to 1705 Ma, although detailed data needed to constrain these events more closely is lacking. The amphibolites bear geochemical similarities to basalts erupted from mid-ocean ridge (Zr-TiO_2, Zr-Y-Nb, TiO_2-V, and Ti/Y-Nb/Y diagrams) and island arc (Ta/Yb-Th/Yb, Zr-TiO_2, Th-Ta-Hf, TiO_2-V, Ti/Y-Nb/Y, and MnO-P_2O_5-TiO_2 diagrams) tectonic settings, display a very distinct subduction zone signature (MORBn spidergram and Th-Ta-Hf diagram), and show a chemical resemblance to calc-alkaline basalts erupted from immature island arcs (MORBn spidergram). Additionally, the association of basaltic sills with what appears to be terrestrial sediments and the lack of Fe-enrichment in the mafic units is also consistent with eruption in a back-arc basin.

The metasediments exhibit a major and trace element similarity to quartzwackes, implying the impetus of granitic material commensurate with derivation from a continental margin system. Furthermore, the metasediments chemically resemble sediments deposited along active continental margins (DFXN plot, K-Na-Si diagram, and Hf-La/Th diagram) evolving, perhaps, into more passive margin type systems (Hf-La/Th and La/Sc-Ti/Zr diagrams). A quartzwacke is also consistent with the current mineralogical composition of the biotite-quartz-plagioclase

gneisses, a mineralogy which suggests a plagioclase- and quartz-rich protolith, unlike the K-feldspar rich protoliths of rift zones.

The granulites of the Wet Mountains appear to have formed at metamorphic temperatures in excess of 850°C and pressures on the order of 9 kb, pressures and temperatures which would be required to produce the mineral and fluid associations seen in the granulite terrane. Most granulite terranes are readily explained by invoking a process of crustal thickening, in excess of 30–35 km, through continent-continent collision, although recent research suggests that many granulites may develop in continental margin arc systems (Bohlen, 1987). Lastly, the leucogranites of the Wet Mountains display lithologic and chemical similarities to leucogranites around the world from collisional settings and plot in within-plate or post-collisional fields on Pearce (1984) type discriminant diagrams (Y+Nb-Rb diagram).

On Fig. 72 the available geochronologic and lithologic relationships are compiled in the form of a geochronologic scale. The recognized relationships suggest that deposition of the metasediments and intrusion of basaltic sills occurred contemporaneously before 1705 Ma and perhaps as early as 1720 Ma. The tectonic data available suggest that the most reasonable setting for the deposition of these sediments is in a back-arc basin developed in or near continental crust, which explains the subduction zone component in the basalts (MAF), along with their arc affinities, and the active to passive continental margin signature of the sediments (QW). Such a setting also fits into the regional tectonic framework of the Proterozoic sequences in Colorado. Many of the terranes in Colorado have well preserved primary textures which show a predominance of pyroclastic and epiclastic material, suggestive of an arc environment and any setting proposed for the Wet Mountains must be constrained by the other terranes.
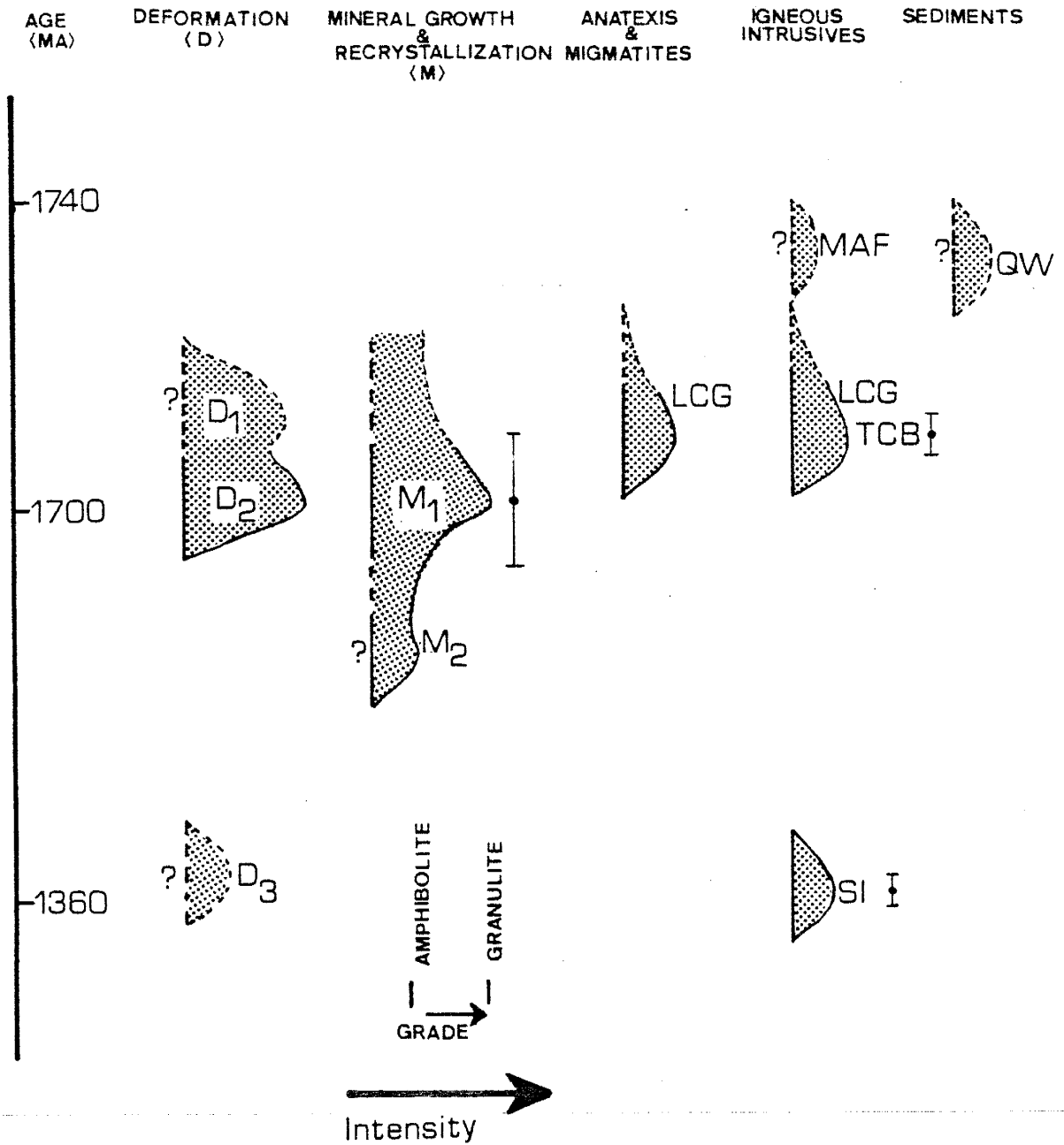
Figure 72: Schematic geochronologic relationships of some key geologic events in the early Proterozoic development of the Wet Mountains (Explanation in text).

The Wet Mountains terrane must have subsequently been deformed (D_1) but how early this event pre-dates the deformational events of 1705 Ma (D_2) is unclear. It seems feasible to envision that these two events may represent a single, continuous event but whether this first deformation had an associated metamorphic episode and what grade it may have been is uncertain. It does seem that the D_2 event produced similar folds, which are common of strongly deformed orogenic belts, with slip directions which are close to vertical, perhaps suggestive of almost horizontal compression. It is the D_2 deformation, the waning stages of which were accompanied by the intrusion of 1705 Ma (TCB) plutons (Tweto, 1980a), however, which is responsible for the dominant structural fabric of the area. Age dating on the granulites also suggests that this is the age of granulite facies (M_1) metamorphism (Bickford, 1986) and anatexis of the amphibolite grade metasediments to produce the leucogranites (LCG). There must subsequently be another metamorphic event of amphibolite facies grade (M_2) which causes retrogression of the granulites to amphibolite grade and a later NW trending deformational event (D_3). The timing of D_3 cannot be determined given existing data, but in the southern Front Range there is a deformation associated with the intrusion of 1400Ma plutons and may be similar to the deformation seen in the Wet Mountains.

Models

Admittedly, many problems exist in the interpretation of how the central Wet Mountains terrane (WM) fits into the regional framework of Proterozoic sequences in Colorado. In particular, gaps in data exist in the surrounding terranes which foster a lack of regional continuity to our understanding.

West of WM are the Proterozoic terranes of the Gunnison, Salida, and Sangre de Cristo areas (Fig. 73). Most of the rocks of the Dubois/Green Mountain

terrane (DGM), 1790–1760 Ma, are sub-marine, bimodal volcanics and volcani-clastic sediments with geochemical characteristics of subduction related volcanics from island arcs (Condie and Knoper, 1986). The Cochetopa/Salida terrane (CS), 1740–1730 Ma, is dominantly comprised of volcaniclastic sediments (65%) with sub-equal amounts of bimodal felsic and mafic volcanics, principally as tuffs and flows, with similarities to volcanics erupted in back-arc basin environments (Condie and Knoper, 1986 and Boardman and Condie, 1986). The Sangre de Cristo terrane (SDC), 1710–1670 Ma, includes variably deformed and metamorphosed volcanic rocks ranging in composition from basalt to rhyolite with affinities to volcanics erupted in continental-margin arc settings and associated back-arc basins (Thacker and Condie, 1986).

North of the Wet Mountains is the Idaho Springs terrane (IS), 1740–1720 Ma, which, in age and lithology, tends to be similar to the Black Canyon terrane (BC), 1740–1720 Ma, and is dominated by metasedimentary gneisses which have been in-terpreted as graywackes and shales (Condie and Martell, 1983). The metamorphic equivalents of these metasediments tend to be biotite gneisses and schists with as-sociated hornblende gneisses, representing basaltic units. Where tectonic setting analysis has been done in the IS, it suggests a source rich in granitic and felsic vol-canic components deposited in continental rifts or near-continent back-arc basins (op. cit.). Plotting some of Condie and Martell's (1983) data from Big Thompson Canyon, a section in the IS, on a Th-La discriminant plot for sediments (Fig. 74) the metasediments have affinities to sediments deposited in basins associated with continental arcs.

Almost nothing is known about the Proterozoic sequences in Colorado which lie south of the Wet Mountains. The Pecos Terrane (PC), 1720 Ma, of New Mexico is the first major Proterozoic exposure south of the WM which has seen extensive
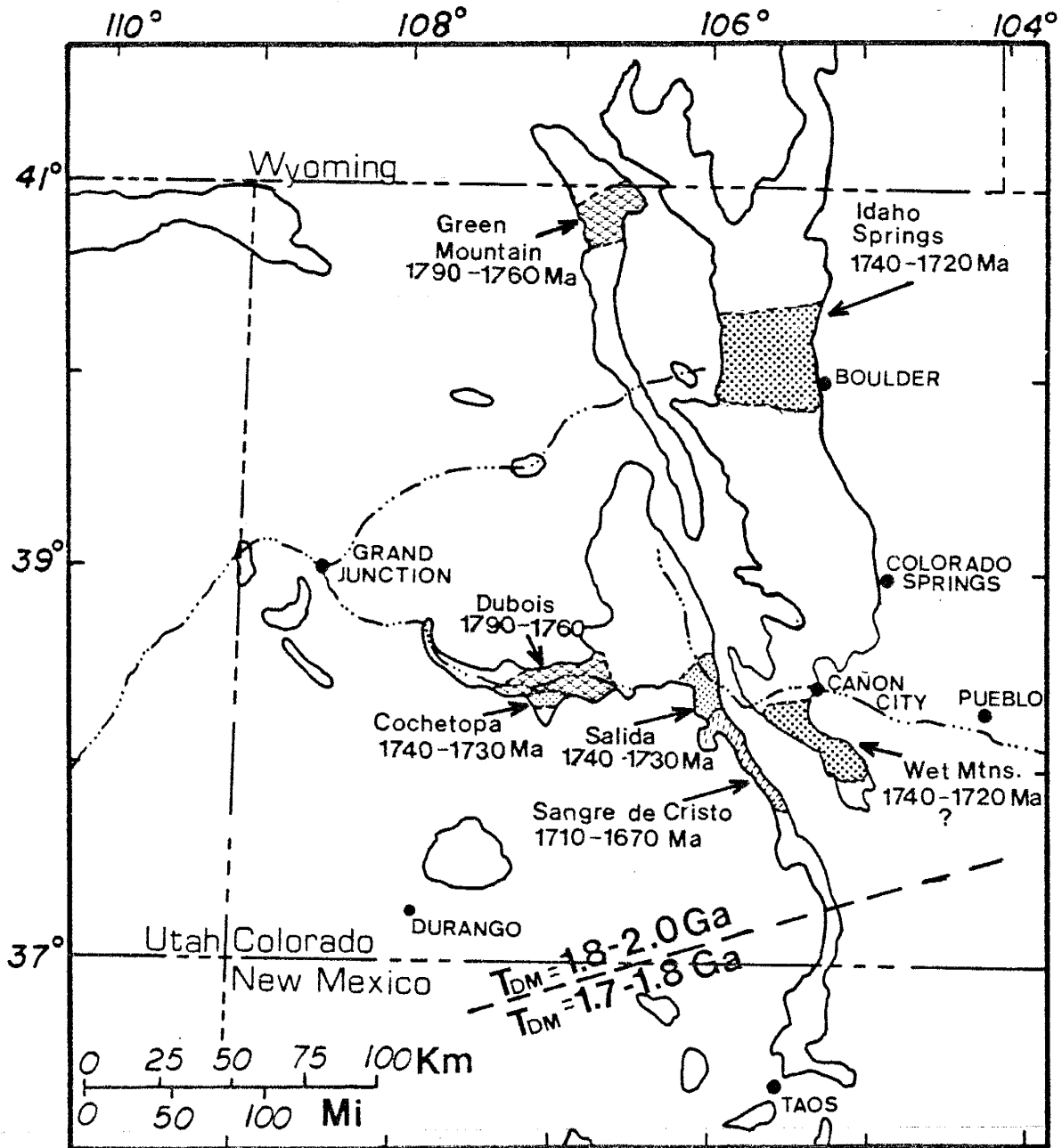
Figure 73: A generalized geologic map of the Precambrian terranes in Colorado and adjacent areas. Shaded areas show key supracrustal areas and ages (modified after Cullers, 1986, Knoper and Condie, 1986, and Nelson and DePaolo, 1985)
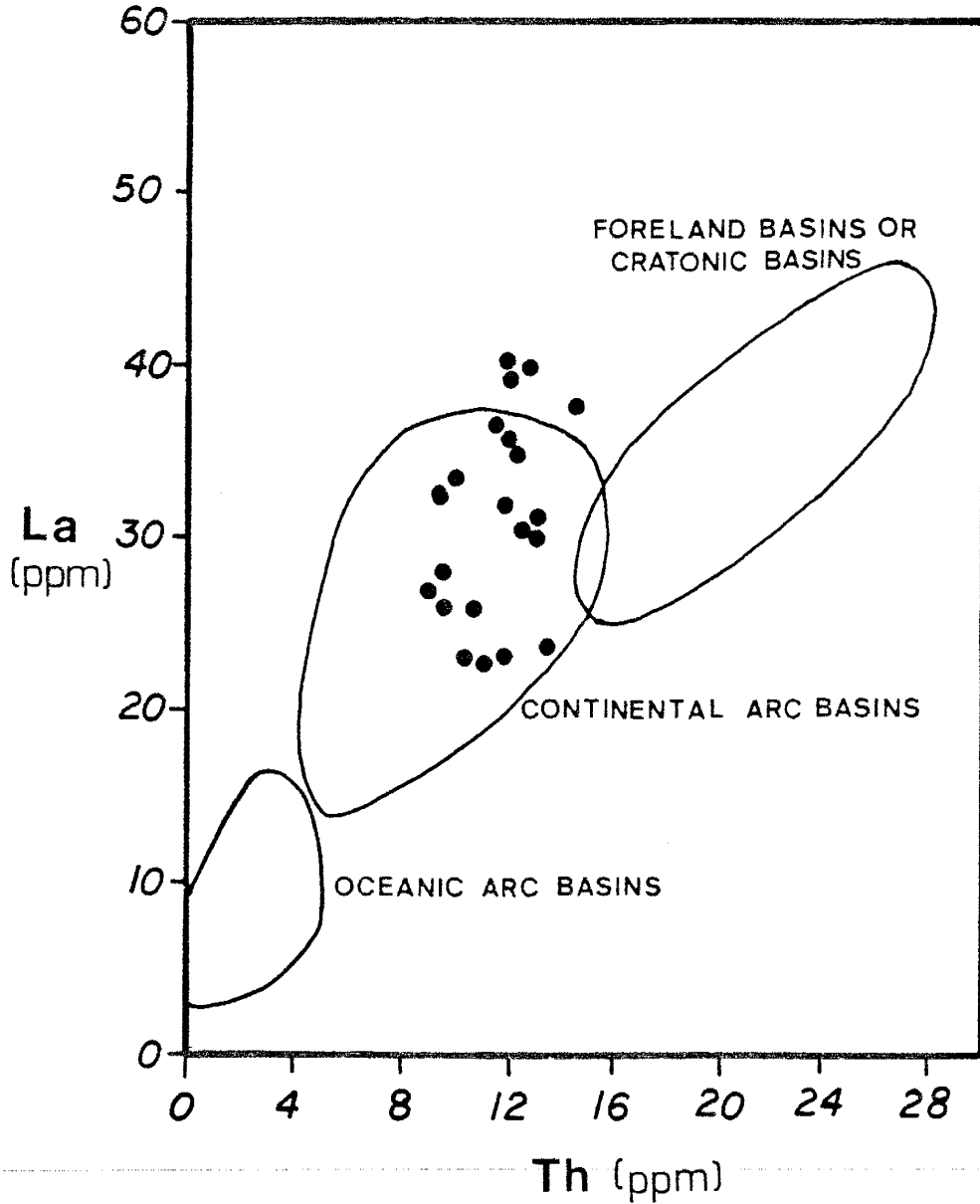
Figure 74: Th-La discrimination diagram for sediments and their tectonic settings (after Bhatia and Crook, 1983). Solid circles represent metagraywackes from the Big Thompson Canyon area of the Idaho Springs terrane (data from Condie and Martell, 1983).

study. The PC is composed of mostly mafic volcanics (45%) and volcaniclastic sediments (40%) and some minor felsic volcanics (15%) which show geochemical similarities to volcanics erupted in evolved oceanic arcs and associated, incipiently opened back-arc basins.

Many scenarios exist on how tectonic processes may have acted to combine the local Proterozoic *fragments* into a more regional framework, but most of these, due to lack of data, remain highly speculative. Two models, however, seem to be receiving the most attention. Reed, et. al., (1987) suggest that there is strong data to support the idea that a major deformational event occurred at about 1710 Ma, based upon the relationship of geochronologic data to structural trends in Colorado. This would support the idea that the WM was emplaced and deformed by 1710 Ma, suggesting that the terrane may be older than about 1720 Ma and that it is older than the SDC to the west, at 1710–1670 Ma. It still remains to be seen if the SDC displays any evidence of the 1710 Ma deformational event, but the striking differences in lithology across the Wet Mountains Valley emphasizes the dissimilarity between the SDC and the WM, since felsic volcanic units dominate the SDC and sediments the WM. Lithologically the WM is most similar to units from the IS since, like the Wet Mountains, the IS is dominated by metasedimentary units. Additionally, the units of the IS bear a geochronologic similarity to the units of the WM, if the WM is older than 1720 Ma, since they fall in the 1740–1720 Ma age group. If they are analogous, this may intimate that the WM may also be of the 1740–1720 Ma age. It may be interesting to note that the metasediments in the Wet Mountains tend to have higher concentrations of Hf, Zr, Th, and Si than those of the Idaho Springs area. It is possible, yet highly speculative, that the Wet Mountains may represent a stratigraphically higher portion of the same sedimentary package and that the higher elemental concentrations could represent

a reflection of increased sediment recycling, mostly in the mineral zircon, in the stratigraphic pile.

The tectonic expression of the 1710 Ma deformational episode is unclear and, interestingly, seems to be the point of greatest contention. The Pecos and Sangre de Cristo terranes should display the effects of this deformation, since they pre-date it. Reed, et. al., (1987) make a strong point of the fact that the deformation throughout Colorado is characterized by a complex, heterogeneous fabric and that this heterogeneity is inconsistent with regional compression or shearing. Rather, they argue that the complex pattern of foliation is more conveniently justified by deformation and metamorphism accompanying the emplacement of voluminous plutons in a magmatic arc system and, indeed, this model has appeal even in the new developing concepts in the genesis of granulites.

Bohlen (1987) offers that many granulite terranes have average geothermal gradients of 30–35°C/km and that initial cooling of granulites from peak metamorphic conditions tends to be nearly isobaric. He also suggests that these characteristics, taken as a whole, imply that many granulites form as a result of anomalous thermal gradients caused by the intrusion of magmas beneath or into a given terrane rather than as a result of increased burial. A likely environment for such granulite formation, he states, would be in a magmatically thickened and heated crust of a continental arc environment.

Alternatively, another way of explaining the rapid formation of new crust at this time would be to invoke a model of arc accretion. Accretion would be a viable model for producing the bedding parallel foliation commonly seen in much of Colorado and northern New Mexico by crustal shortening. It may be that a substantial accretionary event at 1710 Ma would be responsible for the deformation pegged at that time. The apparently horizontal stresses associated with the

1700Ma similar folds in the Mount Tyndall quadrangle would agree with such a model. As for the argument that this cannot explain the complex structural fabric of Colorado, keep in mind that in many areas in Colorado the Proterozoic sequences have seen as many as three strong deformational events. Additionally, plutonism associated with the terminus of some of these events may have significantly disturbed existing fabrics (Tweto, 1980a). Also, it has been suggested that during accretion it is not uncommon to see a structural rotation of stresses as the accretion proceeds which may also complicate the structure.

Although, admittedly, the foliation patterns in Colorado do seem to be complex, some overall structural trends do seem to exist. Throughout Colorado a belt of Precambrian faults extend northeast and seem to have been activated before 1700 Ma (Warner, 1980). This pattern defines a major structural discontinuity referred to as the Colorado Lineament, the northern extension of which is the Wyoming shear zone. At least in the northern part of the state, foliation trends do show a dominant east-northeast to east trend which is also evident in the subsurface and in gravity and aeromagnetic maps (Tweto, 1980a). Tweto (1987) points out that both aeromagnetic and Bouger gravity maps show an east-west pattern, defined by magnetic grain and gravity signatures. These features, he notes, match the surface geology poorly, suggesting a deep crustal feature.

In the southern part of the state a gravity anomaly has been identified which parallels the northeasterly trend in structure seen to the north. Simpson, et. al. (1986) note that a linear gravity low extends northeastward from northern New Mexico across the southeastern corner of Colorado and into Nebraska and suggest that this low may indicate a Precambrian structure, perhaps a high-low gravity pair over a Precambrian suture zone. Such a suture may separate an oceanic arc type terrane to the south, the Pecos terrane in particular, from a

more continental margin arc system to the north and represent the suture of an arc-arc collision. This location also corresponds roughly to the general location where Condie (1986) proposes a boundary based on lithologic constraints and geochemical constraints and where Bennett and DePaolo (1987) show a change in Sm-Nd model ages (Fig. 73) which separate crusts derived from the mantle between 2.0–1.8 Ga (T_{DM}) to the north and 1.8–1.7 Ga to the south. Distinct, sharp changes in the T_{DM} ages of provinces has been taken to infer, in the past, juxtaposition of two age terranes along faults or sutures, although it should be cautioned that DePaolo and Bennett's data is not clearly defined due to lack of detailed data at the boundary. Aleinikoff and Reed (1987), however, note that common Pb ratios from the area suggest that the rocks from northern New Mexico were derived from a more evolved 1.8 Ga source while those of the Colorado province are derived mainly from a 2.0 Ga primitive source.

A possible suture has as yet not been identified at the surface. There is a possibility that it may be covered under younger volcanic and sedimentary units such as those of the Sangre de Cristo terrane or the Burned Mountain Rhyolite in the Tusas Range of New Mexico, 1700 Ma (Reed, et. al., 1987). Many have suggested that the 1700 Ma deformation seen throughout the southwest is associated with accretionary tectonics. Harris et. al. (1987) have observed that there is evidence for north directed, thin-skinned thrusting and north-northwest shortening in the Needle Mountains of Colorado. Karlstrom et. al. (1987) suggest that accretion was responsible for the juxtaposition of two tectonic provinces in central Arizona with contrasting rock-types, deformational styles, metamorphic grades, and chronologies of deformation. They suggest that this may have occurred at about 1710 Ma since they see continentally derived volcanic and sedimentary units of 1710–1692 Ma age lying unconformably on newly accreted continental crust.

In such a scenario, the Pecos arc system would collide with the continental margin arc in Colorado at 1710 Ma. This juxtaposition of terranes would be responsible for the gravity anomaly in southern Colorado, the northeasterly trending structural fabric in the central Wet Mountains, and result in extensive crustal thickening. The crustal thickening, in turn, would cause dehydration and promote the high-P CO_2 metamorphism of the terrane. This is one point this model addresses which the magmatic model does not. The magmatic model, as stated by Reed, et. al. (op. cit.), calls for a high-T but low-P metamorphism, but the LIL-depletion in the granulites and the proposed entrapment pressures of the fluid inclusions in the granulites call for metamorphic pressures on the order of 8-9 kbars. The accretion model provides a much more viable mechanism for developing such high pressures through crustal thickening.

The water purged from the system during accretion may, in turn, promote partial melting of the metasediments, giving rise to the leucogranites as volatile-induced melts. This would explain the affinity of the leucogranites to leucogranites from collisional terranes and the later uplift might result in the retrogression of some of the granulites to amphibolite facies assemblages.

REFERENCES

Abbey, S., 1983, Studies in "standard samples" of silicate rocks and minerals, 1969–1982: *Geol. Survey of Canada Paper 83-15.*

Aleikoff, J. M., Reed, J. C., and Pallister, J. S., 1987, Tectonic interpretations of the Colorado Proterozoic province based on common Pb data from feldspars in 1400Ma and 1700Ma plutons: (abst.) *Geol. Soc. Amer. Abstracts with Programs; Rocky Mountain Regional Meeting,* v19, no. 5, p. 257.

Arth, J. G., 1976, Behavior of trace elements during magmatic processes: a summary of theoretical models and their applications: *Journ. of Research of U. S. Geol. Survey,* v4, p. 41–47.

Bard, J. P., **Microtextures of Igneous and Metamorphic Rocks,** Dordrecht: D. Reidel Pub. Co., 1986.

Barker, F., (ed), **Trondhjemites, Dacites, and Related Rocks,** New York: Elsevier, 1979.

Barth, T. F. W., 1959, Principles of classification and norm calculations of metamorphic rocks: *Journ. of Geol.,* v67, p. 135–152.

Bennett, V. C., and DePaolo, D. J., 1987, Proterozoic crustal history of the western United States as determined by neodymium isotopic mapping: *Geol. Soc. of America Bull.,* v99, p. 674–685.

Berberian, F., and Berberian, M., 1981, Tectano-plutonic episodes in Iran: *in* Gupta, H. K., and Delaney, F. M. (eds.), **Zagros-Hindu Kush-Himalaya: Geodynamic Evolution; Geodynamics Series vol. 3,** Washington: AGU Press.

Berning, J., Cooke, R., Hiemstra, S. A., and Hoffman, U., 1976, The Rössing uranium deposit, southwest Africa, *Econ. Geol.,* v71, p. 351–368.

Bhatia, M. R., 1983, Plate tectonics and geochemical composition of sandstones: *Journ. of Geol.,* v91, p. 611–627.

Bhatia, M. R., and Crook, K. A. W., 1983, Trace element characteristics of graywackes and tectonic setting discrimination of sedimentary basins: *Contrib. Mineral. Petrol.,* v92, p. 181–193.

Bhatia, M. R., and Taylor, S. R., 1981, Trace-element geochemistry and sedimentary provinces: a study from the Tasman geosyncline, Australia: *Chemical Geology,* v33, p. 115–125.

Bickford, M. E., 1986, Geochronology of volcanic and plutonic rocks in the Gunnison, Salida, and Wet Mountains areas, Central Colorado: *in* W. R. Van Schmus [ed.], **IGCP Guidebook on Proterozoic Geology and Geochemistry of Central Colorado,** p. 17–26.

Bickford, M. E., Cullers, R. L., Lanzirotti, A., Noblett, J. B., and Wobus, B. J., 1987, Proterozoic geology of the Wet Mountains, Colorado [abs.]: **Geological Society of America 1987 Annual Meeting, Programs with Abstracts,** v19, no. 7.

Bickford, M. E., Van Schmus, W. R., and Zietz, I., 1986, Proterozoic history of the midcontinent region of North America: *Geology,* v14, p. 492–496.

Boardman, S. J., 1986, Early Proterozoic bimodal volcanic rocks in central Colorado, U. S. A., part 1: petrography, stratigraphy, and depositional history: *Precamb. Res.*, v34, p. 1–36.

Boardman, S. J., and Condie, K. C., 1986, Early Proterozoic bimodal volcanic rocks in central Colorado, U. S. A., part 2: geochemistry, petrogenesis, and tectonic setting: *Precamb. Res.*, v34, p. 37–68.

Bohlen, S. R., 1987, Pressure-temperature-time paths and a tectonic model for the evolution of granulites: *Journ. of Geol.*, v95, p. 617–632.

Boyer, R. E., 1962, Petrology and structure of the southern Wet Mountains, Colorado: *Geol. Soc. of America Bull.*, v73, p. 1047–1070.

Brock, M. R., and Singewald, Q. D., 1968, Geologic map of the Mount Tyndall Quadrangle, Custer County, Colorado: *U. S. Geol. Survey Geologic Quadrangle map GQ-596.*

Castelli, D., and Lombardo, B., 1988, The Gophu La and western Lunana granites: Miocene muscovite leucogranites of the Bhutan Himalaya: *Lithos*, v21, p. 211–225.

Christman, R. A., Brock, M. R., Pearson, R. C., and Singewald, Q. D., 1959, Geology and thorium deposits of the Wet Mountains, Colorado; a progress report: *U. S. Geol. Survey Bull.* 1072-H, p. 491–535.

Clemens, J. D., and Vielzeuf, D., 1987, Constraints on melting and magma production in the crust: *Earth and Planet. Sci. Lett.*, v86, p. 287–306.

Clemens, J. D., and Wall, V. J., 1988, Controls on the mineralogy of S-type volcanic and plutonic rocks: *Lithos*, v21, p. 53–66.

Condie, K. C., 1986, Geochemistry and tectonic setting of early Proterozoic supracrustal rocks in the southwestern United States: *Journ. of Geol.*, v94, p. 845–864.

Condie, K. C., 1982, Plate tectonics model for Proterozoic continental accretion in the southwestern United States: *Geology*, v10, p. 37–42.

Condie, K. C., and Allen, P., 1984, Origin of Archean charnokites from southern India: *in* A. Kröner, **Archean Geochemistry**, p. 182–203, Berlin: Springer-Verlag, 1984.

Condie, K. C., Allen, P., and Narayana, B. L., 1982, Geochemistry of Archean low- to high-grade transition zone, southern India: *Contrib. Miner. Petrol.*, v81, p. 157–167.

Condie, K. C., Bowling, G. P., and Vance, R. K., 1985, Geochemistry and origin of early Proterozoic rocks, Dos Cabezas Mountains, southeastern Arizona: *Geol. Soc. of America Bull.*, v96, p. 655–662.

Condie, K. C., and DeMalas, J. P., 1985, The Pinal Schist: an early Proterozoic quartzwacke Association in southeastern Arizona: *Precamb. Res.*, v27, p. 337.

Condie, K. C., and Knoper, M. W., 1986, Geology and origin of early Proterozoic rocks from the Gunnison area, central Colorado: *in* W. R. Van Schmus [ed.], **IGCP Guidebook on Proterozoic Geology and Geochemistry of Central Colorado**, p. 3–16.

Condie, K. C., and Martell, C., 1983, Early Proterozoic metasediments from north-central Colorado: metamorphism, provenance, and tectonic setting: *Geol. Soc. of America Bull.*, v94, p. 1215.

Copeland, P., and Condie, K. C., 1986, Geochemistry and tectonic setting of lower Proterozoic supracrustal rocks of the Pinal Schist, southeastern Arizona: *Geol. Soc. of America Bull.*, v97, p. 1512–1520.

Cullers, R. L., and Wobus, R. A., 1986, Proterozoic framework of the southern Front Range and Wet Mountains, Colorado: *in* W. R. Van Schmus [ed.], **IGCP Guidebook on Proterozoic Geology and Geochemistry of Central Colorado**, p. 55–68.

Davis, A., et. al., 1979, Trace element geochemistry and origin of late Precambrian, early Cambrian Catoctin greenstones of the Appalachian Mountains: *Univ. Calif. Davis unpub. manuscript.*

De la Roche, H., 1966, Sur l'existence de plusieurs faciés géochimiques dans les schistes paléozoiques des Pyrénées Luchonnaises: *Geol. Rundsch.*, v55, p. 274–315.

Dufour, E., 1985, Granulite facies metamorphism and retrogressive evolution of the Monts du Lyonnais metabasites, Massif Central, France: *Lithos*, v18, p. 97–113.

Ehlers, D., and Blatt, G., **Petrology; Igneous, Sedimentary and Metamorphic**, San Francisco: W. H. Freeman and Co., 1983.

Elthon, D., 1983, Isomolar and isostructural pseudo-liquidus phase diagrams for oceanic basalts: *Amer. Minr.*, v68, p. 506–511.

Elthon, D., 1984, High-pressure equilibria of a high-magnesia basalt and the genesis of primary oceanic basalts: *Amer. Minr.*, v69, p. 1–15.

Essene, E. J., 1982, Geologic thermometry and barometry: *in* Ferry, J. M., (ed.) **Characterization of Metamorphism through Mineral Equilibria, Reviews in Mineralogy, Vol10**, Washington: Miner. Soc. of America.

Floyd, P. A., and Leveridge, B. E., 1987, Tectonic environment of the Devonian Gramscatho basin, south Cornwall: framework mode and geochemical evidence from turbiditic sandstones: *Journ. of Geol. Soc. of London*, v144, p. 531–542.

Furnes, H., Ryan, P. D., Greene, T., Roberts, D., Sturt, B. A., and prestvik, J., 1985, Geological and geochemical classification of the ophiolitic fragments in the Scandinavian Caledonides: *in* **The Caledonide Orogen - Scandinavian and Related Areas, vol 2**, p. 657–669, New York: J. Wiley and Sons, 1985.

Gansser, A., **Geology of the Bhutan Himalaya**, Basel: Birkhäuser-Verlag, 1983.

Gibson, I. L., and Jagam, P., 1980, Instrumental neutron activation analysis of rocks and minerals: *in* Mueke, G. K., (ed.) **Short Course in NAA in the Geosciences** Halifax: Min. Assoc. of Canada.

Goldsmith, J. R., 1976, Scapolites, granulites, and volatiles in the lower crust: *Geol. Soc. of Amer. Bull.*, v87, p. 161–168.

Goldsmith, J. R., and Newton, R. C., 1977, Scapolite-plagioclase stability relationships at high pressures and temperatures in the system $NaAlSi_3O_8 - CaAl_2Si_2O_8 - CaCO_3 - CaSO_4$: *Amer. Mineral.*, v62, p. 1063–1081.

Hall, A., **Igneous Petrology**, New York: Longman Scientific and Technical, 1987.

Hansen, E. C., Janardhan, A. S., Newton, R. C., Prame, W. K. B. N., and Ravindra Kumar, G. R., 1987, Arrested charnockite formation in southern India and Sri Lanka: *Contrib. Mineral. Petrol.*, v96, p. 225–244.

Hansen, E. C., Newton, R. C., and Janadhan, A. S., 1984, Fluid inclusions in rocks from the amphibolite-facies gneiss to charnockite progression in southern Karnataka, India: direct evidence concerning the fluids of granulite metamorphism: *Journ. of Metam. Geol.*, v2, p. 249–264.

Harley, S. L., 1987, Precambrian geological relationships in high-grade gneisses of the Rauer Islands, east Antarctica: *Australian Journ. of Earth Sci.*, v34, p.175–207.

Harris, C. W., Gibson, R. G., Simpson, C., and Eriksson, K. A., 1987, Proterozoic cuspate basement-cover structure, Needle Mountains, Colorado: *Geology*, v15, p. 950–953.

Harris, N. B. W., Pearce, J. A., and Tindle, A. G., 1986, Geochemical characteristics of collision zone magmatism: *in* Ries, A. C., and Coward, M. P., (eds.) **Collision Tectonics: Geol. Soc. of London Spec. Publ. 19**.

Henderson, P., **Rare Earth Element Geochemistry**, Amsterdam: Elsevier, 1984.

Hollister, L. S., and Crawford, M. L., 1986, Melt-enhanced deformation: a major tectonic process: *Geology*, v14, p. 558–561.

Huang, W., and Wyllie, P. J., 1975, Melting relationships in the system $NaAlSi_3O_8 - KAlSi_3O_8 - SiO_2$ to 35 kilobars, dry and with excess water: *Journ. of Geol.*, v83, p. 737–748.

Hubbard, F. H., 1975, The Precambrian crystalline complex of southwestern Sweden: the geology and petrogenetic development of the Varberg region: *Geologiska Föreningens i Stockholm Förhandlinger*, v97, p. 223–236.

Hyndman, D. M., **Petrology of Igneous and Metamorphic Rocks**, New York: McGraw-Hill, 1972.

Jackson, M. P. A, 1976, **High-Grade Metamorphism and Migmatization of the Namaqua Metamorphic Complex around Aus in the Southern Namib Desert, South-West Africa**: Bull. 18, Univ. of Capetown Chamber of Mines, Precamb. Res. Unit.

Jacob, R. E., 1978, Granite genesis and Associated mineralization in part of the central Damara Belt: *in* Verwoerd, W. J., (ed.), **Mineralization in Metamorphic Terranes**, Pretoria: Van Schaik.

Janardhan, A. S., Newton, R. C., and Hansen, E. C., 1982, The transformation of amphibolite facies gneiss to charnockite in southern Karnataka and northern Tamil Nadu, India: *Contrib. Mineral. Petrol.*, v79, p. 130–149.

Jensen, M., 1976, Ontario division of Mines Misc. Paper 66.

Jolly, W. T., 1980, Development and degradation of Archean lavas of the Abitibi area, Ontario and Quebec: *Journ. of Petrol.*, v21, p. 323–363.

Jover, O., and Bouchez, J., 1986, Mise en place syntectonique des granitoïdes del l'Quest du Massif Central français: *C. R. Acad. Sc. Paris*, t303, Série II, n° 10, p. 969–974.

Karlstrom, K. E., Bowring, S. A., and Conway, C. M., 1987, Tectonic significance of an early Proterozoic two-province boundary in central Arizona: *Geol. Soc. of Amer. Bull.*, v99, p. 529-538.

Knoper, M. W., Condie, K. C., Thacker, M., and Lanzirotti, A., 1987, Early Proterozoic tectonic history in Colorado [abs.]: **Geological Association of Canada Special Session on the Trans-Hudson Orogen, abstracts with program.**

Kröner, A., **Precambrian Plate Tectonics**, Amsterdam: Elsevier, 1981.

Lanzirotti, A., 1987, Developing gas geothermometers for high temperature metamorphic fluid inclusions [abs.]: **American Current Research on Fluid Inclusions 1st annual meeting, program and abstracts.**

Lanzirotti, A., and Condie, K. C., 1988, Origin and tectonic significance of early Proterozoic leucogranites and high-pressure granulites in the Wet Mountains, Colorado [abs.]: **Geol. Soc. of America Symposium on Geology and Geophysics of the Mid-Continent Region: G. S. A. Abstracts with Programs**, v20, no. 2.

Lanzirotti, A., and Condie, K. C., 1986, Geochemical characteristics of early Proterozoic rocks from the Mount Tyndall area, Wet Mountains, Colorado [abs.]: *in* W. R. Van Schmus [ed.], **IGCP Guidebook on Proterozoic Geology and Geochemistry of Central Colorado**, p. 104-106.

Le Fort, P., Cuney, M., Deniel, C., France-Lanord, C., Sheppard, S. M. F., Upreti, B. N., and Vidal, P., 1987, Crustal generation of the Himalayan leucogranites: *Tectonophysics*, v134, p. 39-57.

Le Fort, P., 1981, Manaslu leucogranite: a collision signature of the Himalaya; a model for its genesis and emplacement: *Journ. of Geop. Res.*, v86, p. 10545-10568.

Mason, B., and Moore, C. B., **Principles of Geochemistry**, New York: John Wiley and Sons, 1982.

Matte, P., 1983, Two Geotraverses across the Ibero-Armorican Variscan arc of western Europe: *in* Rast, N., and Delaney, F. M., (eds.), **Profiles of Orogenic Belts; Geodynamics Series vol. 10**, Washington: AGU Press.

Middlemost, E. A. K., **Magmas and Magmatic Rocks: an Introduction to Igneous Petrology**, London: Longman Press, 1985.

Mitchell, A. H. G., 1978, Geosynclinal and plate-tectonic hypotheses: significance of late-orogenic Himalayan tin granites and continental collision: *in* 11th **Commonwealth Min. Metall. Congr. of Inst. Min. Metall.**, Hong Kong, p. 79-91.

Mitchell, A. H. G., 1974, Southwest England granites: magmatism and tin mineralization in a post-collision tectonic setting: *Inst. Min. Metall. Trans.*, v83, p. B95-B97.

Miyashiro, A., **Metamorphism and Metamorphic Belts**, London: George, Allen, and Unwin, 1973.

Moench, R. H., Harrison, J. E., and Sims, P. K., 1962, Precambrian folding in the Idaho Springs-Central City area, Front Range, Colorado: *Geol. Soc. of Amer. Bull.*, v73, p. 35-58.

Moore, J. M., 1986, A comparative study metamorphosed supracrustal rocks from the western Namaqualand metamorphic complex: [diss.] Univ. of Capetown, South Africe.

Muecke, G. K., Pride, C., and Sarkar, P., 1979, Rare earth element geochemistry of regional metamorphic rocks: *in* Ahrens, C. H. (ed.) **Origin and Distribution of the Elements**, Oxford: Paragamon Press.

Munasinghe, T., and Dissanayake, C. B., 1980, Pink granites in the Highland Series of Sri Lanka - a case study: *Journ. Geol. Soc. of India*, v21, p. 446-452.

Navarro, E., and Blackburn, W., 1974, Investigations in the basement rocks of Gunnison county, Colorado: the metasedimentary rocks: *N. Jb. Miner. Abh.*, v122, p. 246-267.

Nelson, B. K., and DePaolo, D. J., 1984, 1700-Myr greenstone volcanic successions in southwestern North America and isotopic evolution of Proterozoic mantle: *Nature*, v312, p. 143-146.

Nelson, B. K., and DePaolo, D. J., 1985, Rapid production of continental crust 1.9 b.y. ago: Nd isotopic evidence from the basement of the North American mid-continent: *Geol. Soc. of America Bull.*, v96, p. 746-754.

Newton. R. C., 1986, Fluids of granulite facies metamorphism: *in* Walther, J. V., and Wood, B. J. [eds.], **Fluid-Rock Interactions During Metamorphism**, p. 36-59, New York: Springer-Verlag.

Newton, R. C., Smith, J. V., and Windley, B. F., 1980, Carbonic metamorphism, granulites, and crustal growth: *Nature*, v288, p. 45-50.

Noblett, J. B., Cullers, R. L., and Bickford, M. E., 1987, Proterozoic crystalline rocks in the Wet Mountains and vicinity, central Colorado: *in* **New Mexico Geological Society Guidebook, 38**[th] **Field Conference**, p. 73-82.

Noblett, J. B., 1987, Geology of the Precambrian metamorphic rocks along South Hardscrabble Creek, Wet Mountains, Colorado: *Mountain Geologist*, v24, p. 67-76.

Norrish, K., and Chappell, B. W., 1977, An accurate X-ray spectrographic method for the analysis of a wide range of geologic samples: *Geoc. et Cosmoc. Acta*, v33, p. 431-453.

Norrish, K., and Hutton, J. T., 1969, X-ray fluorescence spectrometry: *in* Zussman, J. (ed.) **Physical Methods in Determinative Mineralogy** London: Academic Press.

Odonne, F., 1987, Hinge migration as a mechanism of superimposed folding: *Journ. of Struct. Geol.*, v9, p. 835-844.

Pearce, J. A., 1987, An EXPERT system for the tectonic characterization of ancient volcanic rocks: *Journ. of Volc. and Geoth. Res.*, v32, p. 51-65.

Pearce, J. A., 1983, Role of the subcontinental lithosphere in magma genesis at active continental margins; *in* C. J. Hawkesworth and M. J. Norry (eds), **Continental Basalts and Mantle Xenoliths**, Cheshire, UK: Shiva Press Ltd.

Pearce, J. A., and Cann, J. R., 1973, Tectonic setting of basic volcanic rocks determined using trace element analyses: *Earth and Planet. Sci. Lett.*, v19, p. 290-300.

Pearce, J. A., Harris, N. B. W., and Tindle, A. G., 1984, Trace element discrimination diagrams for the tectonic interpretation of granitic rocks: *Journ. of Petrology*, v25, p. 956-983.

Perera, L. R. K., 1983, The origin of the pink granites of Sri Lanka: another view: *Precamb. Res.*, v20, p. 17–37.

Pettijohn, F. J., Potter, P. E., and Siever, R., **Sand and Sandstones**, New York: Springer-Verlag, 1973.

Pharaoh, T. C., and Pearce, J. A., 1984, Geochemical evidence for the geotectonic setting of early Proterozoic metavolcanic sequences in Lapland: *Precamb. Res.*, v25, p. 283–308.

Prabhu, M. K., and Webber, G. R., 1983, Origin of quartzofeldspathic gneisses at Montauban les Mines, Quebec: *Can. Journ. of Earth Sci.*, v21, p. 336–345.

Price, N. J., and Audley-Charles, M. G., 1987, Tectonic collision processes after plate rupture: *Tectonophysics*, v140, p. 121–129.

Quensel, P., 1951, The charnockite series of the Varberg district on the southwest coast of Sweden: *Arkiv. Mineral. Geol.*, v1, p. 229–332.

Ragan, D. M., **Structural Geology: An Introduction to Geometrical Techniques**, New York: John Wiley and Sons, 1973.

Ramsay, J. G., **Folding and Fracturing of Rocks**, New York: McGraw-Hill, 1967.

Reed, J. C., 1986, Chronology of deformation and metamorphism in the early Proterozoic terrane of the southern Rocky Mountains [abs.]: *in* W. R. Van Schmus [ed.], **IGCP Guidebook on Proterozoic Geology and Geochemistry of Central Colorado**, p111–112.

Reed, J. C., Bickford, M. E., Premo, W. R., Aleinikoff, J. N., and Pallister, J. S., 1987, Evolution of the early Proterozoic Colorado province: constraints from U-Pb geochronology: *Geology*, v15, p. 861–865.

Reuss, R. L., 1974, Precambrian quartzite-schist sequence in Wilson Park, Fremont County, Colorado: *The Mountain Geologist*, v11, p. 45–58a.

Rogers, J. J. W., Ragland, P. C., Nishimori, R. K., Greenberg, J. K., and Hauk, S. A., 1978, Varieties of granite uranium deposits and favorable exploration areas in the eastern United States: *Econ. Geol.*, v73, p. 1539–1555.

Sawyer, E. W., 1987, The role of partial melting and fractional crystallization in determining discordant migmatite leucosome composition: *Journ. of Petrology*, v28, p. 445–473.

Schenk, V., 1984, Petrology of felsic granulites, metapelites, metabasics, ultramafics, and metacarbonates from southern Calabria (Italy): prograde metamorphism, uplift and cooling of a former lower crust: *Journ. of Petrol.*, v25, p. 255–298.

Scott, G. R., Taylor, R. B., Epis, R. C., and Wobus, R. A., 1978, Geologic map of the Pueblo 1° x 2° quadrangle, south-central Colorado: *U. S. Geol. Survey Miscellaneous Investigations Map I-1022.*

Shaw, D. M., 1972, The origin of the Apsley Gneiss, Ontario: *Can. Journ. of Earth Sci.*, v9, p. 18–35.

Shepherd, T., Rankin, A. H., and Alderton, D. H. M., **A Practical Guide to Fluid Inclusion Studies**, New York: Chapman and Hall, 1985.

Simpson, R. W., Jachens, R. C., and Blakely, R. J., 1986, Isostatic residual gravity analysis of the conterminous United States: *Journ. of Geop. Res.*, v91, p. 8348–8372.

Singewald, Q. D., 1966, Description and relocation of the Ilse fault zone, Wet Mountains, Colorado: *U. S. Geol. Survey Prof. Paper 550-C*, p. C20–C24.

Tankard, A. J., Jackson, M. P. A., Eriksson, K. A., Minter, W. E. L., Hunter, D. R., and Hobday, D. K., **Crustal Evolution of Southern Africa; 3.8 Billion Years of Earth History**, New York: Springer-Verlag, 1982.

Taylor, R. B., 1975, Geologic map of the Black Hawk quadrangle, Gilpin, Jefferson, and Clear Creek counties, Colorado: *U. S. Geol. Survey Geologic Quadrangle Map GQ-1248*.

Taylor, R. B., Scott, G. R., Wobus, R. A., and Epis, R. C., 1975, Reconnaissance geologic map of the Royal Gorge quadrangle, Fremont and Custer counties, Colorado: *U. S. Geol. Survey Miscellaneous Investigations Map I-869*.

Taylor, S. R., and McClennan, S. M., **The Continental Crust: its Composition and Evolution**, Oxford: Blackwell Scientific Publications, 1985.

Tewksbury, B. J., 1985, Revised interpretation of the age of allochtonous rocks of the Uncompaghre Formation, Needle Mountains, Colorado: *Geol. Soc. of America Bull.*, v96, p. 224–232.

Thacker, M., and Condie, K. C., 1986, Early Proterozoic supracrustal rocks from the northern sangre de Cristo mountains and adjacent areas, Colorado [abs.]: *in* W. R. Van Schmus [ed.], **IGCP Guidebook on Proterozoic Geology and Geochemistry of Central Colorado**, p. 122–123.

Thiessen, R. L., and Means, W. D., 1980, Classification of fold interference patterns: a re-examination: *Journ. of Struct. Geol.*, v2, p. 311–316.

Touret, J., and Bottinga, Y., 1979, Équation d'état pour le CO_2 ; application aux inclusions carboniques: *Bull. Minéral.*, v102, p. 577–583.

Trumbell, R. B., 1988, Petrology of flecked gneisses in the northern Wet Mountains, Fremont County, Colorado: *Geol. Soc. of America Bull.*, v100, p. 247–256.

Tweto, O., 1987, Rock units of the Precambrian basement in Colorado: **U. S. G. S. Prof. Paper #1321-A**.

Tweto, O., 1980a, Tectonic history of Colorado: *in* **Rocky Mountain Association of Geologists' 1980 Symposium Guidebook**, p. 5–9.

Tweto, O., 1980b, Precambrian geology of Colorado: *in* **Rocky Mountain Association of Geologists' 1980 Symposium Guidebook**, p. 37–46.

Tweto, O., 1977, Nomenclature of Precambrian rocks in Colorado: **U. S. G. S. Bull. #1422-D**.

Van de Kamp, P. C., 1968, Geochemistry and origin of metasediments in the Haliburton-Madoc area, southeastern Ontario: *Can. Journ. of Earth Sci.*, v5, p. 1337–1372.

Van de Kamp, P. C., and Beakhouse, G. P., 1979, Paragneisses in the Pakwash Lake area, English River Gneiss Belt, Northwest Ontario: *Can. Journ. of Earth Sci.*, v16, p. 1753–1763.

Van de Kamp, P. C., and Leake, B. E., 1986, Petrography and geochemistry of feldspathic and mafic sediments of the northeastern Pacific margin: *Trans. Royal Soc. of Edinburgh*, Earth Sciences Devision, v74, p. 411–449.

Vidal, Ph., Bernard-Griffiths, J., Cocherie, A., LeFort, P., Peucart, J. J., and Sheppard, S. M. F., 1984, Geochemical comparison between Himalayan and Hercynian leucogranites: *Physics of Earth and Planet. Interiors*, v35, p. 179–190.

Vidal, Ph., Cocherie, A., and LeFort, P., 1982, Geochemical investigations of the origin of the Manaslu leucogranite: Himalaya, Nepal: *Geochem. et Cosmochem. Acta*, v46, p.2279–2292.

Wager, L. R., 1963, The mechanism of adcumulus growth in the layered series of the Skaergaard intrusion: *Min. Soc. Amer. Spec. Paper 1*, p. 1–9.

Warner, L. A., 1980, The Colorado Lineament: *in* **Rocky Mountain Association of Geologists' 1980 Symposium Guidebook**, p. 11–21.

Warren, R. G., Hensen, B. J., and Ryburn, R. J., 1987, Wollastonite and scapolite in Precambrian calc-silicate granulites from Australia and Antarctica: *Journ. of Metam. Geol.*, v5, p. 213–223.

Weaver, B. L., and Tarney, J., 1980, Rare-earth geochemistry of Lewisian Granulite-facies gneisses, northwest Scotland: implications for the petrogenesis of the Archean lower continental crust: *Earth and Planet. Sci. Lett.*, v51, p. 279–296.

White, A. J. R., and Chappell, B. W., 1977, Ultrametamorphism and granitoid genesis: *Tectonophysics*, v43, p. 7–22.

Winchester, J. A., and Floyd, P. A., 1977, Geochemical discrimination of different magma series and their differentiation products using immobile elements: *Chemical Geology*, v20, p. 325–343.

Winkler, H. G. F., **Petrogenesis of Metamorphic Rocks**, 2nd ed., New York: Springer-Verlag, 1967.

Wobus, R. A., Epis, R. C., and Scott, G. R., 1979, Geologic map of the Cover Mountain quadrangle, Fremont, Park, and Teller counties, Colorado: *U. S. Geol. Survey Quadrangle Map I-1179*.

Wood, D. A., and Joron, J., 1979, A re-appraisal of the use of trace elements to classify and discriminate between magma series erupted in different tectonic settings: *Earth and Planet. Sci. Lett.*, v45, p. 326–336.

Wright, T. L., and Doherty, P. C., 1970, A linear programming and least squares computer method for solving petrologic mixing problems: *Geol. Soc. of America Bull.*, v81, p. 1995–2008.

Zwart, H. J., 1967, The duality of orogenic belts, *Geol. en Mijnbouw*, v46, p. 283–309.

Appendix 1: Sample Locations[4]

---

[4]All sample locations given in the Universal Transverse Mercator (UTM) system grid.

Sample#	Grid Location	Sample#	Grid Location
LHS-32	4230535mN, 481990mE	LOC-1	4238380mN, 474880mE
LHS-33	4230000mN, 482330mE	LOC-2	4238380mN, 474880mE
LHS-15	4229685mN, 484940mE	LOC-3	4238380mN, 474880mE
LHS-16	4229305mN, 484745mE	LOC-4	4238380mN, 474880mE
LHS-34	4228270mN, 482005mE	LOC-5	4238380mN, 474880mE
LHS-21	4228890mN, 482915mE	LOC-6	4233980mN, 477770mE
LHS-20	4228900mN, 483050mE	LOC-7	4233980mN, 477770mE
LHS-6	4228635mN, 483060mE	LOC-8	4233980mN, 477770mE
LHS-5	4228365mN, 483190mE	LOC-9	4236190mN, 477440mE
LHS-13	4228290mN, 483975mE	LOC-10	4236330mN, 476960mE
LHS-14	4228290mN, 483975mE	LOC-11	4236740mN, 476680mE
LHS-18	4228715mN, 483970mE	LOC-12	4237000mN, 476580mE
LHS-19	4228715mN, 483970mE	LOC-13	4237460mN, 471640mE
LHS-17	4228935mN, 484655mE	LOC-14	4236560mN, 471420mE
LHS-12	4228215mN, 484285mE	LRG2-1	4233690mN, 471890mE
LHS-11	4228080mN, 484360mE	LRG2-2	4233660mN, 471980mE
LHS-10	4228535mN, 485120mE	LWC-28	4232045mN, 459965mE
LHS-38	4227625mN, 483405mE	LWC-27	4232185mN, 459980mE
LHS-9	4228765mN, 481155mE	LWC-30	4230010mN, 460390mE
LHS-8	4229155mN, 480690mE	LWC-29	4230415mN, 460205mE
LHS-7	4229170mN, 480900mE	LWC-23	4230145mN, 459660mE
LHS-35	4229020mN, 479355mE	LWC-24	4230205mN, 459515mE
LHS-22	4227475mN, 486885mE	LWC-31	4229675mN, 460745mE
LHS-25	4227500mN, 487570mE	LWC-25	4229055mN, 460815mE
LHS-24	4227295mN, 487275mE	LWC-26	4228915mN, 460985mE
LHS-23	4227355mN, 487205mE	LWC-33	4228270mN, 460180mE
LHS-1	4225215mN, 487855mE	LWC-32	4227375mN, 460975mE
LHS-2	4225220mN, 487810mE	LWC-22	4226230mN, 460875mE
LHS-3	4225105mN, 487550mE	LWC-21	4226735mN, 461040mE

Table XV: Sample locations in UTM coordinates

Sample#	Grid Location	Sample#	Grid Location
LHS-36	4223310mN, 482520mE	LWC-17	4225875mN, 461715mE
LHS-28	4221815mN, 483660mE	LWC-16	4225815mN, 462310mE
LHS-29	4221545mN, 484340mE	LWC-3	4225395mN, 461235mE
LHS-30	4222615mN, 483390mE	LWC-2	4225210mN, 461405mE
LHS-37	4221665mN, 480610mE	LWC-1	4225225mN, 461490mE
LBM-1	4227485mN, 454805mE	LWC-5	4225205mN, 461600mE
LBM-2	4227565mN, 454720mE	LWC-6	4225220mN, 461655mE
LBM-3	4227935mN, 454660mE	LWC-7	4225235mN, 461710mE
LBM-4	4227935mN, 454660mE	LWC-4	4225020mN, 461630mE
LWC-14	4225200mN, 462610mE	LWC-13	4224900mN, 462495mE
LWC-12	4224880mN, 462360mE	LWC-11	4224895mN, 462115mE
LWC-8	4224895mN, 461745mE	LWC-10	4224630mN, 461625mE
LWC-9	4224895mN, 461285mE	LSC-1	4221255mN, 469935mE
LSC-2	4221295mN, 469905mE	LMT-20	4225045mN, 468995mE
LMT-46	4225225mN, 469060mE	LMT-21	4225030mN, 469340mE
LMT-45	4225490mN, 469890mE	LMT-44	4226040mN, 469645mE
LMT-22	4225220mN, 470350mE	LMT-23	4225320mN, 470895mE
LHS-4	4224960mN, 487385mE	LWC-20	4226240mN, 461360mE
LHS-31	4224685mN, 487095mE	LWC-19	4226445mN, 461560mE
LHS-26	4225495mN, 485135mE	LWC-18	4226035mN, 461590mE
LHS-27	4225055mN, 484890mE	LWC-15	4226025mN, 462425mE
LMT-42	4225695mN, 470800mE	CH-1	4228895mN, 476255mE
CH-2	4228970mN, 476320mE	CH-3	4229105mN, 476485mE
CH-4	4229100mN, 476490mE	CH-5	4229155mN, 476610mE
CH-6	4229150mN, 476605mE	CH-7	4229150mN, 476610mE
CH-8	4228800mN, 476800mE	CH-9	4228780mN, 476790mE
CH-10	4228760mN, 476755mE	CH-11	4228725mN, 476720mE

Table XVI: Sample locations, cont'd

Appendix 2: Analytical Methods

Sample Preparation

All samples which have been chemically analyzed were initially crushed in a steel plate jawcrusher to 2–3cm chips and then ground to <200 mesh using a rotary ceramic plate pulverizer. Only specimens devoid of Fe-staining, quartz veins, and megascopic porphyroblasts have been analyzed.

X-Ray Fluorescence

Major elements and some trace elements (Rb, Sr, Zr, Y, Nb, V, Ni, and Pb) were analyzed with a Rigaku 3064 XRF spectrometer and assosciated PDP11 computer at the New Mexico Bureau of Mines and Mineral Resources X-Ray Laboratory. XRF fusion disks were used for major element analysis, made from $\sim$ 5g sample and fused with 2–4g *Spectroflux*-105 and with $\sim$0.04g NH_4NO_3 as an oxidizing agent. Powder pellets were used for trace element analysis using 5–7g sample, to ensure infinite thickness, pressed with a boric acid backing and several drops of polyvinyl alcohol, to help adhesion, at 10 tons/in^2 pressure. Analytical methods are similar to those of Norrish and Hutton (1969) and Norrish and Chappell (1977). Y, Sr, Nb, Zr, Rb, and Pb were analyzed on 9-23-85, majors on 12-18-85, and V on 2-10-86.

Neutron Activation Analysis

Trace elements Cs, Ba, Hf, Sc, Ta, Cr, Co, U, Th, La, Ce, Sm, Eu, Tb, Yb, and Lu were analyzed by instrumental neutron activation analysis (INAA) using $\sim$300mg sample, sealed in polyethylene vials. The samples were irradiated

at the Annular Core Research Reactor at the Sandia National Laboratories. All samples except LMT2-2, LMT-55, and LOC-14, which were irradiated 12-14-86, were irradiated 11-8-85 for a total time of 10,000sec at a power level of 1MW and a total deposited energy of 10,000MJ. Counting began on 11-14-85 (short count) and the long count began on 1-8-86. Elements Sm, La, Lu, Sc, Co, Ba, Tb, and Yb were taken off the short count and Cr, Cs, Ce, Eu, Hf, Ta, and Th off the long count. The analyzing system consists of an ND6600 multichannel analyzer, an LSI11 computer, and two coaxial, intrinsic Ge detectors. NBS materials NBS-1633a and a Cs isotope were used as calibration standards. Analytical methods are after Gibson and Jagam (1980).

Electron Probe Microanalysis

Electron probe microanalysis was conducted by R. C. Newton at the University of Chicago's ARL fully automated EDS microprobe facility (1984).

Fluid Inclusion Analysis

Thermometric analysis of fluid inclusions were conducted in June, 1987 on a Linkam TH600 heating-freezing stage. Twenty inclusions were analyzed from two chips which were doubly polished to 0.3μm polish and 0.3mm thickness. Calibration on water yielded a freezing temperature of $+0.5°C$. Analytical method is similar to Roedder (1984).

Appendix 3: Precision of INAA method

Sample LMT-19 was analyzed in triplicate with three separate samples acting as unknowns. The first sample was analyzed in Nov. 1985, and the other two in Dec. 1986.

	Nov. 85	Dec. 86a	Dec. 86b
Cs	0.1	0.1	0.1
Ba	205	183	180
Hf	1.5	1.6	1.5
Sc	39.5	39.4	38.6
Ta	0.33	0.39	0.32
Cr	141	166	143
Co	37.1	37.8	36.2
U	0.6	0.4	0.4
Th	0.5	0.6	0.6
La	9.4	9.3	9.5
Ce	23.3	31.4	24.1
Sm	3.28	3.05	3.35
Eu	1.02	1.22	1.03
Tb	0.39	0.40	0.40
Yb	1.53	1.37	1.36
Lu	0.26	0.22	0.23

Table XVII: Replicate analyses of LMT-19 on INAA

Appendix 4: Standard Values Using INAA

Standard materials G-2 (USGS), AN-G (GIT-IWG), and BLCR (NMT) were analyzed as unknowns using INAA. Shown in the following table are the determined trace element contents and the percent difference between actual and observed concentrations (Θ). Observed values are reported in the number of significant figures appropriate to the method, but Θ is dependent upon the number of significant figures reported in the literature for the standard (Abbey, 1983).

	G-2	Θ	AN-G	Θ	BLCR	Θ
Cs	1.4	0	0.03		1.9	
Ba	1905	0.26	31	8.8	345	
Hf	8.0	0	0.4	5.3	3.7	
Sc	3.6	2.9	7.9	20	24.3	
Ta	0.80	0	0.15	0	0.34	
Cr	7.9	0	38.7	22	105	
Co	4.3	20	20.3	19	24.7	
U	2.0	4.8			1.4	
Th	24.8	0			3.3	
La	91.6	0	1.6	0	9.1	
Ce	164.3	2.5	3.87	17	21.3	
Sm	7.15	0	0.65	0	3.46	
Eu	1.403	0	0.265	27	0.964	
Tb	0.47	0	0.17	0	0.69	
Yb	0.88	2.3	0.68	20	2.7	
Lu	0.10	0	0.10	17	0.44	

Table XVIII: Analyses of G-2, AN-G, and BLCR

Appendix 6: Distribution Coefficients

Mafic K_ds (solid/liquid)						
	Grnt	Opx	Oliv	Mgt	Cpx	Plag
La	0.03	0.007	0.00001	0	0.07	0.15
Ce	0.03	0.008	0.00001	0	0.1	0.12
Sm	0.22	0.02	0.0006	0	0.40	0.067
Eu	1.0	0.02	0.001	0	0.40	0.35
Tb	3.0	0.05	0.002	0	0.5	0.06
Yb	5.0	0.15	0.02	0	0.6	0.07
Lu	5.5	0.18	0.016	0	0.6	0.06
Sr	0.012	0.02	0.015	0	0.10	2.0
K	0.02	0.014	0.17	0	0.011	0.17
Rb	0.04	0.02	0.01	0	0.02	0.13
Ba	0.02	0.013	0.01	0	0.005	0.25
Tb	3.0	0.05	0.002	0	0.5	0.06
Ta			0.03	0.5	0.06	0.04
Nb	0.1	0.15	0.01	0.7	0.1	0.01
Zr	0.3	0.03	0.01	0.1	0.1	0.01
Hf	0.15	0.04	0.04	0.4	0.3	0.01
Ti	0.3	0.1	0.02	7.5	0.4	0.04
Y	2.0	0.2	0.01	0.2	0.5	0.03
V			0.05	25	1.2	
Rhyolite K_ds (solid/liquid)						
	Kspar	Mgt	Plag	Biot	Garnt	
Rb	0.35	0	0.04	2.2	0.01	
Nb	0.05	2.5	0.06	5	0.5	
Y	0.1	2	0.1	0.03	35	

Table XX: Distribution coefficients

Appendix 7: Modes and Melting Proportions

Garnet Lherzolite		
	mode (%)	melt (%)
Opx	28	5
Oliv	64	5
Cpx	3	45
Garn	6	45
Metasediments		
	mode (%)	melt (%)
Kspar	10	34
Mgt	1	1
Plag	39.5	31
Biot	19	4
Garn	0.5	1
Qtz	30	29

Table XXI: Modes and melting proportions

wt %	OPX CH1	OPX CH2	AMPH CH1	AMPH CH2	BIOT CH1	BIOT CH2	PLAG CH1	PLAG CH2
SiO_2	50.56	50.05	40.78	40.21	35.52	34.68	61.07	61.42
TiO_2	0.00	0.00	2.35	2.29	6.14	6.50	0.00	0.00
Al_2O_3	0.74	0.61	11.66	11.11	14.57	14.24	24.11	23.82
FeO	30.76	31.39	20.29	20.48	20.07	21.75	0.00	0.00
MnO	2.43	1.86	0.00	0.00	0.00	0.00	0.00	0.00
MgO	15.90	15.13	8.39	7.39	9.61	8.70	0.00	0.00
CaO	0.75	0.67	12.70	12.36	0.00	0.00	5.68	6.09
Na_2O	0.00	0.00	1.13	1.18	0.00	0.00	7.55	8.36
K_2O	0.00	0.00	1.80	1.80	10.23	9.79	1.81	0.42
Cl	0.00	0.00	0.35	0.79	0.32	0.63	0.00	0.00
Σ	101.14	99.71	99.45	97.61	96.38	96.29	100.24	100.13
							An 27.2	An 29.0

Notes : Minerals virtually unzoned.

CH-1 Pyrite, ilmenite, magnetite, apatite, zircon, quartz, K-feldspar also present.

CH-2 Ilmenite, magnetite, apatite, zircon, quartz, K-feldspar also present.